Analyzing the hydraulic design for the new basin in the IJmuiden outer harbor

Investigating the influence of long waves on basin and ship resonance

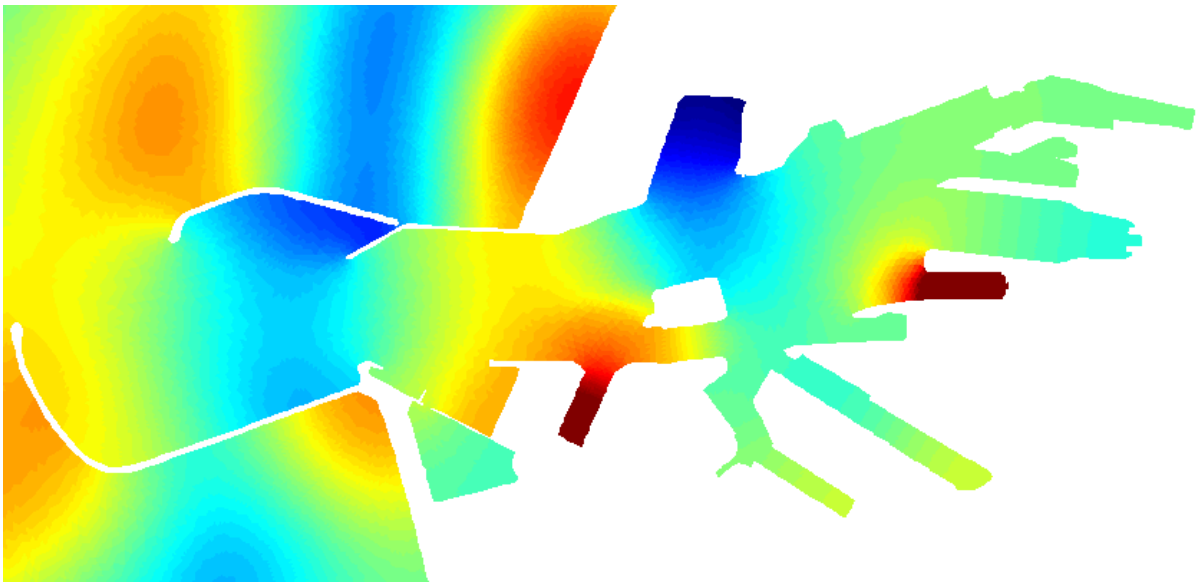

Master of Science Thesis

Author:
Philip Kaufmann

Graduation committee:
Prof. ir. Tiedo Vellinga
Dr. ir. Robert Jan Labeur
Ir. Michiel de Jong
Ir. Bas Wijdeven

November 17, 2011

Faculty of Civil Engineering and Geosciences

DHV Consultancy and Engineering

Preface

This thesis work is the final part of my MSc study for the Hydraulic Engineering specialization 'Ports & Waterways' at the Faculty of Civil Engineering of the Delft University of Technology. The thesis subject was commissioned by by DHV Consultancy and Engineering.

The thesis describes the subject 'Analyzing the hydraulic design for the new basin in the IJmuiden outer harbor' with the subtitle 'Investigating the influence of long waves on basin and ship resonance'.

I am greatful to all the people who were involved in the track of beginning to finalizing my master thesis. I would like to thank my graduation committee for their supervision and support: Prof. ir. Tiedo Vellinga (Delft University of Technology) as head of the committee; Dr. ir. Robert Jan Labeur (Delft University of Technology) for always making time for me, for his feedback and extensive advise concerning encountered hydraulic issues; Ir. Michiel de Jong (Delft University of Technology) for providing the thesis subject and opportunity to perform the research at DHV and Ir. Bas Wijdeven (DHV Consultancy and Engineering) for his advise and substantive feedback at the DHV office. Furthermore I would like to thank DHV Consultancy and Engineering for the provided opportunity and office facility they have offered me to write my thesis.

Graduation committee:

Prof. ir. Tiedo Vellinga	Delft University of Technology
Dr. ir. Robert Jan Labeur	Delft University of Technology
Ir. Michiel de Jong	Delft University of Technology
Ir. Bas Wijdeven	DHV Consultancy and Engineering

Acknowledgments

Besides the graduation committee, I would like to show my gratitude to the following persons who have assisted me in the research process:

All DHV employees from the RK and HWG divisions who were always ready to assist me or provide me of advise; Especially I would like to thank Johan Henrotte, Tijmen Smolders, Roald Treffers, Thijs de Boer, Lars Hoogduin, Joas Boeyinga and Frank Dekker.

Apart from DHV employees I would like to thank the following external specialists:

Judith van Os from Deltares, for always providing extensive support concerning the PHAROS model setup. Jo Pinkster, for providing the data concerning bulk carrier response. Gert Jan van den Brenk from DNH, for making available the raw data of the AWAC measurements. Peter van de Meerakker and Roland van Velzen, general director and technical director of the port of IJmuiden NV, for the possibility to interview them and the provided information they granted about the harbor of IJmuiden.

Summary

To improve the lightering conditions of bulk carriers in the outer harbor of IJmuiden, the lightering facility will be transfered to a new harbor basin that will be implemented at the location of the dredging depot in the former Averij harbor. The Dutch Directorate-General for Public Works and Water Management (RWS) demands that down time of the lightering operations inside the new basin does not exceed 5% of the operating time of 365 days a year, 24 hours a day.
Down time of the lightering operation can be caused by several issues. This thesis investigates the contribution of long waves with wave periods between 10 and 250 seconds to the down time conditions. Theoretically this long wave climate can cause high ship response as incoming wave periods are close to the bulk carrier's natural periods. The long waves can also cause resonance in the new basin or in the outer harbor as a whole. A coupled system of basin resonance and ship response is also investigated as the two separate resonance systems can enforce each other for certain wave periods.

Investigating a 200.000 DWT bulk carrier's Response Amplitude Operators for an open water situation concludes that the bulk carrier experiences enforced movement in its horizontal motions for wave periods around 250 seconds and in its vertical motions for wave periods between 15 and 20 seconds. In the real time situation the ship's horizontal motions will be damped by the mooring system and the high resonance periods will not be met.

The numerical wave model PHAROS has been used to analyze whether resonance patterns arise in the outer harbor basins for a wave period band between 10 and 250 seconds. It is concluded that the new basin can experience resonance for wave periods between 100 and 250 seconds. The highest wave amplification of 4.5 times the incoming wave height at sea occurs for an incoming wave period of 147 seconds. The amplified wave height inside the new basin will not contribute to down time conditions as the amplified wave height is lower than the critical wave height of 0.80 meter.
The implementation of the new basin has a positive effect on the area of the outer harbor behind the Fort island. Especially in the Hoogoven harbor and at the Noorder ship lock wave agitation decreases. However, standing waves may arise between the new basin and the opposing IJmond harbor if sufficient wave energy is present in the incoming wave climate.

The results of the coupled system of basin resonance and bulk carrier vertical response do not result in a contribution to the down time criteria. Although amplified waves can become a factor 4.5 larger than the incoming wave heights, earlier investigation and observations and analyses in this study show that the incoming wave energy for long waves is low and the probability of incoming waves amplifying into waves of critical wave heights that cause down

time to the lightering process is very little. The contribution to the down time of the new basin is very small in comparison to the contribution of wind and locally generated wind waves.

Contents

List of Figures

List of Tables

Chapter 1

General introduction

1.1 Motivation for the study

DHV Consultancy and Engineering (DHV), the initiator of this study, is involved in the development of a new basin in the outer harbor of the port of IJmuiden. The project is assigned by the Dutch Directorate-General for Public Works and Water Management (RWS).

The reason for the construction of the basin is to provide a new location for the lightering of bulk carriers sailing to Amsterdam. The port of IJmuiden is accessible for ships with a maximum draught of 17,80 meter, however the depth of the North Sea channel (connecting the port of IJmuiden with Amsterdam) is less. When bulk carriers with destination Amsterdam have a draught deeper than 13,75 meter they have to be lightered in the outer harbor before they are able to sail through the Noorder ship lock into the North Sea channel.

1.1.1 Current situation for lightering in the outer harbor

In the current situation lightering of these bulk carriers happens at the IJ-palen. This mooring facility is located in the outer harbor south of the former Averij harbor (see figure 1.2). The IJ-palen consist of two berthing dolphins, three buoys and a bollard. The Port of Amsterdam is the operator of the mooring facility that has been in use since 1998.

Figure 1.1: Overview of the outer harbor of IJmuiden

Figure 1.2: Overview of the IJ-palen and the sludge depot

1.1.2 Complications for the lightering facility at the current location

In 2007 it was determined that the lightering of ships at the IJ-palen can cause nautical complications. These complications occur due to the position of the lightering facility. A ship moored to the IJ-palen narrows the approach channel of the Noorder ship lock significantly, making it difficult for other ships to maneuver through the channel.
The complications also account for a moored ship at the IJ-palen itself. Due to suction forces of passing ships through the approach channel mooring lines have broken, causing a ship to sail away from the mooring facility. These complications can cause dangerous situations in the outer harbor of the port of IJmuiden.

Figure 1.3: Impression of the lightering in progress [34]

1.1.3 Solution for the lightering facility

RWS has decided that to solve the bottleneck the lightering facility has to be transferred to another destination. The best alternative for a new destination is the former Averij harbor

situated north of the IJ-palen (see figure 1.2). The former Averij harbor has lost its original goal as refuge harbor in 1979, twelve year after it had been built. Since then it served as a sludge depot to store contaminated dredging materials.
The solution consists of the total demolition of the sludge depot and the creation of a new port basin with a water depth of - 20 meter NAP. The IJ-palen berthing facility will be transferred into the former Averij harbor such that ships can be moored and lightered without causing complications to the existing waterway from and to the Noorder ship lock (see figure 1.4).

Figure 1.4: Impression of the future layout of the former Averij harbor

1.2 Problem definition

For the hydraulic design of the new basin it is important to understand the operational wave conditions in the new basin. These wave conditions can affect the nautical operations and the mooring conditions of bulk carriers in the basin. The study emphasizes on long waves as well as harbor resonance. Local wind waves seem to have little effect on moored bulk carriers.

At the moment it is unknown whether there are complications due to the occurrence of long waves or resonance in the existing harbor basins of the outer harbor.

The layout and hydraulic design of the new basin may have effects on the operational conditions of the current layout of the outer harbor. It could be possible that the new basin has positive effects on the wave conditions of the existing harbor basins.

1.3 Study objective

The objective of this thesis is to analyze the hydraulic design for the new basin. The design of the basin must assure minimal influences of adverse wave impacts (long waves and harbor resonance) on moored bulk carriers inside the basin. It will also be investigated whether changing the geometry of the new basin improves the outcomes of the study.

It has to be made certain that the design of the new basin does not have negative effects on the existing harbor basins and possibly even improves the wave conditions in the existing harbor basins.

1.4 Study approach

A primary study has to be carried concerning the current situation of the outer harbor of IJmuiden. This includes information about the port's layout and revetments as well as the hydraulic conditions. When this data is analyzed an understanding is formed of the appearing conditions inside the harbor.

It will be analyzed what the downtime criteria are for the new basin and the bulk carriers moored at the lightering facility. It is important to determine the critical hydraulic conditions during which ships suffer difficult mooring or (un)loading conditions. Without this information it can not be concluded whether obtained data and theoretical findings concerning the harbor conditions cause any problems in the new basin.

Not only wave heights can cause down time conditions, wave periods of long waves causing a bulk carrier to experience severe movement should also be analyzed. When it is determined what the wave periods are with negative impact on moored bulk carrier motions, it can be investigated whether these periods are present in the outer harbor.

Next to the bulk carrier, the new basin can also experiences resonance caused by certain wave periods. Based on simplified mathematical formulations, calculations will be carried out to determine the resonance periods of the new basin and current harbor basins. This analysis gives a first impression whether problematic wave conditions can occur in the new basin due to basin resonance.

The next step is analyzing the wave climate inside the outer harbor to determine whether the problematic wave periods are present in the outer harbor.
Through pressure box and AWAC measurements wave spectra can be analyzed providing information about the presence of these wave periods inside the outer harbor. This analysis can determine whether the theoretically obtained resonance wave periods are indeed present in the outer harbor.
As stated the theoretical findings have been determined using simplified mathematical formulations. Furthermore these calculations only analyze designated parts (the basins) of the outer harbor separately. To obtain more precise results concerning the outer harbor as a whole, a hydraulic model will be applied to investigate the wave configurations inside the new basin and to investigate the interaction between the new basin and the existing harbor basins concerning standing wave patterns and basin resonance.

A study will be carried out using a mathematical mild slope equation model. This model provides wave agitation inside the port of IJmuiden for given wave periods based on the mild slope equation. In the model runs concerning the existing layout of the outer harbor will be compared with the layout of the outer harbor including the new basin. It will be determined which wave periods cause basin resonance and these results will be compared with earlier results concerning bulk carrier resonance. Runs will also be carried out considering a different

geometry of the new basin, results will be compared with the current layout and conclusions can be drawn whether changes the layout provides better model results.
This way it can be determined whether the new basin itself experiences resonance situations that cause severe movement to the bulk carrier. It will also be analyzed whether the implementation of the new basin creates adverse wave resonance in the other basins.

The bulk carrier experiences severe movement due to basin resonance or heavy ship response. However these two resonance system combined in a coupled system could enforce each other if both systems react to the same wave periods. Therefore the coupled system will be analyzed for every degree of free ship motion.

1.5 Report structure

Chapter 2 provides information of present hydraulic conditions at the outer harbor.

The general design criteria, bulk carrier natural periods and the resonance periods of the new basin and current harbor basins are the subject of Chapter 3.

Chapter 4 analyzes the wave conditions inside and just outside the outer harbor. On the basis of one dimensional energy spectra it will be determined what wave periods are present in the outer harbor.

The outcomes of the implementation of the new basin in a mathematical model are discussed in Chapter 5. Results concerning the existing situation of the outer harbor and the future situation concerning the new basin will be compared.

Chapter 6 analyzes the coupled system of basin resonance and ship response to incoming wave periods.

The conclusions and recommendations of this study are provided in Chapter 7.

Chapter 2

Hydraulic conditions

2.1 Layout and bathymetry of the outer harbor

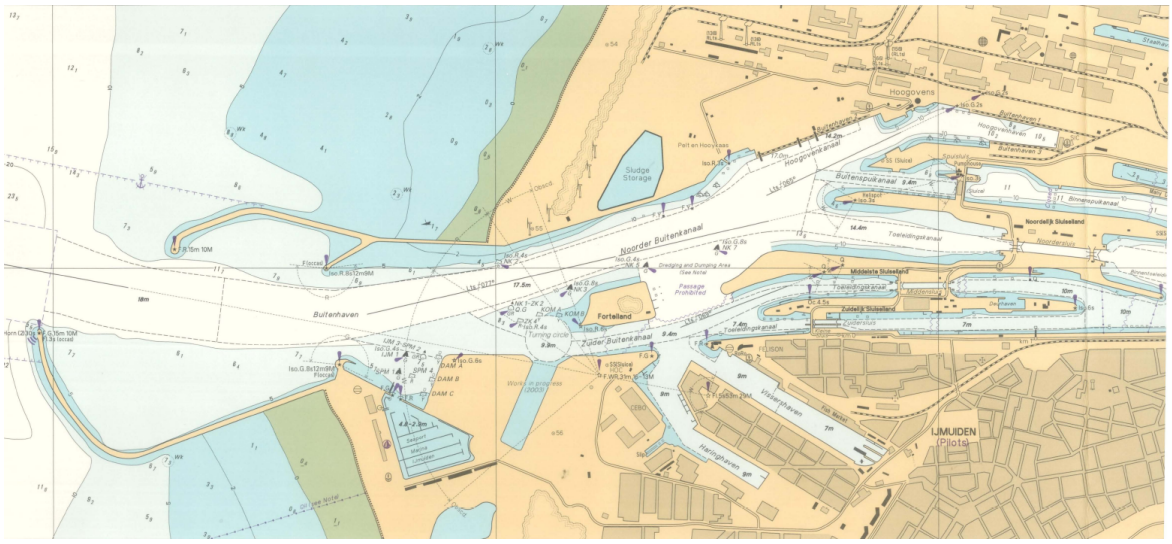

Figure 2.1: Nautical map of the outer harbor (source: RWS)

The existing outer harbor consists of three basins and a marina at the southern boundary as can be seen in figure 2.1. The harbor entrance is situated at the North Sea and is connected to the hinterland by three ship locks connecting the port of IJmuiden with the North Sea channel. At the north of the ship locks a discharge sluice is located, this system is able to discharge water from the North Sea channel into the outer harbor. The harbor channel has a water depth of 18 meter below NAP when entering the outer harbor from the North Sea. Just west of the Fort island the channel parts into two separate channels. The deepest of the two channels is located north of the Fort island and navigates ships to the Noorder ship lock. This channel has a minimum depth of 14.4 meter below NAP. The second channel is located south of the Fort island and functions as a connection for the southern harbor basins with the North Sea and the other two ship locks. This channel is shallower than the northern channel and has a minimal depth of 7.4 meter below NAP (see figure 2.2).
In direction from east to west the first two basins are named the Vissers harbor and the Haring harbor (see figure 1.1). The Vissers harbor has a depth of 9 meters below NAP at

the entry of the harbor, this depth decreases to 7 meter below NAP when nearing the end of the basin. The Haring harbor has a depth of 9 meters below NAP. The third basin is called the IJmond harbor and has a constant depth of 11 meters below NAP. All three basins have vertical sheet pile revetments. Next to the IJmond haven, outside the old outer harbor, a marina is situated. The marina has a maximal depth of 5 meters below NAP and functions as a berthing harbor for leisure yachts (see figure 2.1).
As stated above the outer harbor entrance is situated at the North Sea. As the North Sea has an average depth of 10 to 15 meters below NAP near the Dutch coast, an approach channel called the IJ-geul has been implemented for ships to enter the harbor of IJmuiden. Dimensions of the channel are provided in Table 2.1

Table 2.1: Dimensions of the IJmuiden harbor approach channel [3]

Approach channel parameters	Dimension
Average channel depth (m)	- 21.0 NAP
Channel width (m)	450 - 600
Channel length (km)	43.0
Maximum draught (m)	17.8

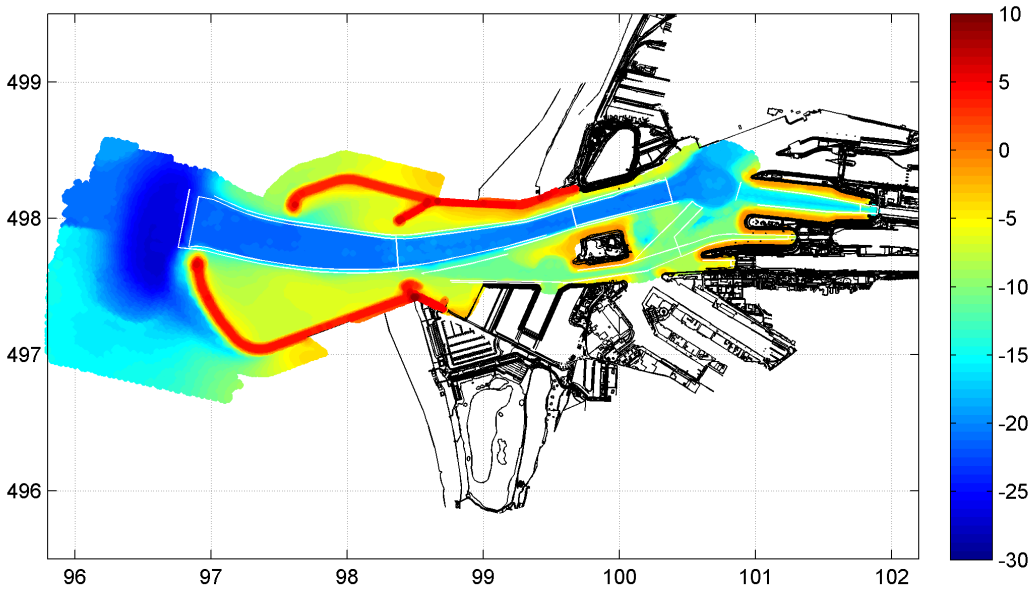

Figure 2.2: Bathymetry of the outer harbor (m) (source: RWS and DHV [22])

2.2 Water levels and tidal conditions

Water levels outside the harbor of IJmuiden for the period between 1981 - 2009 have been downloaded from Waterbase [30]. The data is obtained through a measuring pole located at the entrance of the outer harbor (see appendix A.1 for the exact location). The water levels of the downloaded data set vary between 2 meter above NAP and 1.5 meter below NAP with an extreme water level of 3.12 meter above NAP which occurred during a north-west wind condition with a velocity above 15 m/s. Extreme low water levels occur during eastern wind conditions with velocities above 10 m/s.

Apart from the downloaded data from Waterbase, the website Waternormalen [31] provides general characteristics of water levels in the outer harbor of IJmuiden. The characteristics are added in appendix A.2. From the provided data from Waternormalen it can be seen in the appendix that the extreme water level of 3.12 meter above NAP, provided by waterbase, has a return period of 1/20 years. Table 2.2 provides the important tidal, average and extreme water level conditions and their return periods.

Table 2.2: Important average and high water level conditions

Condition	Water level
Mean High Water level	0.97 m NAP
Mean Low Water level	-0.73 m NAP
Spring tide High Water level	1.15 m NAP
Spring tide Low Water level	-0.75 m NAP
Neap tide High Water level	0.75 m NAP
Neap tide Low Water level	-0.64 m NAP
Mean Sea Level	0.02 m NAP
1/1 year High Water level	2.35 m NAP
1/10 year High Water level	2.90 m NAP
1/100 year High Hater level	3.60 m NAP
1/10.000 year High Water level	5.15 m NAP
1/1 year Low Water level	-1.70 m NAP
1/10 year Low Water level	-2.05 m NAP

2.3 Currents in the outer harbor

Currents arise in the outer harbor because of a combination of sluice discharges and tide. Waterbase [30] provides discharge data of the discharge sluice located north of the Noorder ship lock (see figures 1.1 and 2.1). The discharge sluice can discharge water by means of free flow or by the use of pumps. These discharge capacities of the sluice have been documented by DHV [22]. Table 2.3 shows the discharge properties of the sluice.

Table 2.3: Discharge capacities of the discharge sluice

Sluice discharge option	Discharge (m^3/s)
Maximum average daily discharge under free flow	300
Maximum daily discharge under free flow	500
Maximum daily discharge capacity by use of pumps	260
Maximum discharge by combinations of free flow and pumps	700

DHV has carried out an analysis of the combination of the sea and discharge currents inside the outer harbor using a simplified two dimensional flow model [22]. The model considered normative tidal conditions in combinations with the sluice discharges. The port designer's handbook [36] states that currents higher than 1 m/s interfere with the mooring conditions of a bulk carrier. Maximum currents 0.1 m/s were modeled at the entrance of the new basin. The results of the analysis show that current velocities are negligible for the hydraulic design of the new basin.
As Tata steel (the former Hoogovens) is situated at the harbor of IJmuiden there is also an intake and discharge of cooling water by the factory. However the discharge of this cooling water vary between 4 to 7 m^3/s. The maximum discharge capacity is unknown. A realistic maximum is estimated to be be around 10 to 20 m^3/s [22]. This capacity is only a few percent of the total discharge through the outer harbor to sea.

2.4 Sedimentation

Information about the sedimentation and erosion process at the IJmuiden harbor has been derived from a sedimentation study carried out by RWS in 2003 [15]. For more detailed information reference is made to this report.
After the implementation of the IJmuiden harbor breakwaters in the period between 1867 and 1876, the adjacent coastline gradually moved seawards. The sedimentation of the coastline extended over a distance of 2 to 3 kilometer at both sides of the harbor but was much bigger north of the harbor in comparison to the southern coastline. Adjacent to these sedimentation areas an erosion area was situated at both sides of the harbor stretching out over an area of 4 to 5 kilometers. About a 100 years after the implementation of the breakwaters a sedimentation equilibrium was achieved for the area of IJmuiden.
After the extension of the breakwaters in the 1960's, sedimentation of the northern and southern coast arose again. However, the southern coast sedimentation was much higher in comparison to the northern coastline. The so called Kennemer beach, just south of the southern breakwater (figure 2.3), increased significantly due to the sedimentation [15]. It is

determined that the sedimentation area south of the harbor expands in southern direction. This sedimentation process is still present in current situation, however the sedimentation pattern decreases during the years. The report concludes that in the near future a sedimentation equilibrium will be established. It has been estimated [15] that a new sedimentation equilibrium will be derived in a about 30 years just south of the harbor going up to 70 years when moving along the coastline in southerly direction.

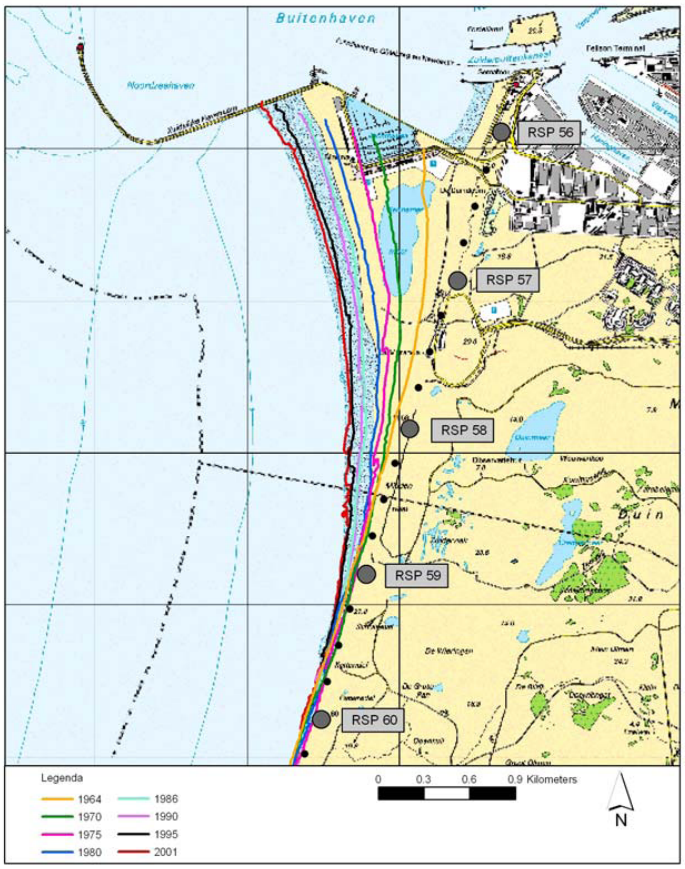

Figure 2.3: Position of the 0 meter NAP line at the Kennemer beach during the period between 1964 and 2001 (source: RWS [15])

2.5 Wind conditions

Wind conditions are obtained from the KNMI website [25]. The data is retrieved by the measuring station s225 IJmuiden for the period of 1952 to 2010. This station is situated at the "buitenhaven IJmuiden""location (see appendix A.1). The website provides a distribution of normal wind conditions and an extreme value distribution. These distributions are shown in appendix A.3. In figure 2.4 a directional distribution of the wind velocities has been presented based on the available data [22].

It can be concluded that the majority of the wind comes from the west to south west direction. In addition a significant number of occurrences concern eastern winds. The maximum

wind velocity measured in the data set by the KNMI is around 25 m/s, corresponding to a force of 10 on the scale of Beaufort. Based on the extreme value distribution this wind velocity has a 1/50 year probability of occurrence. Wind forces of 8 on the scale of Beaufort (critical for crane movement [42]) occur less than 1% of the time.

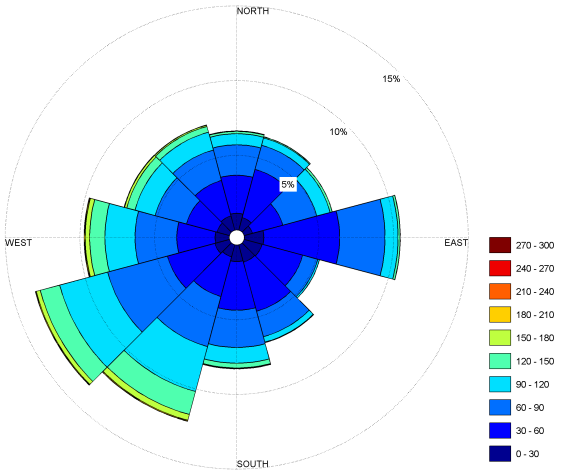

Figure 2.4: Directional distribution of wind velocities (cm/s), (source: DHV [22])

2.6 Wave conditions

2.6.1 Wave conditions outside the harbor

Wave conditions outside the port of IJmuiden have been determined using data collected from two locations outside the harbor.

1. A wave buoy, measuring wave spectra, located at an old ammunition dump 30 km of the coast of IJmuiden
(measurement period: 1980 - 2009) Provided by waterbase [30]

2. A wave pole located just outside of the outer harbor of IJmuiden
(measurement period: 2002 - 2010). Provided by the Port of Amsterdam

Appendix A.1 shows the exact location of the two measurement systems.
In appendix A.4 a summary of the normal wave conditions provided by DHV is included. In figures 2.5 and 2.6 directional distributions of the wave heights and wave periods are derived out of the provided data [22].
From the data it can be concluded that 75% of the waves at the ammunition dump are coming from south west to north east direction. The mayority of the waves come from the north west (45%), another significant direction is the south west accounting for 25% of the waves.

The highest wave measured at the ammunition depot had a significant wave height of 8 meter. The wave had a average wave period of 9 seconds. The longest average wave period

of the dataset provided by the spectral measurements is 12 seconds and the average wave height is 1 meter.

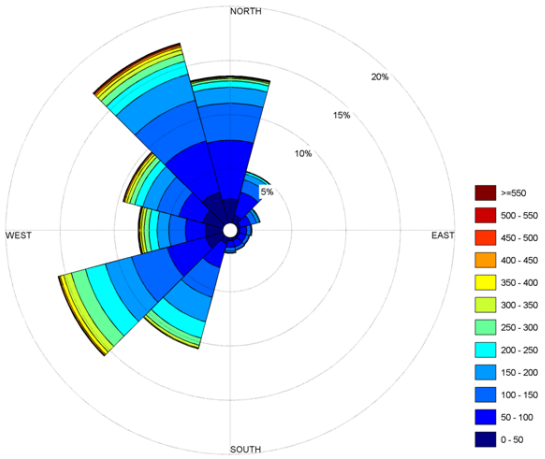

Figure 2.5: Directional distribution of wave height (H_{m0}) at the ammunition dump (cm) (source: DHV [22])

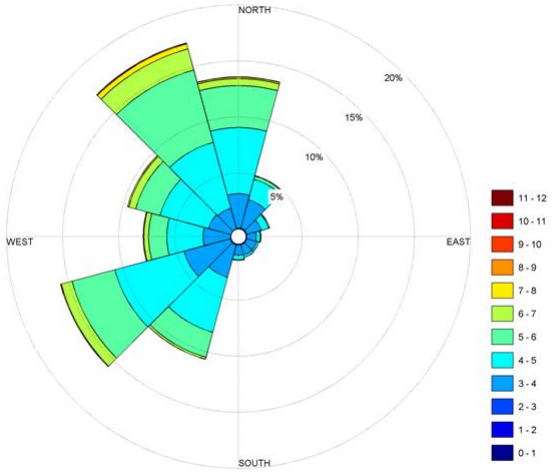

Figure 2.6: Directional distribution of wave periods (T_p)at the ammunition dump (s) (source: DHV [22])

The highest measured significant wave height of the dataset derived at the wave pole just outside of the harbor is 6,2 meter and has an average wave period of 8 seconds. The highest average period obtained from the dataset is 9 seconds and the average wave height at the location is 1 meter.
There are no statistics available about extreme wave height conditions at the measurement locations. DHV has carried out an extreme wave height analysis for the sea at IJmuiden which concluded that the 1/1 year probability of occurrence wave has a wave height of 5 meter [22]. This matches the statistics of extreme wave heights in the proximity of IJmuiden,

presented in the HR2006. Both graphs are added in appendix A.5 It has to be taken into account that this is an approximation.

2.6.2 Wave conditions inside the outer harbor

Wave action inside the outer harbor has not been measured in the past. Until recent measurement, no data was available. From the summer of 2010 RWS has started to obtain wave data from the outer harbor. Data has been obtained in two different ways. By means of AWAC measurements and by means of pressure boxes.

The data obtained by the use of AWAC measurement systems is capable of measuring waves with wave periods up to 30 seconds. The data has been provided by the RWS office in IJmuiden [37] for this thesis and will be analyzed extensively in chapter 4.

The data obtained through pressure boxes is not available for this thesis. However the data has been processed by Arcadis and Deltares [6] and results will be taken into account in chapter 4 when analyzing the data from the AWAC measurements. This will create a complete view of the energy spectrum in the outer harbor.

Pressure boxes were installed at three locations in the outer harbor: in the IJmond harbor, at the Midden sluice and in the Vissers harbor. Energy density spectra have been derived concerning waves with large periods (wave periods of 50 seconds and larger). The report [6] provides spectral plots for all three locations in the outer harbor for eight selected moments in time between March and June 2010. These moments have been chosen as the significant wave heights at the three location at those moments were highest in the obtained data. Figures 2.7 and 2.8 shows the measured energy spectra at the pressure box installed in the IJmond harbor.
For energy spectra concerning all three of the locations and the setup and data preparation of the pressure boxes, reference is made to appendix A.6.

As can be seen in figures 2.7 and 2.8 the energy spectra cover a large range of very low wave frequencies of 0.1 up to 0.002 Hz (coinciding with wave periods of 50 seconds to 167 minutes). The figures clearly show that waves with very low frequencies penetrate the outer harbor at these given moments. Some of the energy spectra show energy peaks around 0.005 Hz, these peaks comply with very long wave periods.

Earlier studies on very long waves in the outer harbor carried out by Alkyon (2001) [5] and by WL Delft Hydraulics (1987) [32] confirm the results of the measured data of very low frequency waves inside the outer harbor.
These studies have shown, with help of measured data and computer models that seiches with wave periods of around 11 and 30 minutes cause harbor resonance. The 30 minute seiche shows a first mode standing wave pattern. In the far end of the harbor, at the sluices and Hoogoven harbor, the incoming wave is amplified a factor 12 to 14. The 11 minute seiche shows a mode two standing wave pattern and the incoming wave is amplified a factor 4 to 5 near the end of the harbor.
Alkyon [5] concludes that seiches appear almost continuously in the outer harbor of IJmuiden. However, the probability of occurrence of amplified wave height of more than a few

decimeters are low. For example a seiche with a amplified wave height of 1 meter in the back of the outer harbor occurs less than once per year [5].

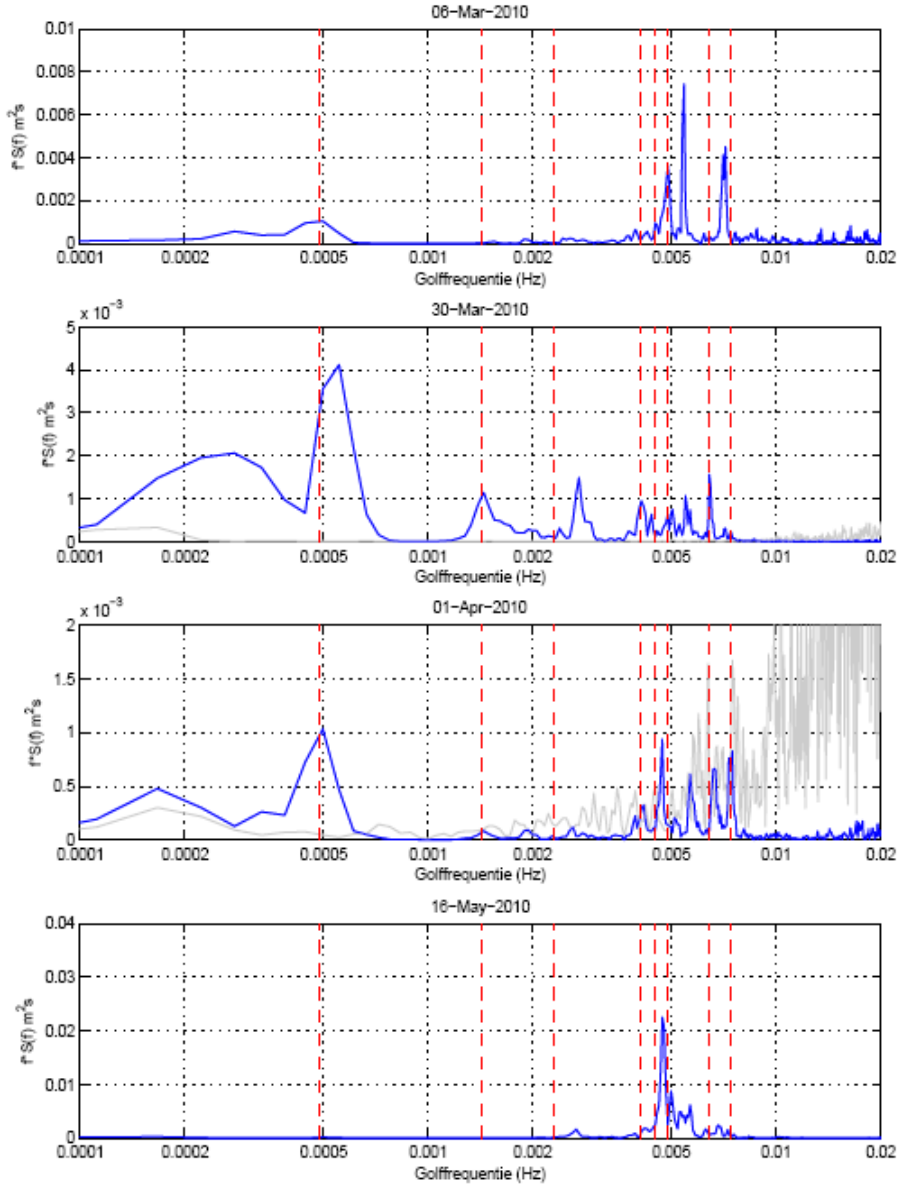

Figure 2.7: One dimensional wave spectra derived at the IJmond harbor [6]

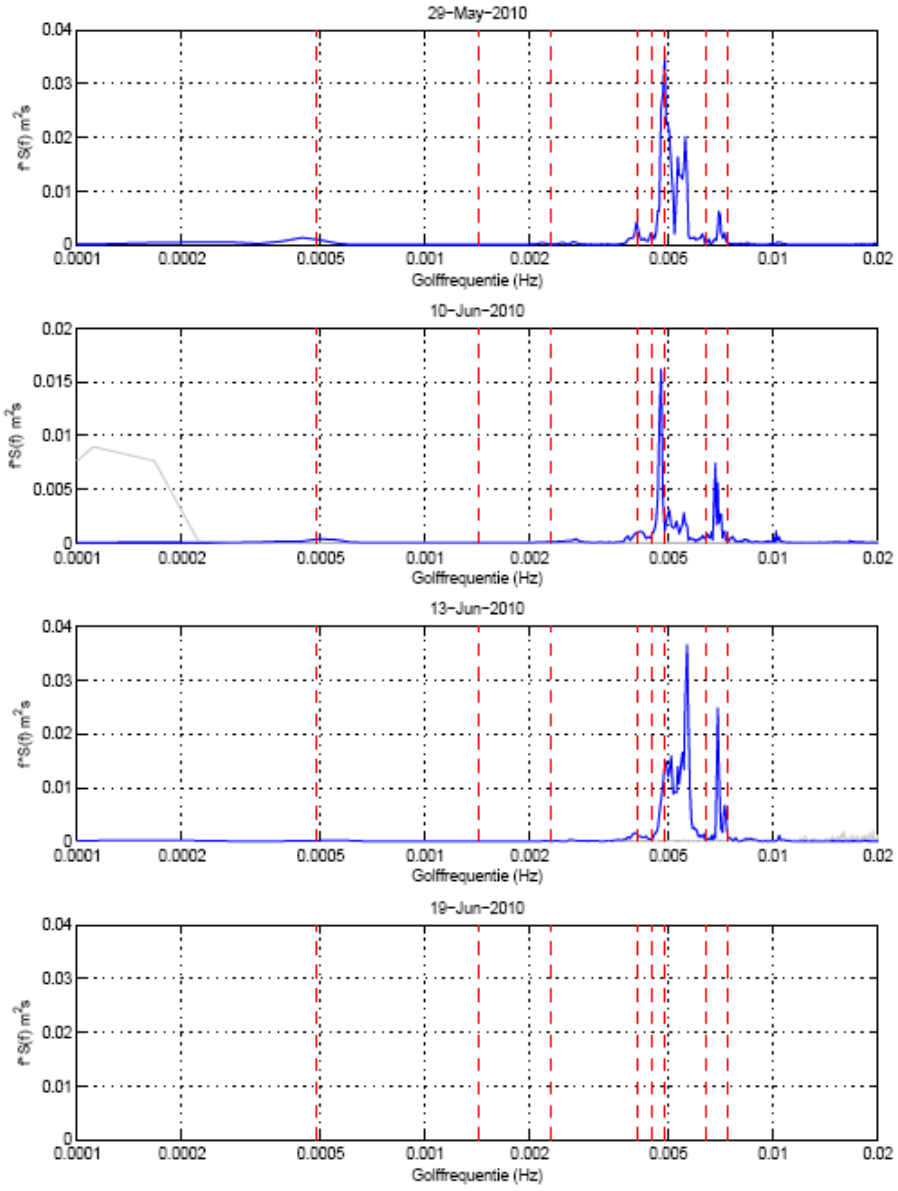

Figure 2.8: One dimensional wave spectra derived at the IJmond harbor [6]

Chapter 3

Design criteria

3.1 Introduction

Chapter 2 provides information about the hydraulic conditions for the outer harbor in the current situation. It is expected that the implementation of the new basin will have influence on and will probably change this situation. This chapter emphasizes on the new basin. The chapter consists out of three sections. The first section explains the function, the general dimensions and the downtime criteria of the new basin. It also provides information about the vessels making use of the basin and the loading operation restrictions which should be taken into mind.
The second section considers the type of bulk carrier that will be lightered in the new basin in further detail. Incoming wave periods that cause severe ship movement to the bulk carrier are analyzed and conclusions concerning the results will be drawn.
As a bulk carrier can also experience movements when the basin itself will experience resonance, the last section of the chapter discusses wave periods that cause resonance to arise in the outer harbor basins. The emphasis of this analysis will lay on the new basin, but all the harbor basins will be analyzed to create an understanding of sensitive wave periods that cause resonance to the outer harbor basins.

3.2 Criteria considering the function of the new basin

As stated in chapter 1.1.3 a new harbor basin will be implemented in the former Averij depot. This new basin will have the objective to serve as the new lightering location (in stead of the current location situated at the IJ-palen) for bulk carriers sailing to Amsterdam. Next to the lightering of the bulk carrier the basin must be capable of providing shelter and berth facilities to inland vessels that transport the lightered bulk to the terminals in Amsterdam. The goal of the study is to analyze the impact of the wave climate on the lightering process concerning the new basin and new situation of the outer harbor. To determine adverse wave impacts, the design criteria and down time conditions of the new basin should first be analyzed, before conclusions can be drawn.

3.2.1 General design criteria for the new basin

RWS and DHV have documented criteria for the hydraulic design of the new basin [33] [11]. The most important criteria to determine the downtime for the new basin are listed in this chapter.

- The basin operating time is 365 days, 24 hours a day.
- The total downtime of the new basin may not exceed 5% of the operating time.
- The basin will serve as a lightering and refuge facility for bulk vessels
- The lightering will be carried out by two floating cranes positioned at the same side of the bulk vessel

3.2.2 Layout dimensions for the new basin

The new harbor basin should provide sufficient maneuvering space for the vessels to move without complications. DHV has derived the general dimensions of the new basin layout [18] following the guidelines from the design rules provided by the port design handbook [36].

- The width of the new basin is determined to be 4 x the width of the bulk carrier:	180 m.
- The length of the basin should be $LOA_{bulkcarrier}$ + 30 m:	330 m
- The space between the front of the ship and the shore should be:	15 - 30 m
- Criterion stated by RWS is that the new basin has a depth of:	20 m below NAP

Based on these criteria DHV has created a number of variants of the new basin. In consideration with RWS the most suitable variant [19] has been chosen to be constructed as layout for the new basin. Figure 3.1 shows the layout of the chosen variant.

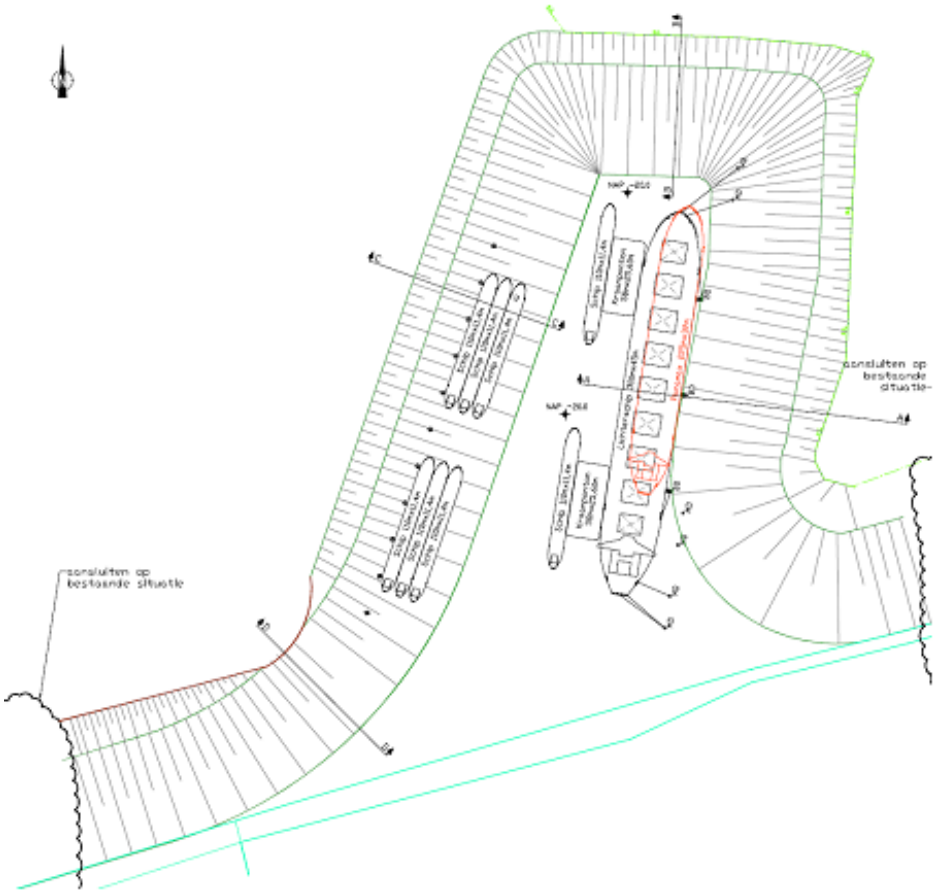

Figure 3.1: The chosen variant for the new basin layout (source: DHV [19])

A sloping shoreline for the entire new basin will be implemented instead of a vertical revetment. The slope of the shoreline has a 1:5 ratio from the bottom of the basin at 20 meter below NAP until the slope reaches the depth of 10 meter below NAP. From there the slope changes into a 1:3 ratio until it reaches a level of 5 meter NAP.
The bulk carrier will be moored just east of the middle of the new basin. The mooring facilities are located east of the bulk carrier. Due to the determining westerly wind conditions it is better and more convenient to moor a ship at the lee shore. In addition, in case mooring lines break, the bulk carrier will be pushed against the mooring system instead of drifting away when the fenders would be situated at the other side of the ship. The mooring position of the bulk carrier also makes the ship easy accessible for the barges and cranes to lighter the ship from the port side.
The mooring system exists out of three breasting dolphins, two mooring dolphins at the front of the ship and four mooring dolphins at the back of the ship (see figure 3.1)
In the chosen variant the bulk carrier is less sensitive to effects of passing ships than in the existing situation. Due to the perpendicular position of the bulk carrier towards the northern harbor channel and the passing ship direction, it is less sensitive to water level decreases due to these passing vessels.

3.2.3 Dimensions of the bulk carrier

The basin should be able to berth and lighter bulk carriers with the following maximum dimensions:

* DWT:	180.000 - 200.000 DWT
* LOA:	290 to 300 m
* Width of the vessel:	45 m
* Loaded draught of the vessel:	17,80 m
* Lightered draught of the vessel:	13,75 m

These are the dimensions of typical bulk carriers currently mooring at the IJ-palen. In the new lighter facility there will be no change in ship dimensions. The lighter location will be moved inside the new basin but the bulk carriers to be lightered remain of the same dimensions.

3.2.4 Dimensions of the barges

Bulk from the carrier is lightered onto smaller barges. It is important to determine downtime conditions for these smaller ships. When the conditions are still appropriate for the bulk carrier, it could be the case that it is an unworkable situation for the smaller barges. Since criteria set by RWS attend to the matter of multiple ship dimensions of the barges, the normative dimension used by DHV is a ship of the CEMT class Va [11].

The dimensions for these barges are:

* LOA:	110 m
* Width of the vessel:	11,4 m
* Loaded draught of the vessel:	4 m

3.2.5 Dimensions of the floating cranes

As stated in chapter 3.2.1 two floating cranes will be used for the lightering of the bulk carrier. There are a number of floating cranes that can be used for the lightering process.
The dimensions of a prominent floating crane (type Hippopotamus) are:

* Crane length:	58 m
* Crane width:	25,6 m
* Crane draught:	3,06 m

3.2.6 Down time conditions for the new basin

Down time conditions should not exceed 5% of the harbor operating time 3.2.1. Important aspects related to the downtime conditions of moored bulk vessels and the cargo handling process are:

1 Down time considering the tugboats berthing the bulk carrier

2 Down time considering the cargo handling equipment (un)loading the carriers

3 Down time considering the movement of the bulk carriers

4 Down time considering the movement of the inland waterway freight vessels

To define the down time conditions the next sections describe the generally obtained conditions considering the vessels dimensioned in chapter 3.2.3. The derived down time limits described in the next sections are commonly used in the design of port facilities and are based on internationally accepted standards and recommendations based on figures provided by PIANC, the port's design handbook and the Spanish standard ROM [42] [36] [35].

3.2.7 Operating limits for tugboats and mooring boats

Due to wind generated or short periodic waves, tugboats have operating limits. Tugboats start to lose efficiency in controlling the mooring operations when encountering a wave climate with significant wave heights of more than 1 to 1.50 meter [42].

3.2.8 Wind restrictions for down time conditions

It is generally recommended that crane equipment used for handling the cargo of carriers will not operate during wind conditions of 20 m/s or higher (Beaufort scale 8) [42]. Moored carriers in the new basin are being lightered by floating cranes. These cranes have to halt their operations during the exceedence of wind conditions mentioned above.

3.2.9 Restrictions on ship movements for moored vessels

Moored ships are continuously in movement due to the impact of current, waves and wind. Ship motions are described by the 6 degrees of freedom (see figure 3.2).

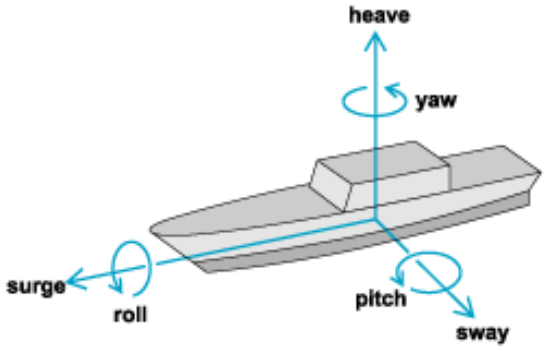

Figure 3.2: The six degrees of free movement for a ship

The movements in the horizontal plane (surge, sway and yaw) are related to the forces in the fenders and mooring systems that tend to counteract the movement or displacement of the ship from its equilibrium position. Movement in the vertical plane (roll, pitch and heave) are the natural movements of a free floating ship.

The wave action is mainly responsible for the unacceptable ship movement and forces in mooring systems. Values of maximum significant wave heights that have generally been assumed as acceptable for ships at berth are shown in Table 3.1 for bulk carriers. The wave heights are not affiliated to a wave period, it is purely stated that when waves exceed these maximum wave heights, it leads to downtime conditions [35]. For the maximum significant wave heights of CEMT Va inland vessels the characteristics of bulk vessels smaller than 30.000 DWT are maintained as reference. These are obtained out of the port designer's handbook [36]. For the Bulk carriers the maximum significant wave heights of bulk carriers with 30.000 - 100.000 DWT is maintained [36].

Table 3.1: Maximum significant wave heights for ships at berth in the new basin (source: Spanish ROM [35])

Type of ship	Limiting wave height at berth Hs (m)
Bulk carrier	0.80 - 1.50
Inland CEMT Va vessel	0.80

Table 3.2 shows the maximum wave heights for (un)loading operations of the bulk carrier. Again the limiting wave height is based on bulk carriers with 30.000 - 100.000 DWT. The table shows significant wave heights for two possible scenarios for incoming wave directions. The maximum wave height is dependent on the angle of the incoming waves.
For berthing the bulk carrier and the inland vessels in the new harbor the limiting significant wave heights will be 0.80 meter.

Table 3.2: Maximum significant wave heights for (un)loading operations of a bulk carrier for different wave directions (source: Spanish ROM [35])

Type of ship	Limiting wave height Hs (m)	
	0°(head on or stern on)	45°- 90°
Dry bulk carrier loading	1.50	1.00
Dry bulk carrier unloading	1.00	0.80

The figures in the two tables can generally be accepted for wave periods up to 10 seconds. For longer periods the figures have to be reduced [35]. Based on experience, PIANC working group 24 [35] states that locally generated waves inside the basin will generally have smaller periods and will therefore have relatively little effect on the moored carriers. For the lightering process of the coal carriers in the new basin the limiting significant wave height will be 0.80 meter.

3.3 Criteria considering bulk carrier resonance

Severe ship movement is not only caused by wave heights of primary waves (as discussed in chapter 3.2.9). Ship movement can also be caused when a ship's natural periods are close to the period of an incoming wave. Independent of the wave height a ship can suffer severe movement if this is the case. Depending on their type, dimensions and loading conditions, all vessels have well defined natural periods. For all six degrees of free ship movement, if one of these natural periods coincides with incoming wave periods, resonance may occur which will considerably increase the vessels swinging motions. It is therefore important to determine these natural periods for the bulk carrier moored in the new basin.

3.3.1 Earlier investigation on large ship resonance periods

The Spanish ROM states that considering the natural periods for heave, pitch and roll motions are usually over 8 seconds for the larger displacement vessels (ships larger than 60 meters), it is the long swell waves which most affect the vertical motions of vessels [35]. The port designer's handbook [36] states that natural periods of large vessels, concerning horizontal movement, would be one minute or more.

The precise natural frequencies for the six degrees of freedom of a ship depend on many ship properties. The study of a ship's natural frequencies needs the help of several mathematical models. Modeling a bulk carrier concerns a very detailed maritime study and is not within the scope of this thesis. However it is important to understand the frequencies of a bulk carrier berthing in the new basin.
To come with first assumptions on resonance frequencies of the bulk carrier, a study has been carried out on existing publications and documents to find examples of ships with similar dimensions as a 200.000 DWT bulk carrier. The natural frequencies of these ships can be taken into account when investigating the wave frequencies present in the outer harbor.

- Van der Molen and Hoes (2009) [39] state that typical natural periods for surge sway and yaw for bulk carriers are around 2 to 3 minutes. Natural periods concerning these three movements for container vessels are around 1 minute. Natural periods for pitch, roll and heave are between 10 and 25 seconds for sea going vessels.

- Van der Molen (2006) [40] has determined that a 60.000 DWT coal carrier with a L_{pp} of 215 meters shows energy peaks in it's surge spectrum at 0.007 and 0.011 Hz (wave periods of 140 and 90 seconds).

- De Bont (2010) [12] has studied a container carrier with a LOA of 294 meters, a width of 32 meters and a draught of 9 meters. The carrier was berthed at a quay wall. The investigation provided energy spectra for surge sway and yaw. Energy peaks for the surge, sway and yaw motion appeared in all three directions for frequencies of 0.004 and 0.01 Hz (wave periods of 100 and 250 seconds).

- Ligteringen (2001) [26] shows that for a 65.000 DWT bulk carrier natural periods for roll appear around 12 seconds.

- Bingham (2000) [8] has investigated the motions of a 72.000 metric ton total displacement LPG carrier with a LOA of 220 meter and a width of 40 meter. The investigation concludes that for surge and sway energy peaks appear around 0.02 Hz (wave period of 50 seconds). For roll peaks arise 0.1 Hz (wave period of 10 seconds), for yaw around 0.03 Hz (wave periods of 33 seconds), for heave around 0.01 Hz (wave period of 100 seconds) and for pitch around 0.07 Hz (wave period of 14 seconds).

When analyzing the results provided in chapter 3.3.1 it can be concluded that most of the outcomes state that ship resonance is caused by long waves of 100 seconds or more. Especially when looking at the movements that can interfere with the mooring system (surge, sway and yaw) wave periods between one and three minutes are causing ship resonance.
However when looking at the vessel types and vessel dimensions little correlation or even a relation can be found between ship dimensions and resonance periods. Appendix B.1 shows the analysis carried out on possible relations for ship dimensions and resonance periods. It is concluded that based on these publications it is hard to predict the resonance frequencies for the 200.000 DWT bulk carrier.

3.3.2 Natural periods of a 200.000 DWT bulk carrier

The results of chapter 3.3.1 do not provide any guidance in determining the resonance periods for a 200.000 DWT bulk carrier. Therefore it is decided to leverage the knowledge of a marine expert.
After a consult with em. prof. dr. ir. Pinkster, the former head of Marine Technology at the TU Delft, it was decided that the best way to approach the resonance frequencies is to model the fully loaded bulk carrier (300 x 45 x 17.80m) for an open water situation for a depth of 20 meters in a DELFRAC model. This is a three dimensional diffraction model specialized in calculating ship resonance. Figure 3.3 shows the dimensions of the modeled bulk carrier in DELFRAC. Bigger images of the modeled ship dimensions are provided in appendix B.2.

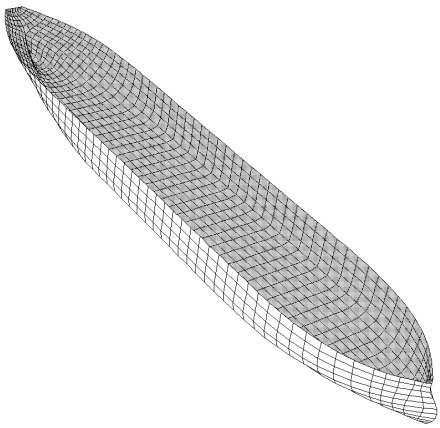

Figure 3.3: The bulk carrier modeled in DELFRAC

The analysis concerns incoming regular waves in different angles for wave periods between 6 and 250 seconds. The incoming wave angles are 0, 30, 60 and 90 degrees concerning the

stern of the vessel.
Mr. Pinkster has provided the data derived out of the DELFRAC model and from these data the Response Amplitude Operators (RAO's) for all six degrees of free motions of the ship have been determined. The RAO's for the surge sway and heave motion will be discussed in this chapter as they are considered to have the most influence on the lightering process [36]. The analysis assumes that the bulk carrier is situated in open water instead of moored at the lightering facility inside the new basin, this implies that the outcomes do not reflect the real situation. However the analysis provides the best data about resonance frequencies available for this investigation.

When looking at the surge movement of the bulk carrier it can be concluded that the highest ship motion concerning surge occurs for the low wave frequencies belonging to wave periods up to 250 seconds (see figure 3.4). This is the case for all incoming wave directions except for waves arriving straight at the stern. This is obvious as these waves arrive perpendicularly to the surge motion of the bulk vessel and therefore cannot influence this motion.
The increase of the surge amplification for wave frequencies approaching zero can be explained by the fact that water particles will move in an elliptical motion for shallow water situations. As the frequency range approaches zero wave lengths will become larger, increasing the the shallow water criteria. The elliptical movement of the water particles will increase in horizontal directions increasing the ship movement in the surge direction. In theory the ship will follow the motion of the long tidal waves on shallow water [14].

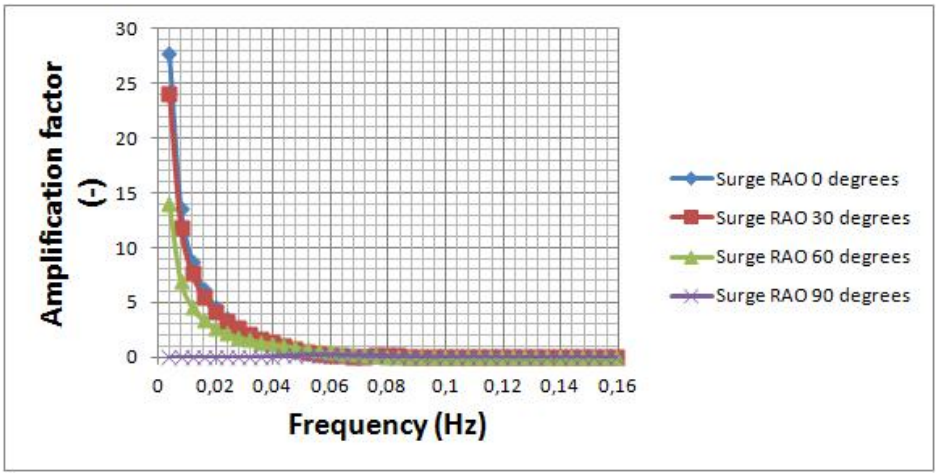

Figure 3.4: RAO results for surge movement of the bulk carrier

When looking at the DELFRAC results for the bulk carrier's sway motion (figure 3.5) it can be concluded that results are identical, only in the opposite incoming wave direction. This is what is expected as the sway movement is perpendicular to surge. Therefore waves arriving perpendicular to the ship (in an angle of 90 degrees) have most effect on the sway motion and as waves arrive in a more parallel direction the effect on the sway motion have less effect on this motion. As is the case for surge motion the low wave frequencies cause the highest ship movement.

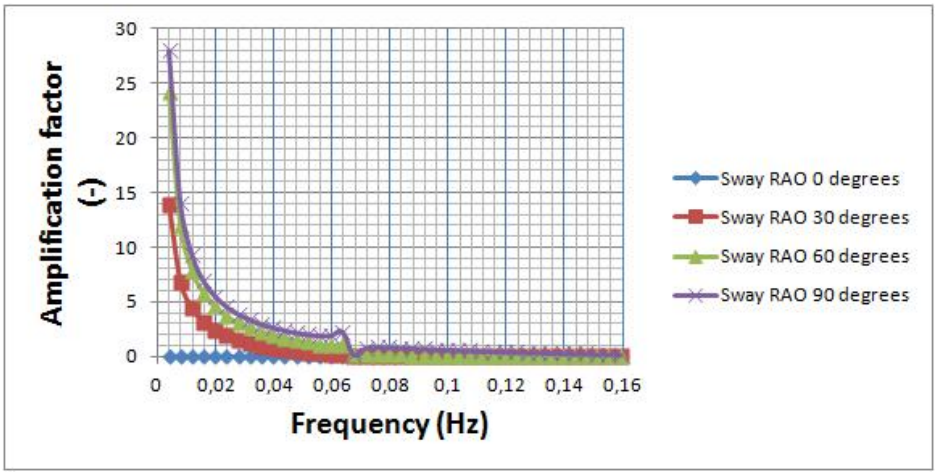

Figure 3.5: RAO for sway movement of the bulk carrier

When looking at the vertical ship movement (figure 3.6 shows the results for heave) it can be seen that peaks for the bulk vessel lie between 14 and 20 seconds.

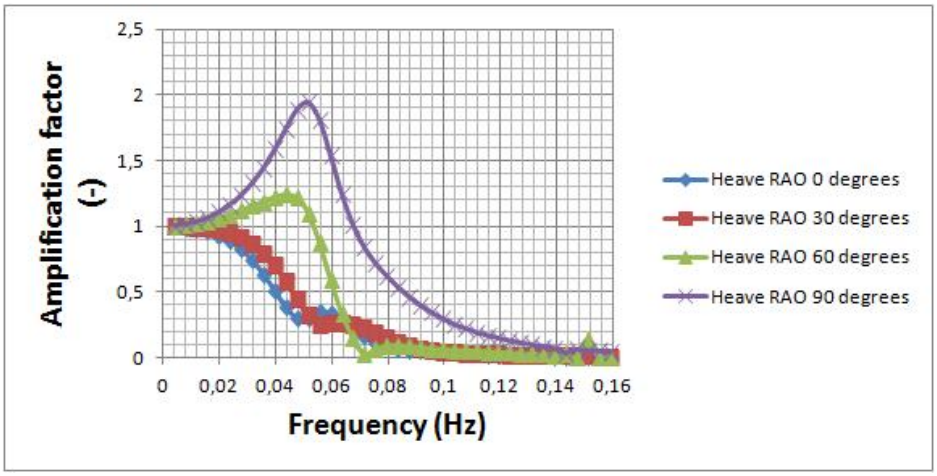

Figure 3.6: RAO for heave movement of the bulk carrier

This complies with the general assumptions that wave periods between 8 and 25 seconds are responsible for vertical ship movement (see chapter 3.3.1). The RAO analysis shows that when the wave frequency approaches zero the amplification of ship heave approaches 1 (see figure 3.6). For very long waves, as explained for the horizontal ship movement, the ship will follow the water particle movement. Therefore the vertical ship movement will be identical

to the wave height belonging to the long wave [14].
The results for the RAO's in all six degrees of free movement for the bulk vessel are added in appendix B.2 and are summarized in table 3.3.

Table 3.3: Resonance periods between 6 and 250 seconds for a 300 meter bulk carrier in open water, considering all six degrees of free movement

Type of movement	Peak value period (sec.)
Surge	250
Sway	250
Yaw	250
Heave	20
Roll	15
Pitch	20

It can be concluded that incoming waves with wave periods of around 250 seconds cause the highest wave amplification concerning horizontal ship movement. However these results are based on a ship in open water. In the new basin ship motions will not reach these high periods as the motions will be damped by the mooring system.
Incoming waves with wave periods between 15 to 20 seconds cause the highest wave amplification concerning the vertical movement of a 300 meter long 200.000 DWT bulk carrier.

3.4 Resonance periods of the IJmuiden harbor basins

Chapter 3.3 demonstrated that a ship will experience resonance if energy peaks arise at wave periods that coincide with the ship resonance periods. However, severe ship movement can also occur if the basin in which the ship is moored experiences resonance due to the incoming wave period. Therefore it has to be analyzed what the resonance periods are concerning the IJmuiden harbor basins.
Appendix C.1 provides an explanation of the phenomenon of basin resonance and how resonance periods can be determined considering the basin geometry.

3.4.1 Resonance periods of the outer harbor basins

For calculating the resonance periods, dimensions used for the length and width of the basins will be implemented conform the criteria mentioned in appendix C.1. Table 3.4 provides the dimensions of all the outer harbor basins.

Table 3.4: Dimensions of the outer harbor basins (m)

Basin name	Basin length (m)	Basin width (m)	Basin depth below NAP (m)
The new basin	360	220	20
The IJmond harbor	394	192	11
The Vissers harbor	1075	130	8
The Haring harbor	668	120	9

With these dimensions several mode standing waves have been calculated that cause resonance in the outer harbor basins. As the emphasis of the study lays on the new basin, this harbor basin will be highlighted first.
The resulting resonance periods for the new basin are shown in table 3.5.

Table 3.5: Table of resonance periods (sec) of the new basin

		basin length		
		1^{st} mode	2^{nd} mode	3^{rd} mode
basin width	0^{th} mode	103	35	21
	1^{st} mode	25	21	17
	2^{nd} mode	14	13	12
	3^{rd} mode	10	10	10

The basin resonance periods appear to have values between 10 and 103 seconds. Incoming wave heights for these given wave periods will amplify in anti nodes inside the new basin. Amplification factors of the incoming waves are unknown in this study and therefore nothing can be said yet about the magnitude of the effect on the moored bulk carrier.
As can be seen in table 3.5, higher mode standing waves will occur for waves with shorter wave lengths and wave periods. The interesting waves are the long waves with long wave periods that cause severe horizontal ship movement. Therefore, only the first mode standing

waves in the harbor basins will be treated in this section. When interesting, higher mode standing waves will be pointed out. For the higher mode standing waves for every separate harbor basin reference is made to appendix C.2. This appendix provides tables concerning the first three modes of standing waves and associated explanations for all harbor basins.

Table 3.6 summarizes the wave periods that cause a first mode standing waves in the different basins situated in the outer harbor.
The IJmuiden harbor NV states that the existing basins do not experience resonance due to incoming waves [27]. It is interesting to investigate the resonance periods of these existing basins. As through the acquired information [27] the assumption arises that these wave periods do not contain enough energy to create basin resonance in the existing outer harbor basins. In chapter 4 the wave climate penetrating the outer harbor is investigated and conclusions can be drawn on this assumption.

Table 3.6: Resonance periods belonging to a first order standing wave in the outer harbor basins (sec)

Basin name	Wave periods for first mode standing waves (sec)
The new basin	103
The IJmond harbor	149
The Vissers harbor	476
The Haring harbor	286

3.4.2 Standing waves between the IJmond harbor and the Averij depot

Thus far analyses have been carried out looking at the harbor basins separately. However, resonance could also occur between two opposing shores or basin ends. An example of this is a standing wave between the end of the IJmond basin and the opposing shore of the Averij depot (see figure 3.7).
Table 3.7 provides the wave periods belonging to the modes of these waves.

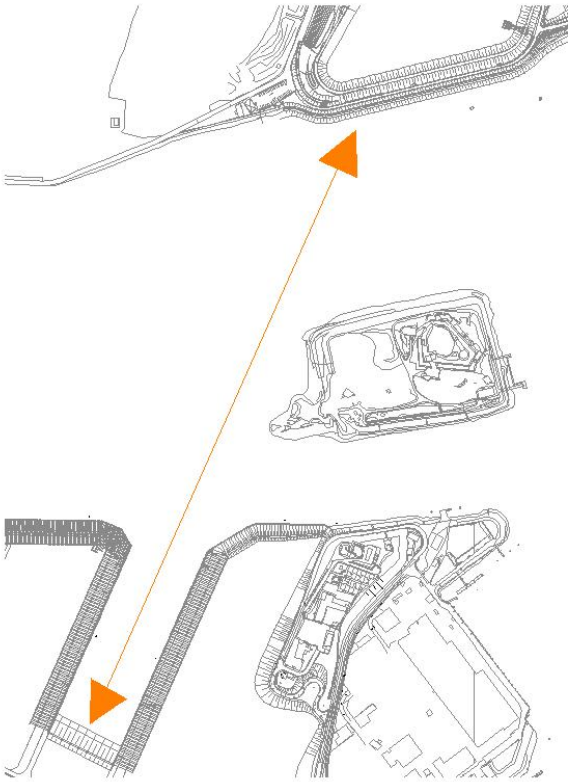

Figure 3.7: Overview of the harbor area between the IJmond harbor and the opposing shore

Table 3.7: Resonance periods (sec) of standing waves between the IJmond harbor and the opposing shore

basin length		
1^{st} mode	2^{nd} mode	3^{rd} mode
185	93	62

According to the IJmuiden harbor NV [27] These periods do not cause problematic situations in the current harbor situation. However, after the new basin is implemented in the outer harbor a new situation can occur concerning harbor basin resonance. A standing wave can arise between the two ends of the IJmond harbor and the new basin. Therefore the wave periods causing standing waves will change because of the shift in length over which the wave can propagate. Table 3.8 provides the wave periods based on the new situation.

Table 3.8: Resonance periods (sec) of standing waves between the IJmond harbor and the new basin

basin length		
1^{st} mode	2^{nd} mode	3^{rd} mode
286	141	89

When looking at the new basin, these wave periods are close to the resonance periods showing the highest horizontal movement amplification of the bulk carrier in open water (see figures 3.4 and 3.5). However the question arises whether these very long bulk carrier natural periods are met as the mooring system will cause damping to the horizontal ship movement.

3.5 Conclusions

RWS states that the total downtime of the new basin may not exceed 5% of the operating time. Downtime of the lightering process occurs when wind conditions are 20 m/s or higher as the cranes cannot handle the cargo safely anymore. This wind condition occurs less than 1% per year (see chapter 2.4).
Down time will also occur when incoming waves have heights higher than 0.80 meter as the ship's vertical movement becomes too large for the unloading process.

Not only wave heights can cause down time, bulk carriers can also experience horizontal and vertical movement when incoming wave periods coincide with the ship's natural periods. The results for these natural periods have been obtained by analyzing a bulk carrier in open water. The results are not representative for the moored ship condition, as the mooring system will strongly damp the ship's movement and questions arise whether the long natural periods can be met. For the bulk carrier in open water results show that wave periods between 10 and 25 seconds are responsible for the highest amplification for vertical ship movement and long wave periods analyzed up to 250 seconds for the horizontal ship movement.

Ship movement may also be triggered by standing waves in the new basin itself. Standing waves can arise between the end of the IJmond harbor and the end of the new basin.

The phenomenon of seiches (discussed in chapter 2.6.2) will not enforce the movement of the bulk carrier as these waves have periods higher than 250 seconds. It is therefore chosen not to study the effect of seiches for the new basin.
As waves with wave periods lower than 10 seconds (typical wind waves) do not affect ship movement and do not cause basin resonance, these waves are also not interesting for the study on severe bulk carrier movement. However it has to be determined whether the locally generated wind waves do not exceed the critical wave height of 0.80 meter inside the new basin as they will then create down time.

Chapter 4

Spectral analyses of the wave climate in the outer harbor

4.1 Introduction

In chapter 3 it is determined that down time conditions of the new basin are caused by specific wave periods. However, until now it is not clear whether these wave periods do arise in the outer harbor. This chapter analyses the wave climate present in the outer harbor to determine which wave periods are present in the outer harbor.

As stated in chapter 2.6.2 there is no long term data available concerning the outer harbor of IJmuiden. However in the recent past RWS has started to obtain wave data from several locations inside the outer harbor.
The provided information on wave action in the outer harbor is split and discussed in two separate sections in this chapter. The first section analyzes the wave data concerning very long waves (wave periods of 50 seconds and higher). As explained in chapter 2.6.2 the actual data is not available for this thesis, however a report created by Deltares and Arcadis [6] provides one dimensional energy spectra derived at certain locations inside the outer harbor. These spectra will be analyzed and compared with the results for basin resonance frequencies derived in chapter 3.4.1. It can then be determined whether the theoretical approach complies with the measured data of the outer harbor. The Alkyon study on seiches in the outer harbor [5] provides information on measured wave heights inside the outer harbor belonging to the long waves. The measured wave heights from this report will also be discussed.

The second section concerns a detailed investigation of AWAC measurements carried out in the outer harbor. The AWACs measure wave periods between 2 and 30 seconds. As the data provided by the AWACs is made available by RWS [37], analyses will be carried out concerning wave spectra, peak wave periods and significant wave heights.

4.2 Wave periods longer than 50 seconds in the outer harbor

4.2.1 Equipment setup and data preparation

Results for the long wave action in the outer harbor have been obtained from a technical report provided by Arcadis and Deltares [6] and the Alkyon report on seiches [5]. For this

research data was obtained from pressure box measurements. These pressure boxes were installed in the IJmond harbor, at the Midden ship lock and in the Vissers harbor. The pressure boxes measured water levels at an interval of 2 Hz. The data has been average over periods of 15 seconds and transferred into continue signals without intervals. All results have been filtered with a high pass Butterworth filter to filter out the astronomical tide [6].
Spectral plots have been derived for eight selected moments in time. These moments have been chosen as the significant wave heights at the three location at those moments were highest in the obtained data.

4.2.2 Long wave spectra for wave periods higher than 50 seconds

For all three locations spectra have been plotted for eight different moments in time between March and June 2010. The spectra only include wave conditions for these specific eight moments and therefore it is pointed out that conclusions drawn from these one dimensional energy spectra could be inaccurate. However these spectra have been chosen as they show the eight moments concerning highest wave action during the four months of measurement. The spectra show a large range of very low frequencies from 0.0001 up to 0.02 Hz (see appendix A.6). Therefore the spectra can be analyzed to see whether the calculated basin resonance frequencies in chapter 3.4.1 comply with the measured data. Unfortunately for long wave measurements (as mentioned in chapter 4.2.1) one dimensional energy spectra have been provided for three locations of which only two are of use for the comparison of measured and calculated basin resonance frequencies. These two locations concern the IJmond harbor and the Vissers harbor. The information obtained from the Midden ship lock pressure box will be analyzed concerning the measured amplified wave heights in the outer harbor. The wave height data will provide information about amplified wave heights present in the outer harbor.
It useful to compare the measured data for these two basins with the theoretical calculations. When the results agree it can be concluded that the approach in chapter 3.4.1 to calculate basin resonance can be approved. Figure 4.1 shows the measured one dimensional energy density spectrum of the IJmond harbor for four moments in time. Spectra considering Both the IJmond harbor and the Vissers harbor for all measured moments are included in appendix A.6.

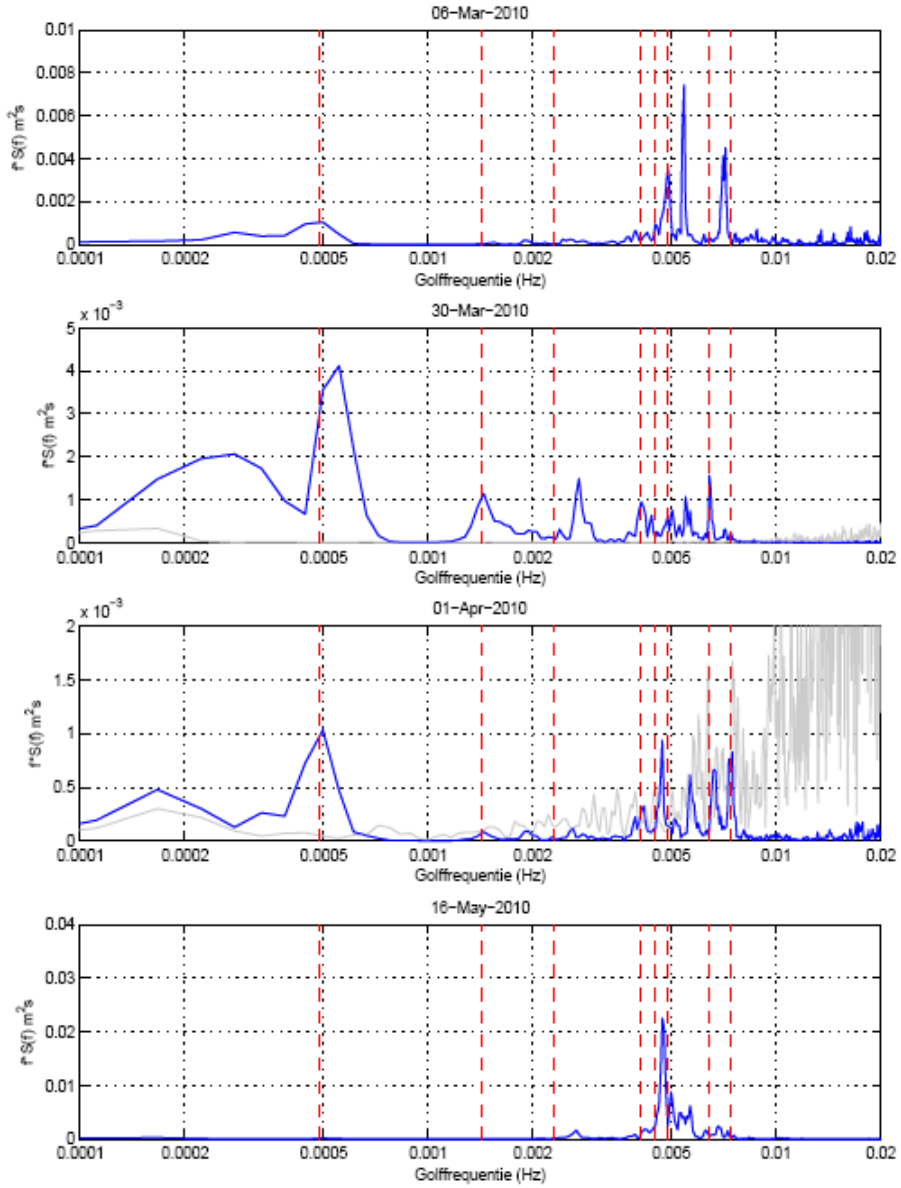

Figure 4.1: One dimensional energy density spectra derived at the IJmond harbor [6]

4.2.3 Measured spectra concerning the IJmond harbor

When looking at figure A.5 and A.6 in appendix A.6, measured energy peaks in the IJmond harbor are displayed for seven moments in time. When looking at the energy spectra it can be stated that energy peaks tend to arise around 0.005 Hz (wave period of 200 seconds) and around 0.007 Hz (wave period of 133 seconds). When these energy peaks are compared to the calculated resonance frequencies in chapter 3.4.1. It can be seen that the calculated first

mode frequency of 0.0066 Hz (a wave period of 151 seconds) is very close to the peak around 0.007 Hz in the measured spectra. It seems that this standing wave does occur in the IJmond harbor.
The measured energy peak around 0.005 Hz (complying with a wave period of 200 seconds) does not comply with any standing wave period concerning the calculated resonance periods for the IJmond harbor (see table C.4 in appendix C.2). However, when looking at table 3.8 this energy peak complies with the calculated wave period of a first mode standing wave between the IJmond harbor and the opposing shore.

4.2.4 Measured spectra concerning the Vissers harbor

When looking at figure A.7 and A.8 in appendix A.6, measured energy peaks in the Vissers harbor are displayed for seven moments in time. When looking at the energy spectra it can be stated that energy peaks tend to arise around 0.002 Hz (wave period of 500 seconds) and around 0.005 Hz (wave period of 200 seconds). When these energy peaks are compared to the calculated resonance period for the Vissers harbor in table 3.6. It can be seen that the calculated first mode standing wave period of 476 seconds is coinciding with the peaks around 0.002 Hz (wave period of 500 seconds) in the measured spectra. It seems that this first mode standing wave occurs in the Vissers harbor.
The measured energy peak around 0.005 Hz (wave period of 200 seconds) does not comply with any standing wave period concerning the Vissers harbor (see table C.6 in appendix C.2). However, if a standing wave between the Vissers harbor and the south east shore of the Fort island could occur it follows from the theory that the first mode of this standing wave would occur at a frequency around 0.005 Hz. This could comply the energy peaks that arise around 0.005 Hz in the measured spectra in figures A.7 and A.8.

4.2.5 Measured amplified wave heights at the end of the outer harbor

The previous chapters demonstrated the presence of energy peaks for long wave periods inside the outer harbor. However nothing is concluded about the amplified wave heights. To determine whether high wave amplification arises in the outer harbor results from the Alkyon report [5] have been analyzed. Although the measured data are limited (a couple of months of measurements) it provides information on amplified wave heights inside the outer harbor. Figure 4.2 shows the measured wave heights for measured wave periods between 2 and 8 minutes. This period band includes the wave periods showing the energy peaks in chapter 4.2.3 and 4.2.4.

Probability of occurrence				Probability of exceedence			
Hs in cm			% Per year	Hs in cm		% of exceeding	Average per year
0	-	1	13.48	> 0		100.00	365 days
1	-	2	62.46	> 1		86.52	316 days
2	-	3	16.42	> 2		24.06	88 days
3	-	4	4.96	> 3		7.64	28 days
4	-	5	1.75	> 4		2.67	10 days
5	-	6	0.73	> 5		0.92	81 days
6	-	7	0.15	> 6		0.19	17 days
7	-	8	0.03	> 7		0.04	4 days
8	-	9	0.02	> 8		0.02	86 min
9	-	10	-	> 9		-	- min
10	-		-	> 10		-	- min

Figure 4.2: Measured amplified wave heights for wave periods between 2 and 8 minutes [5]

The figure indicates that the amount of energy for long waves with wave periods between 2 and 8 minutes will not result high wave amplification in the outer harbor.

4.2.6 Conclusions for wave periods of 50 seconds and higher

When analyzing the spectra considering very long waves it can be concluded that wave periods belonging to energy peaks match the calculated wave periods of first mode standing waves in chapter 3.4 causing resonance in the IJmond and Vissers harbor. It has to be kept in mind that the provided data is very limited and only concerns two basins of the outer harbor.
The IJmuiden harbor NV stated that ships inside the basins do not suffer from basin resonance [27]. This could indicate that although wave periods causing basin resonance show energy peaks in the outer harbor, the energy belonging to these waves is too small to cause wave amplification that interferes the basin operations. This assumption is substantiated by the resulting wave heights for measured long waves obtained from the Alkyon study [5] on wave periods between 2 and 8 minutes.

4.3 Analyzing wave penetration for wave periods up to 30 seconds

In the first section of this chapter it is explained that no data but only results provided by Arcadis and Deltares were available for very long waves inside the outer harbor. For waves up to 30 seconds data obtained from AWAC measurements in November 2010 is available. This data will be analyzed in this section to understand the present wave climate in the outer harbor.

The AWAC setup only measures wave periods between 2 and 30 seconds (this will be explained in chapter 4.3.1), it is concluded in chapter 3.3.2 that important periods concerning horizontal ship movement can be of values up to 200 seconds. However, resonance periods concerning vertical ship movement are in the range of 10 to 25 seconds (see chapter 3.3). Therefore it is important to understand whether waves concerning these periods are present in the outer harbor basins.

4.3.1 Derived data from AWAC measurements

The AWAC setup measures wave height and period using the unique acoustic surface tracking (AST) feature. A short acoustic pulse is transmitted vertically towards the water surface and the time lag between the transmitted ping and its reflection is used to generate a time series of the surface elevation. The AWAC has a measuring frequency of 1 Hz with time intervals of 30 minutes. This measuring time is divided by a current measurement of 720 seconds followed by a wave measurement of 1024 seconds. The remaining time is used for the analysis of the data [28].

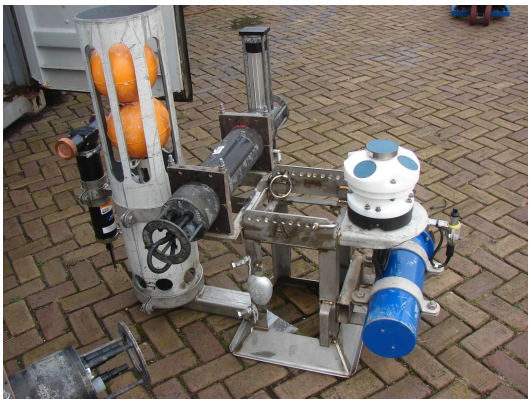

Figure 4.3: AWAC measuring system setup used in the outer harbor (source: RWS [37])

The goal of RWS was to have two permanent AWAC measuring setups located at the northern and southern breakwater ends and to switch one AWAC setup every two weeks between the Averij depot and discharge channel locations. Unfortunately during the first session (Nov - Dec) an error occurred during the data collection at the southern breakwater resulting in a lack of data for that period.
Although the data set is very small to come up with substantiated conclusions it is one the only sources providing information about wave conditions inside the outer harbor. Therefore

the information provided by the AWAC measurements will be analyzed to create better understanding of wave penetration in the outer harbor.
The AWAC measurements provide data about wave conditions at four locations in the outer harbor. Two locations are situated just outside of the northern and southern breakwaters. The other two locations concern a location just in front of the Averij depot and a location in front of the discharge sluice, figure 4.4 shows the exact locations and table 4.1 the coordinates.

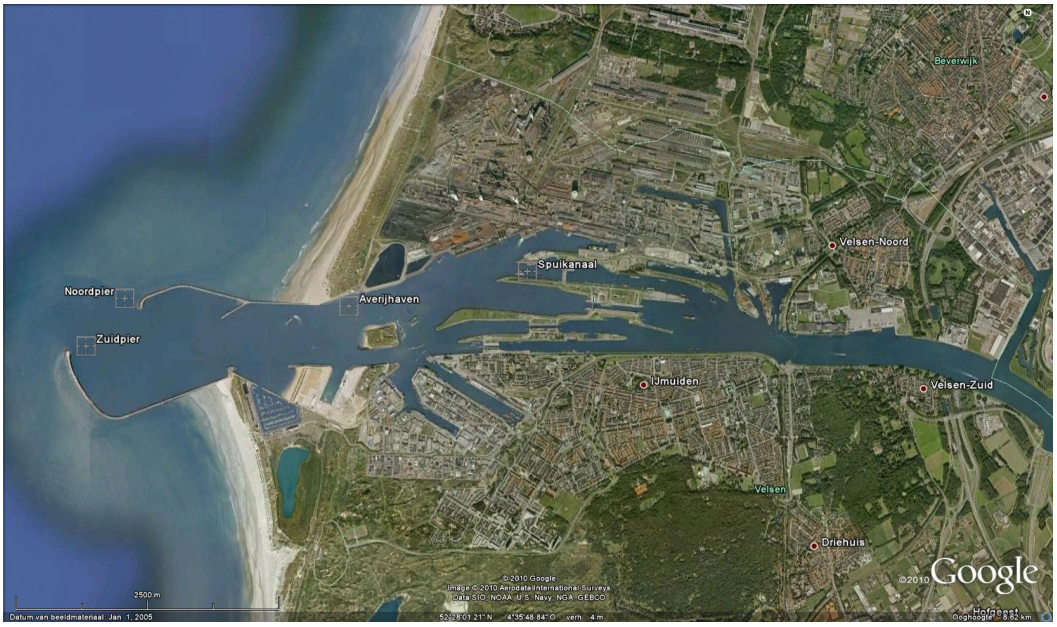

Figure 4.4: Locations of AWAC measurement systems (source: RWS [37])

Location	Latitude	Longitude	Depth (m)	Period
Northern breakwater	5228'05.7463	432'25.3044	-9.77	8 Nov - 8 Dec, 20 Dec - 17 Febr
Southern breakwater	5227'51.1438	432'05.8774	-16.95	8 Dec - 11 Febr
Averij depot	5228'03.4307	434'18.0881	-17.52	8 Nov - 26 Nov, 16 Dec - 19 Jan
Discharge channel	5228'14.1057	435'48.4911	-10.92	26 Nov - 13 Dec, 19 Jan - 17 Febr

Table 4.1: Coordinates of measure locations (source: RWS [37])

The AWAC setup outside the breakwaters were permanently installed for November and December, for the two locations inside the harbor the AWAC setup was moved every two weeks.
Every 30 minutes the AWAC provides a one dimensional wave spectrum with a complying significant wave height and peak wave period concerning a frequency band between 0.03 and 0.49 Hz (wave periods of 2 to 30 seconds). RWS has made a distinction between swell and wind waves for every spectrum. Data between the range of 0.03 and 0.1 Hz (wave periods of 10 to 30 seconds) have been labeled as swell, data obtained for the frequency range between 0.1 and 0.49 Hz (wave periods of 2 to 10 seconds) have been categorized as wind waves. In the following chapters it will be analyzed what happens to the waves during the travel from the sea towards the outer harbor. It has been chosen to use the data from the AWAC

locations of the setup just outside the northern breakwater and the setup in front of the Averij depot. The reason that data obtained at the southern breakwater is not chosen is that this data is incomplete due to errors during the measurements. The data obtained at the location just in front of the Averij depot can give good insights in wave periods and wave heights that could penetrate the new basin.
The data from these two locations can be compared to create an understanding of the wave propagation into the outer harbor. During the measurements a storm occurred the 12^{th} of November, data from the storm will be analyzed separately to investigate whether different wave conditions occur.

4.4 Analyzing wave spectra

The AWAC measurements provide spectra for every 30 minutes. It is not useful to create an average spectrum out of all these separate spectra. Therefore it has to be determined whether the spectra correlate with each other before conclusions can be drawn.

4.4.1 Spectra at the northern breakwater

As every 30 minutes a spectrum is generated, the collection of these spectra measured in November 2010 (Appendix D shows these figures) does not provide a clear view of the energy distribution over the wave frequencies. To get a better understanding of the representative wave spectrum, a distinction between the spectra measured during the 12 November storm and normal conditions is made for the measurements. For both the storm as the normal conditions a single spectrum representative for the entire database of spectra has been chosen for the analysis.

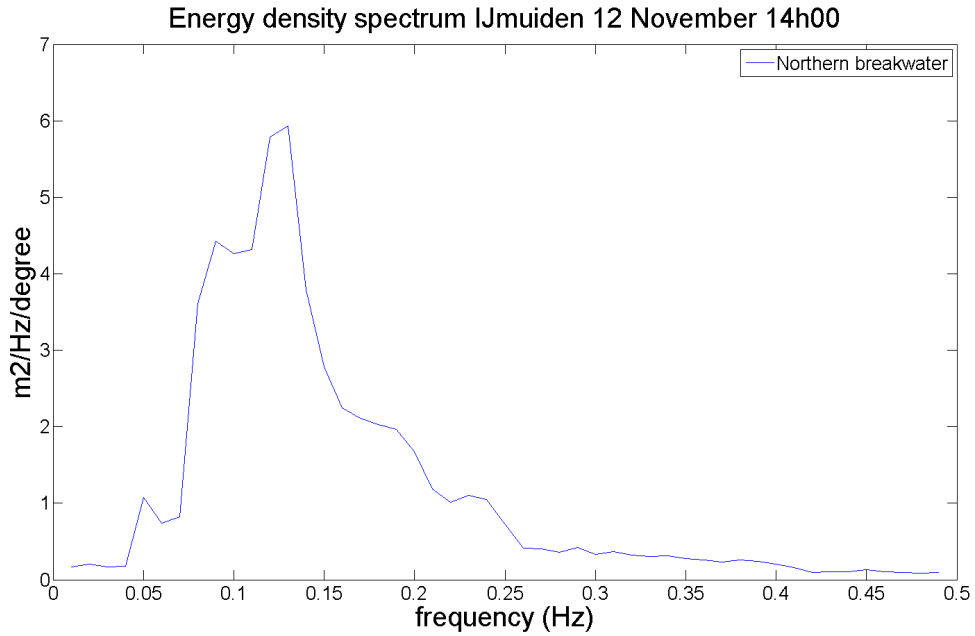

Figure 4.5: One dimensional energy density spectrum measured during the 12 November storm

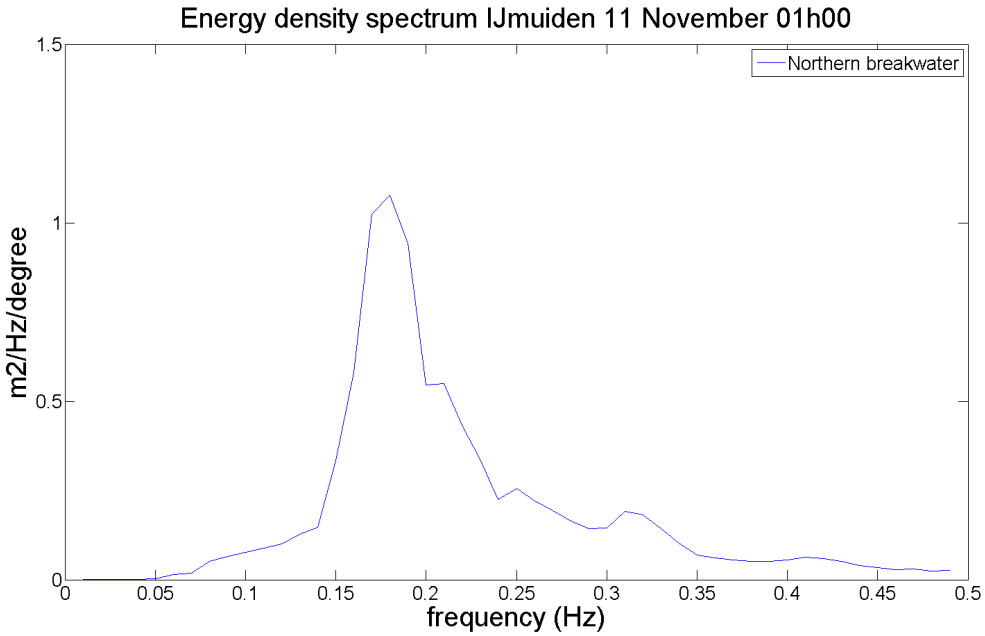

Figure 4.6: One dimensional energy density spectrum measured during November, not including the 12 November storm

It can be seen in figure 4.5 that the majority of the energy arises for frequencies between 0.05 and 0.015 Hz (wave periods between 7 and 20 seconds) during the storm. When looking at figure 4.6 (data obtained during normal conditions) it can be seen that the energy peak values decrease significantly for all frequencies. The energy peak shifts towards shorter waves in the frequency range of 0.15 to 0.20 Hz (wave periods of 5 to 7 seconds), which are typical frequencies concerning wind waves. Although energy peaks shift to higher wave frequencies, an amount of energy is present for normal conditions between 0.05 and 0.1 Hz (wave period between 10 and 20 seconds).

4.4.2 Spectra at the Averij depot

The data derived at the Averij depot have been treated similarly as at the northern breakwater to obtain a single spectrum for the storm condition and the normal condition. The two spectra are shown in figures 4.7 and 4.8, the entire collection of measured spectra at the Averij depot is shown in Appendix D.

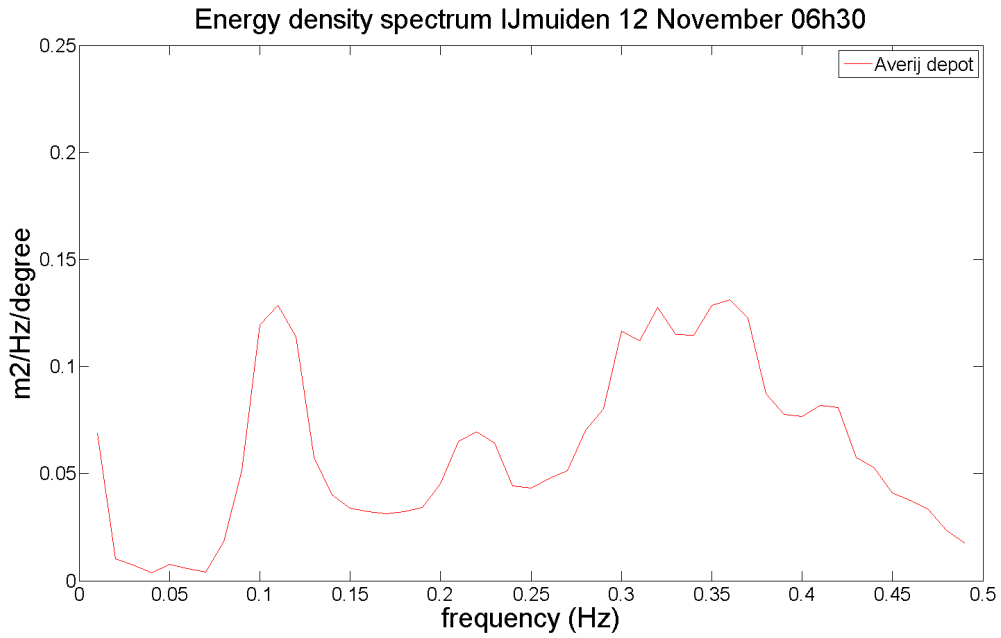

Figure 4.7: One dimensional energy density spectrum measured during the 12 November storm

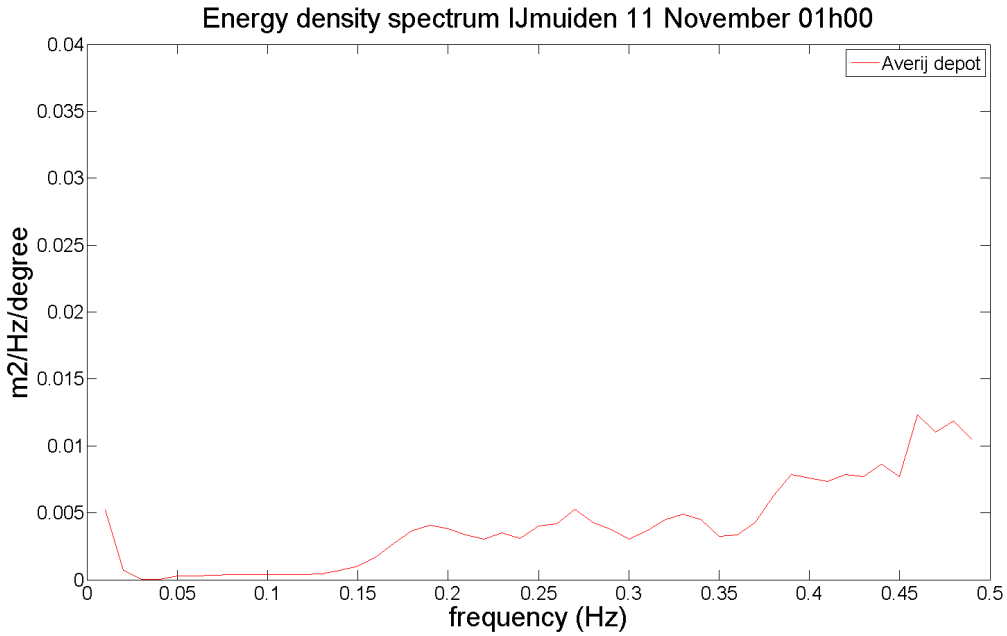

Figure 4.8: One dimensional energy density spectrum measured during November, not including the 12 November storm

When looking at both spectra it can be stated that the energy peaks are situated at typical wind wave frequencies. Inside the outer harbor the emphasis of the wave climate can be put on the presence of wind waves. However during storm condition a significant peak arises around 0.1 Hz inside the basin. To determine whether this peak arises all the time or only during certain events, the same distinction between the storm and the remaining spectra is made as for the data obtained at the northern breakwater. It can clearly be seen when looking at figure 4.7 and 4.8 that the peak around 0.1 Hz arises during the 12 November storm. This indicates that during the storm long waves penetrate the outer harbor. When looking at figure 4.8, representative for calm weather conditions, it can be concluded that the penetration of long waves into the outer harbor is not occurring during the rest of the time. When looking at the wave energy in general it can be stated that peak values have shifted towards higher frequency values in comparison to the measured data at the northern breakwater. It appears that the wave energy at the higher frequencies in the outer harbor is created by the generation of local wind waves.

4.4.3 Conclusions

Just outside the outer harbor high energy peaks arise for waves between 7 to 14 seconds. The majority of these peaks is caused by the 12 November storm. During calm weather conditions energy peaks shift to higher wave frequencies, however energy remains visible for waves with periods around 10 seconds. When looking at the wave energy inside the outer harbor, a shift of energy can be observed towards higher wave frequencies with peak values around a wave period of 3 seconds.
Energy levels have decreased significantly inside the outer harbor pointing out that wave energy is dissipated through the course of penetrating the outer harbor. Although there is a clear shift in energy peaks inside the outer harbor an energy peak still arises during the 12

November storm around 0.1 Hz. This indicates that during the storm a percentage of long waves does penetrate the outer harbor.

4.5 Analyzing wave periods

4.5.1 Scatter plots of the peak periods

From the one dimensional wave spectra peak periods of the waves have been derived. To get a better understanding of the incoming wave periods in the outer harbor these plots have been created to look at the relation between the wave periods that are measured just outside and inside the harbor. The results are obtained out of the one dimensional energy spectra and will therefore provide the same outcomes, however when visualizing the wave periods as a scatter plot a better idea is obtained of the relation between wave periods outside and inside the outer harbor.

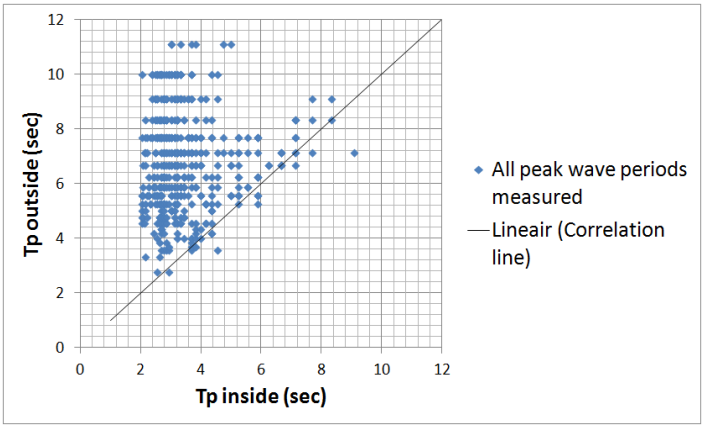

Figure 4.9: Relation between peak periods measured in November at the northern breakwater (y axis) versus the Averij depot (x axis)

Figure 4.9 shows the relation between all the measured peak periods inside and outside the outer harbor. It can be seen that the majority of the peak periods have higher values for the outside measurements compared to the measurements inside the outer harbor. This again indicates that wave periods from outside the harbor do not propagate into the harbor very frequently. However a number of data points do show correlation in the graph. These are the data points situated on and near the $x = y$ line in the graph. To determine whether this correlation of peak periods is inherent to certain weather conditions the seperation of the storm and the calm weather conditions is carried out again.

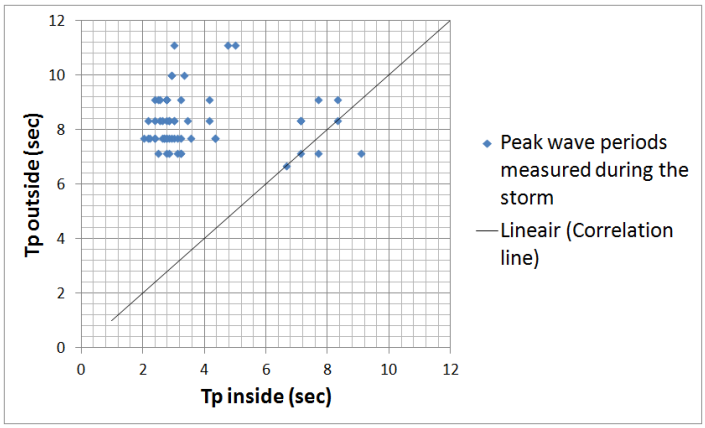

Figure 4.10: Relation between peak periods measured during the storm at the northern breakwater (y axis) versus the Averij depot (x axis)

Figure 4.10 shows the data concerning the 12 November storm. The graph shows two clouds of data points. The first cloud shows a group of peak periods between 7 and 11 seconds that are present at the northern breakwater while inside the harbor waves were measured with peak periods that are significantly lower. The second cloud shows a group of peak periods around 7 to 9 seconds that shows correlation for waves outside and inside the outer harbor. This is the cloud that corresponds with the energy peak at 0.1 Hz, derived in chapter 4.4.2.

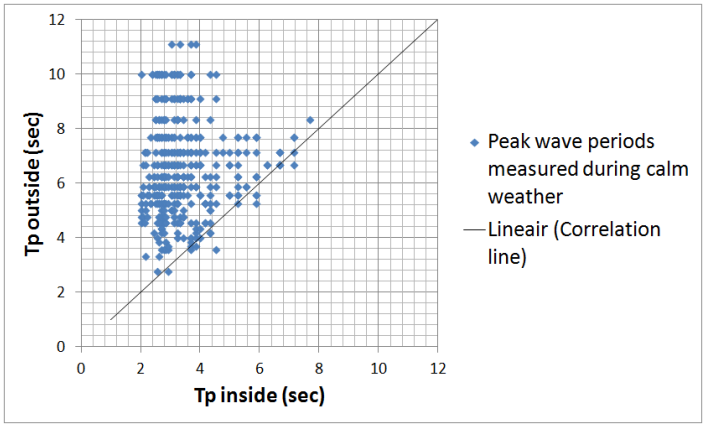

Figure 4.11: Relation between peak periods measured during calm weather at the northern breakwater (y axis) versus the Averij depot (x axis)

However, when looking at figure 4.11 it can be seen that during calm weather conditions, despite of the large cloud showing no correlation between the two measurement locations, correlation can also be found between the peak periods for several data points between 3 and 8 seconds. Since the majority of these data points concern short wave periods it is assumed that these waves are being generated at the two locations at the same time. Still, figure 4.11 shows that even during calm weather conditions waves with peak periods around 7 and 8 seconds do show correlation for some data points, indicating that wave penetration occurs during calm weather conditions.

4.5.2 Conclusion

When looking at the graphs showing the peak periods at the northern breakwater and near the Averij depot it can be concluded that the wave periods measured at the northern breakwater do not show a lot of correlation. This suggests that only a small percentage of waves penetrate the outer harbor. However, during the storm a cloud of data appears around the peak periods of 7 to 9 seconds that shows correlation for the data obtained at the two locations. This indicates that during storm conditions wave penetration of the outer harbor increases.

4.6 Analyzing wave heights

Apart from incoming wave frequencies it is important to understand what the wave height of incoming waves is in the outer harbor. As stated in chapter 3.2.9, ships could suffer downtime due to high waves that appear in the outer harbor. It is therefore important to determine whether high waves from the North sea can easily penetrate the outer harbor.

4.6.1 Waves offshore

Offshore waves have been measured at the Ammunition depot 30 kilometers offshore and at a wave pole located just in front of the outer harbor. The exact locations have been shown in appendix A.1. When the data of the ammunition depot and the wave pole are compared for the same wave period, it shows that waves arriving from the direction south west to west (210 - 270 degrees) have similar wave heights for both locations. However, when looking at waves coming from west to north west direction (270 - 330 degrees) it can be seen that waves at the ammunition dump are 12% higher than waves measured at the wave pole. This indicates that wave heights are not strongly reduced between the two measurement points (see figures 4.12 and 4.13)

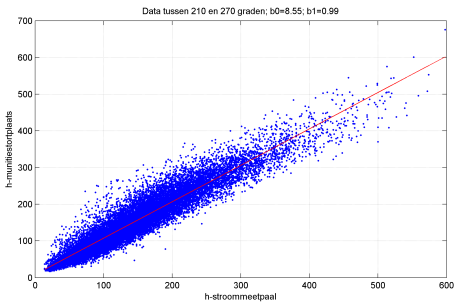

Figure 4.12: Comparison of significant wave heights at the ammunition depot vs the wave pole at IJmuiden. Waves are arriving under 210 - 270 degrees. (source: DHV [22])

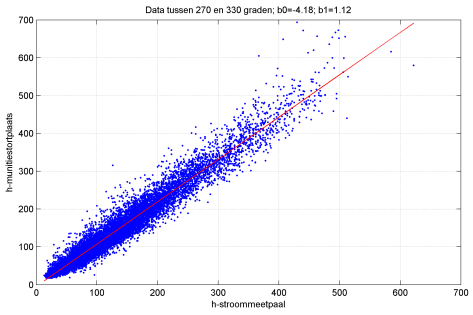

Figure 4.13: Comparison of significant wave heights at the ammunition depot vs the wave pole at IJmuiden. Waves are arriving under 270 - 330 degrees. (source: DHV [22])

There are no statistics available about extreme wave height conditions at the two offshore measurement points. DHV has carried out an extreme wave height analysis for the sea at IJmuiden which concluded that the 1/1 year probability of occurrence wave has a wave height of 5 meter. This matches the statistics of extreme wave heights in the proximity of IJmuiden,

presented in the HR2006. Both graphs are added in appendix A.5 It has to be taken into account that this is an approximation.

4.6.2 Scatter plots of the significant wave heights

To see whether there is correlation between the waves inside and outside the harbor, data obtained from the AWAC measurements has been analyzed for November 2010. Figure 4.14 shows the results of the relation for waves measured outside and inside the harbor.

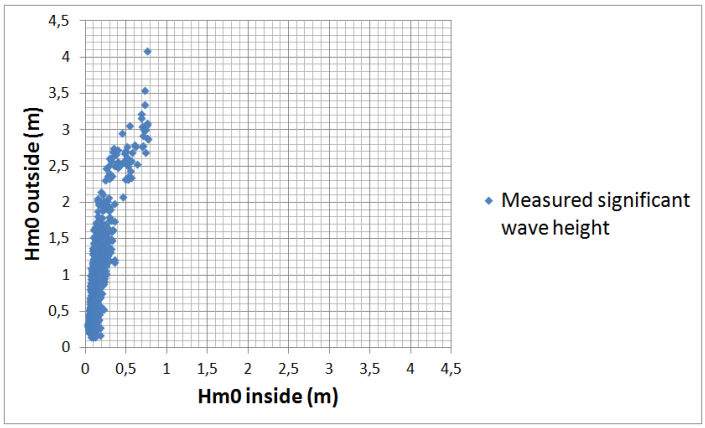

Figure 4.14: Relation between the significant wave height (m) measured in November 2010 at the northern breakwater (y axis) versus the Averij depot (x axis)

Figure 4.14 clearly shows that there is no correlation between wave heights outside and inside the outer harbor. To understand the wave relation during extreme conditions, the wave data derived during the storm have been separately plotted another time in figure 4.15.

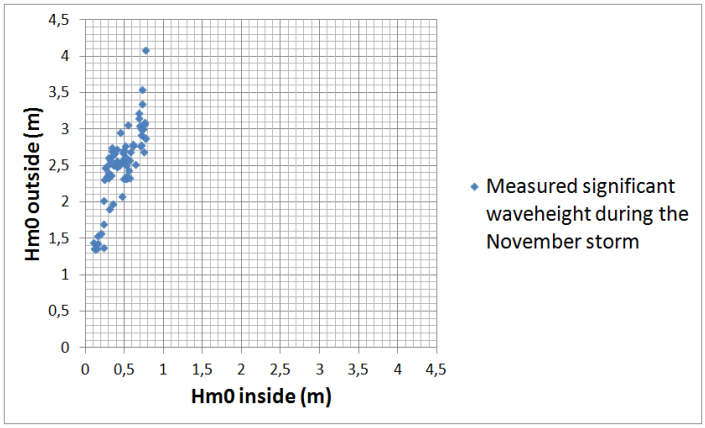

Figure 4.15: Relation between the significant wave height (m) measured during the November storm at the northern breakwater (y axis) versus the Averij depot (x axis)

As could be expected the highest measured wave heights in figure 4.14 were measured during this storm. For the highest measured wave of 4.1 meter outside the northern breakwater, the wave height inside the harbor does not exceed the critical down time condition criteria of 0.80 meters (see downtime criteria in chapter 3.2.9). However a number of measured wave

heights inside the outer harbor does approach this value.
The two figures showing the relation between the wave heights inside and outside the harbor do indicate that wave height of waves penetrating the harbor is strongly reduced. It could also be that the resulting wave height of waves penetrating the outer harbor is even that small that the wave setup inside the outer harbor is primarily caused by locally generated wind waves and that wave heights of primary waves will not cause down time to the lighter process. This will be further analyzed in chapter 4.6.3.

4.6.3 Scatter plots of the swell waves

In chapter 4.6.2 it is analyzed that waves measured in the outer harbor have a significant wave height that is much smaller then wave heights measured at the northern breakwater. However wave heights of 0.77 meters [29] are measured inside the outer harbor close to the new basin. In the analyses carried out it is not defined whether the waves measured inside the outer harbor are locally generated or have penetrated the harbor from outside. When looking at the spectra measured in the outer harbor during the storm (see figure 4.7) it was stated that energy peaks arise around 0.1 Hz during the November storm. It is important to define what part of the measured wave inside the harbor during this storm condition is related to the incoming longer waves. It is explained in chapter 4.3.1 that the AWACs make distinction between swell and wind waves. Therefore it is possible to filter out the waves measured for wave periods of 10 to 30 seconds at the measurement locations. Figure 4.16 shows the relation between swell waves measured outside and inside the outer harbor.

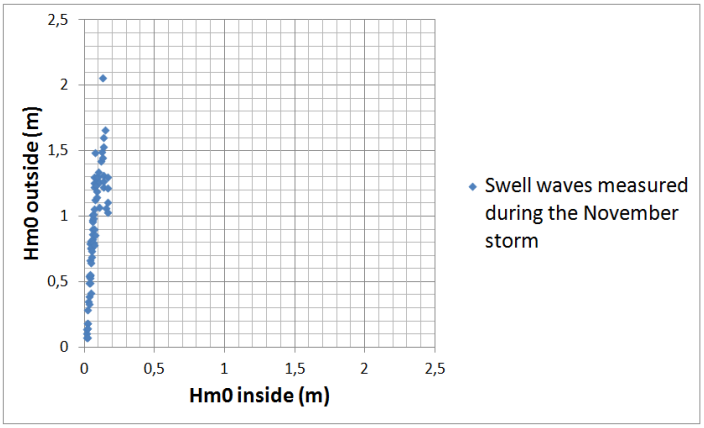

Figure 4.16: Relation between the significant wave height (m) measured during the November storm at the northern breakwater (y axis) versus the Averij depot (x axis)

The contribution of swell (maximum Hm0 of 0.17 meter) is little to the total Hm0 measured inside the harbor (maximum Hm0 of 0.77 meter, see figure 4.15), indicating that the majority of the total significant wave height measured inside the outer harbor is created by locally generated wind waves. This enforces the conclusion that the wave height of penetrating waves in the outer harbor is very small and the majority of the wave height of waves present in the outer harbor is accounted for by the locally generated wind waves.

As stated in chapter 4.6.2 the measured value of 0.77 meter is close to the critical wave height of 0.80 meter. To determine the probability of occurrence of this wave height a numerical wave model study performed by DHV on local wave generation in the outer harbor

is investigated [20].
As this study purely looks at wind generated waves, the contribution of wind waves measured by the AWAC will be evaluated instead of the total significant wave height of 0.77 meter. The significant wave height of the wind wave contribution to the total significant wave height is 0.75 meter [29]. As can be seen in table 4.2 [20] the maximum calculated significant wave height with a return period of 1/1 year is 0.7 meter at a location close to the new basin.

Wind direction (°)	Modeled Hs for wind wave (m)
210	0.6
240	0.7
270	0.7
300	0.5
330	0.4

Table 4.2: Modeled significant wave heights over different wind directions for locally generated wind waves with a return period of 1/1 year [20]

To understand the probability of occurrence of a 0.75 meter wave height it can be referred to the result of the return periods of a 0.7 meter wave height. As the return period of a 0.7 meter wave height is once per year, it can be concluded that the chance of a 0.75 meter wave height occurring in the basin will be smaller.
A total down time of 5% per year is allowed 3.2.1, the contribution of local generated wind-waves to the 5% down time per year is less then 1/365. This is less than 0.3% of the total 5% which amounts to a percentage of 6% of the total downtime.
When comparing this 0.3% contribution to the down time contribution caused by wind (see 2.4) it can be seen that wind contribution (1% per year) is far more dominant than the locally generated wind waves. It can be concluded that locally generated wind waves are not the most important component in the contribution to down time of the new basin. Especially as it may be assumed that strong wind conditions are responsible for the 1/1 year wind wave occurrence. Therefore the 0.3% contribution of wind waves may fall under the 1% contribution of wind to the down time conditions of the new basin.
It should be taken in mind that although wind waves alone do not contribute severely to down time conditions, a combination of wind waves with basin resonance could.

4.6.4 Conclusion

It can be concluded that significant wave heights outside the outer harbor are much higher than inside the outer harbor. When looking at the waves inside the outer harbor, the majority of the wave height is created by locally generated wind waves. As these waves have peak periods shorter than 10 seconds the wind waves do not cause severe ship movement to a moored bulk carrier.

4.7 Relation between peak wave periods for given wave heights

Wave peak periods and significant wave heights have been analyzed separately from each other for the outer harbor. It has been concluded that wave peak periods show little correlation inside and outside the outer harbor. However in some cases correlation is present. Therefore an analysis is carried out to see whether there is a relation between the correlation of wave periods outside and inside the outer harbor in combination with certain measured significant wave heights measured at the northern breakwater. This could provide extra information about certain moments that wave penetration occurs more strongly than during other moments.

4.7.1 Scatter plots of peak periods concerning certain significant wave heights

		Tp (sec)							
		2,0 to 4,0	4,1 to 6,0	6,1 to 8,0	8,1 to 10,0	10,1 to 12,0	12,1 to 14,0	14,1 to 16,0	16,1 to 18,0
Hm0 (m)	0 to 0,2	0,0%	0,7%	0,1%	0,3%	0,4%	0,0%	0,0%	0,0%
	0,2 to 0,4	0,7%	7,0%	4,2%	5,4%	3,0%	0,0%	0,0%	0,0%
	0,4 to 0,6	2,3%	9,3%	4,1%	5,6%	6,3%	1,0%	0,3%	0,7%
	0,6 to 0,8	2,3%	8,3%	2,5%	3,1%	5,2%	2,5%	0,0%	0,1%
	0,8 to 1,0	0,3%	6,1%	7,4%	2,1%	2,4%	0,8%	0,0%	0,0%
	1,0 to 1,2	0,0%	5,9%	7,8%	0,2%	0,2%	0,0%	0,0%	0,0%
	1,2 to 1,4	0,0%	5,1%	5,3%	0,1%	0,0%	0,0%	0,0%	0,0%
	1,4 to 1,6	0,0%	1,4%	2,4%	0,1%	0,0%	0,0%	0,0%	0,0%
	1,6 to 1,8	0,0%	0,9%	2,2%	0,0%	0,0%	0,0%	0,0%	0,0%
	1,8 to 2,0	0,0%	0,0%	1,8%	0,2%	0,0%	0,0%	0,0%	0,0%
	2,0 to 2,2	0,0%	0,0%	0,8%	0,2%	0,0%	0,0%	0,0%	0,0%
	2,2 to 2,4	0,0%	0,0%	0,8%	0,6%	0,0%	0,0%	0,0%	0,0%
	2,4 to 2,6	0,0%	0,0%	0,4%	0,8%	0,2%	0,0%	0,0%	0,0%
	2,6 to 3,0	0,0%	0,0%	1,0%	0,8%	0,3%	0,0%	0,0%	0,0%
	3,0 to 4,0	0,0%	0,0%	0,3%	0,4%	0,1%	0,0%	0,0%	0,0%
	4,0 to 6,0	0,0%	0,0%	0,1%	0,0%	0,0%	0,0%	0,0%	0,0%
	higher than 6,0	0,0%	0,0%	0,0%	0,0%	0,0%	0,0%	0,0%	0,0%

x > 5%
2,5< x < 5%

Figure 4.17: Scatter plot table showing the distribution of significant wave heights (m) over the peak periods measured at the northern breakwater

		Tp (sec)							
		2,0 to 4,0	4,1 to 6,0	6,1 to 8,0	8,1 to 10,0	10,1 to 12,0	12,1 to 14,0	14,1 to 16,0	16,1 to 18,0
Hm0 (m)	0 tot 0.1	13,3%	2,4%	0,0%	0,0%	0,0%	0,0%	0,0%	0,0%
	0.1 tot 0.2	27,8%	5,5%	2,2%	0,2%	0,0%	0,0%	0,0%	0,0%
	0.2 tot 0.3	10,3%	3,0%	0,6%	0,2%	0,0%	0,0%	0,0%	0,0%
	0.3 tot 0.4	13,5%	1,0%	0,2%	0,2%	0,0%	0,0%	0,0%	0,0%
	0.4 tot 0.5	1,3%	0,3%	0,0%	0,2%	0,0%	0,0%	0,0%	0,0%
	0.5 tot 0.6	2,1%	0,0%	0,0%	0,0%	0,0%	0,0%	0,0%	0,0%
	0.6 tot 0.7	13,6%	0,0%	0,0%	0,0%	0,0%	0,0%	0,0%	0,0%
	0.7 tot 0.8	2,1%	0,2%	0,0%	0,0%	0,0%	0,0%	0,0%	0,0%

x > 5%
2,5< x < 5%

Figure 4.18: Scatter plot table showing the distribution of significant wave heights (m) over the peak periods measured at the Averij depot

Figures 4.17 and 4.18 show the distribution of significant wave heights over the measured peak frequencies for both measurement locations. It can be seen that as concluded in the previous paragraphs the gravity of the wave action lies between 4 and 12 second wave periods at the northern breakwater. This high distribution cloud (the dark green colored cells) shifts

to the wave periods between 2 to 4 seconds at the location just outside the Averij depot. In figure 4.18 it can be seen that for wave periods between 8 and 10 seconds waves have been measured inside the outer harbor. This corresponds with the measured and correlating wave data during the November storm inside the outer harbor (see chapter 4.5.1).
To determine the relation between wave periods outside and inside the outer harbor, scatter plots have been created for given significant wave heights measured at the northern breakwater. Figure 4.19 to figure 4.24 on the next page show these plots.

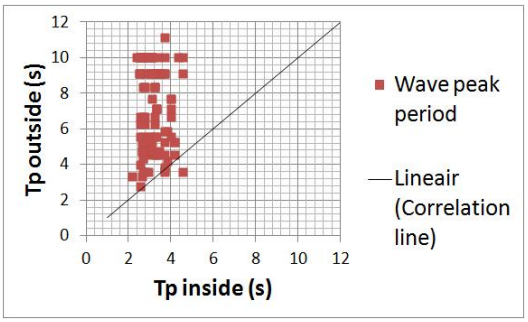

Figure 4.19: Relation between peak periods measured in November at the northern breakwater (y axis) versus the Averij depot (x axis), H_{m0} 0 - 0.5 meter

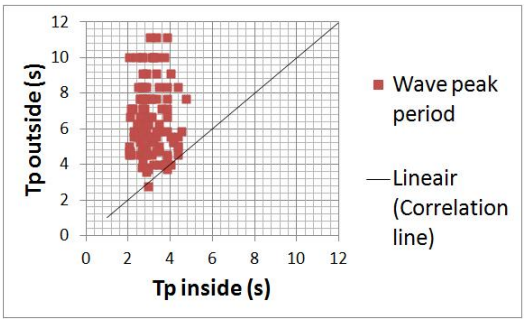

Figure 4.20: Relation between peak periods measured in November at the northern breakwater (y axis) versus the Averij depot (x axis), H_{m0} 0.5 - 1.0 meter

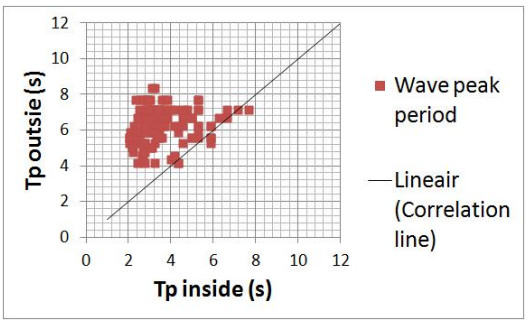

Figure 4.21: Relation between peak periods measured in November at the northern breakwater (y axis) versus the Averij depot (x axis), H_{m0} 1.0 - 1.5 meter

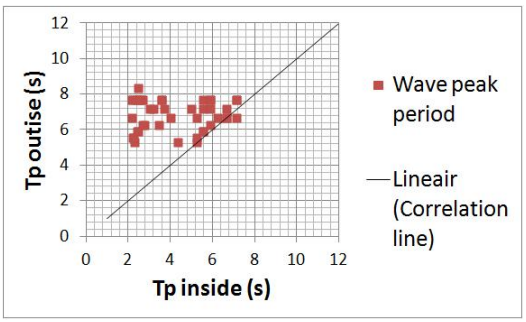

Figure 4.22: Relation between peak periods measured in November at the northern breakwater (y axis) versus the Averij depot (x axis), H_{m0} 1.5 - 2.0 meter

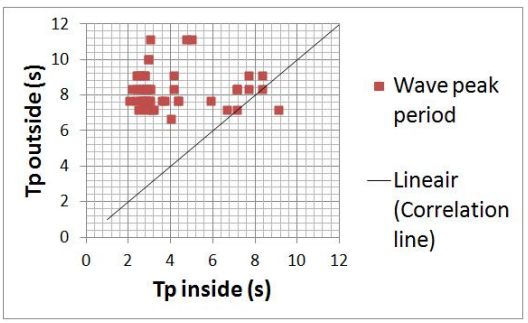

Figure 4.23: Relation between peak periods measured in November at the northern breakwater (y axis) versus the Averij depot (x axis), H_{m0} 2.0 - 3.0 meter

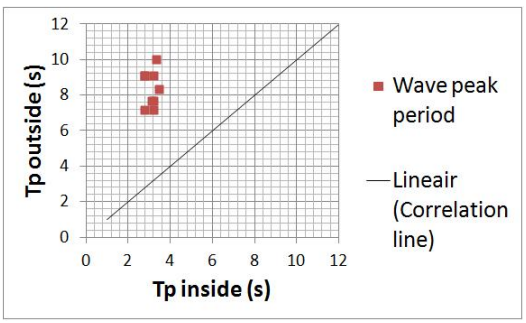

Figure 4.24: Relation between peak periods measured in November at the northern breakwater (y axis) versus the Averij depot (x axis), H_{m0} ¿ 3.0 meter

It can be seen that for significant waves heights up to 1 meter (see figures 4.19 and 4.20) at the northern breakwater the measured peak periods inside are much smaller than outside. There is correlation for peak periods between 2 and 4 seconds. As wind conditions for both locations can be assumed similar (only a few hundreds meters distance between the

two locations) it can be stated that this correlation indicates the local generation of waves outside as well as inside the harbor at the same time by the wind.
When waves heights at the northern breakwater increase (see figures 4.21 to 4.23) it can be seen that two clouds of data points start to appear in the graphs. It can be stated that in all three graphs the left cloud of data points can be explained by the generation of local wind waves inside the harbor, while part of the longer waves measured at the northern breakwater do not penetrate the outer harbor. The right cloud of data points show the larger wave periods (between 6 to 9 seconds) that do penetrate the outer harbor. This conclusion confirms the energy peaks that arise around 0.1 Hz at the northern breakwater at the same time as at the Averij depot described in chapter 4.4.
Figure 4.24 however does not show this correlation for longer waves anymore while it would be expected that for the largest waves the distribution between the two data clouds would be the most obvious. After analyzing the data it appeared that the disappearance of this right data cloud is due to the fact that during the top of the storm the AWAC setup at the northern breakwater stopped measuring peak periods. The reason for this is unclear. To check whether indeed this is just a measurement flaw the one dimensional spectrum at the Averij depot, only concerning significant wave heights higher than 3 meter measured at the northern breakwater, has been derived and shown in figure 4.25.

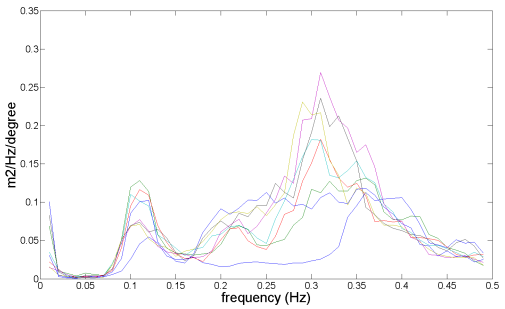

Figure 4.25: Spectra measured at the Averij depot for significant wave heights above 3 meter measured at the northern breakwater

The figure indicates the same energy peak around 0.1 Hz as the other derived spectra at the Averij depot during the storm (see chapter 4.4.2). This confirms that the lack of data at the correlation line around 8 seconds is indeed a measurement flaw for the wave peak periods for waves higher than 3 meter. Figure 4.25 indicates that the pattern of two clouds of data shown in figures 4.21 to 4.23 will have to be the same for waves higher than 3 meter at the northern breakwater.

4.7.2 Conclusion

The scatter plots enforce the conclusions derived in the previous chapters that locally generated waves are normative for the wave climate inside the outer harbor. The plots showing relations for peak periods for waves measured outside and inside the outer harbor, separated for different significant wave heights, show that wave penetration for waves between 6 to 9 seconds occurs for significant wave heights of 1 meter or higher. These wave heights occurred during the November storm. The analysis concludes that wave penetration of these waves does not occur during normal weather conditions but occurs during conditions as a storm.

4.8 Conclusions concerning the AWAC measurements

At the northern breakwater, just outside the outer harbor, energy peaks in the one dimensional wave spectra arise for waves between 7 to 14 seconds. The majority of these peaks is measured during the 12 November storm. During calm weather conditions the energy peaks shift slightly to shorter wave periods at the northern breakwater, however energy is present for waves around 10 seconds.
Inside the outer harbor energy peaks shift towards the higher frequencies (compared to the spectra outside the harbor) coinciding with shorter waves with energy peak values around 3 seconds. During the November storm a energy peak arises around 0.1 Hz for the measured spectra in the outer harbor, indicating that waves of these frequencies do penetrate the outer harbor. The values of the energy peaks inside the harbor are significantly lower than outside the harbor, showing a large energy dissipation of incoming frequencies.
When looking at the relation between significant wave heights outside and inside the harbor, the analyses show a large decay of the wave heights. The majority of the waves inside the harbor occur for short periods indicating that local wind wave generation inside the harbor is dominant in comparison to wave penetration of longer waves.
Finally when analyzing the scatter plots indicating the relation between peak periods outside and inside the harbor for different wave heights at the northern breakwater, the earlier conclusion that long waves penetrate the outer harbor during the 12 November storm can be enforced as the scatter plots clearly show correlation for the wave periods around 7 to 9 seconds for measured waves of 1 meter or higher (occurring during the storm).

4.9 Next steps

Thus far the following aspects have been analyzed:
- Wave periods that cause ship response of a 200.000 DWT bulk carrier
- Wave periods that cause resonance to the harbor basins
- The wave energy present in the outer harbor of IJmuiden

It has been stated that down time is caused by:
- Extreme wind conditions exceeding 20 m/s
- Significant wave heights exceeding 0.80 meter
- Severe ship movement as reaction on incoming long wave frequencies
- Basin resonance due to incoming long wave periods

It is concluded in chapter 2.4 that the exceedence of the critical wind velocity happens less than 1% a year and that significant wave height of locally generated wind waves has very little contribution to the down time condition in the new basin (see chapter 4.6.4).

Although seiches and locally generated wind waves are present in the outer harbor it is analyzed that these waves are not of influence to the severe movement and thus down time conditions of the new basin. wave periods of seiches are too long to cause the bulk carrier to react. Wave periods of locally generated waves are to small and wave heights of these waves are also to little to cause problematic situations in the new basin.

The measured data show that calculated resonance periods in chapter 3.4 do coincide with

actual wave agitation for the given measurement locations. However, there are few measurement locations available to get an understanding of wave action in the entire outer harbor and measured energy levels are low. Another uncertainty is that it is unknown how the existing harbor basins will react when the new basin is implemented. The wave periods causing resonance in the existing basins are calculated, but possible changes to these resonance periods due to the implementation of the new basin are unknown.
It is assumed that measured energy peak frequencies of the IJmond and Vissers harbor and calculated resonance wave periods in chapter 3.4.1 match the first mode standing waves arising in the basins. However it could be that the measured peak values belong to other phenomenons than a first mode standing wave and that the correlation between theory and results is accidental. Therefore more research is necessary to enforce these conclusions.

To form a better insight on these ignorances, it is determined to model the existing harbor in a numerical model capable of simulating long wave action in harbor areas. Chapter 5 will explain the abilities of this model in detail and why the model is chosen.

Chapter 5

Modeling of long waves inside the IJmuiden harbor

5.1 Introduction

In chapters 3 and 4 relations between the incoming wave climate and resonance frequencies of the harbor basins have been analyzed and it has been concluded that wave periods arise in the outer harbor that may cause resonance in the harbor basins.

However, these analyses are purely carried out looking at the basins separately. There is nothing known about the interaction between the existing basins among each other and with the new basin. Standing wave patterns could not only occur inside harbor basins itself but also between certain harbor areas. More important, conclusions drawn concerning the new basin are theoretical as the new basin does not yet exist.
The wave data derived from the pressure boxes and AWAC measurements in chapter 4.3 concern only a couple of explicit locations inside and just outside the harbor. From these analyses conclusions have been drawn concerning the reaction of all basins on incoming wave frequencies. However it is not certain whether this is the case.

In short, conclusions derived in the previous chapters have to be analyzed in further detail. Therefore the outer harbor will be implemented into a numerical wave model. This enables to get a better view of the wave interaction for given wave periods for the outer harbor as a whole. The goal of this model analysis is to determine whether the calculated resonance periods of the harbor basins in chapter 3.4.1 do occur when a given wave period propagates into the outer harbor.
Since a new basin will be implemented in the outer harbor, it is important to investigate in a model whether this implementation will influence the resonance periods in the harbor basins currently present and to determine whether possible changes can be positively or negatively interpreted.

5.2 PHAROS (Program for HARbor OScillations)

Before a model can be selected it is important to state what desired results a model should provide. Looking at the objective of the thesis, the intension is to determine whether long

waves penetrate the outer harbor and create additional movement to a moored bulk carrier in the new basin. Therefore it is important for a model to include refraction, diffraction and reflection of the incoming waves. Absorption factors of the embankment of the harbor basins should also be able to be adjusted in the model.

After inspecting several models that could be used, it has been concluded that a numerical model called PHAROS, developed by Deltares, has the right abilities to reach the objective. In the following paragraphs it will be explained why the model is a good choice to provide answers for the questions asked in chapter 5.1.

PHAROS is a numerical wave model for the simulation of wave agitation and wave resonance in harbor basins. The model is based on the mild-slope equation, which governs linear wave propagation over a mildly sloping bathymetry, with no restrictions to the water depth [1].

The following processes are modeled by PHAROS:

- Diffraction
- Refraction due to depth variations
- Refraction by ambient currents

The model includes the effects of:

- Dissipation by wave breaking
- Dissipation by bottom friction
- Partial reflection from complex seawalls, rubble mounds, beaches etc.
- Partial transmission due to over topping or permeability

The model computes wave propagation including these processes for a given wave period. The incoming wave signal is prescribed at a model boundary in a way that allows reflected waves to pass and move out of the model domain. The effect of directional spreading (short-crested waves) and energy spreading over multiple wave periods (a spectrum) can be accounted for by combining the output of multiple computations.

Furthermore, PHAROS offers the possibility to carry out computations for a large number of long wave periods in a user-defined range of frequencies to study long wave resonance and seiching of harbors.
It is therefore concluded that PHAROS is a model that is capable of analyzing the wave resonance inside the outer harbor.

5.3 Available PHAROS models

Chapter 3.3.2 has analyzed ship response to incoming waves for periods up to 250 seconds. In chapter 3.4.1 it has been analyzed that the harbor basins react to wave periods starting

from 10 seconds. Therefore it should be investigated how the harbor reacts to incoming wave periods between 10 and 250 seconds.
Before explaining the modeling approach it has to be explained that two PHAROS models concerning the outer harbor of IJmuiden are available. The models concern the current layout of the outer harbor without the new basin. The difference between the two models is in the use of the mild slope equation, the model grid size used for the calculations and the desired outcomes of the calculations. The models concern:

- A "long" wave model, developed to calculate wave agitation for wave periods between 30 and 250 seconds
- A "short" wave model, developed to calculate wave agitation for wave periods between 2 and 20 seconds

The long wave model is constructed to investigate harbor resonance and has the ability to create output locations and show wave agitation for a large range of frequencies for the given locations.
The short wave model is originally constructed to provide results for wave penetration in the outer harbor concerning given wave heights and wave periods belonging to determined probabilities of exceedence. It is not possible for this model to create output locations that show wave agitation. As for the shorter waves an output location is not a representative source for wave agitation at a given location. Wave agitation only meters away from this output location can be very different. Therefore, to configure the wave agitation for a certain location in the harbor, the average wave height is calculated by means of looking at all the modeled wave heights within a given radius of the desired location.

As the goal of this study is to investigate wave action inside the outer harbor for wave periods between 10 and 250 seconds it can be seen that the long wave model is the most appropriate model to use. Especially since it is very suitable to provide outcomes of wave agitation peaks for given locations. Therefore the model is well suitable to analyze basin resonance by creating output locations in all the ends of the basins.
However this model is adequate for waves from 30 to 250 seconds. For waves with periods between 10 and 30 seconds this model is not accurate anymore as the resolution of the model decreases.
The resolution is the number of grid nodes per wave length concerning the smallest wave length run through the model. For the long wave model this is around 15 nodes in the outer harbor [6]. However when waves with smaller periods are modeled, this resolution becomes less and exceeds the minimal accepted 8 nodes per wave length [41]. Figure 5.1 and 5.2 show the resolution inaccuracies for a 30 second and 25 second wave modeled in the long wave model.

Figure 5.1: Resolution inaccuracies concerning the long wave model for a 30 second wave period

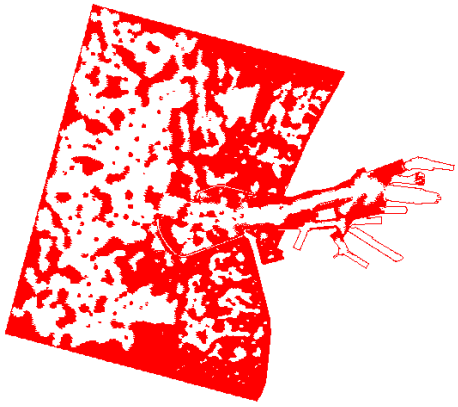

Figure 5.2: Resolution inaccuracies concerning the long wave model for a 25 second wave period

The areas pointed out in red indicate that the model resolution is very low for those areas. It can be seen that for wave periods smaller than 30 seconds the model is not adequate any more to provide accurate results. Therefore the short wave model will be used to model waves with periods between 10 and 30 seconds and the long wave model will be used to calculate the wave agitation for waves between 31 and 250 seconds.

5.3.1 Model calibration and validation

The available long and short wave models were already calibrated and validated by means of the obtained wave data from the measurements inside the outer harbor in 2010 [29]. For a detailed explanation of the calibration and validation, reference is made to the model instrumentation [6].
As measurements have only taken place for a couple of months, use has also been made of an earlier report written by Alkyon in 2001 [5]. This reports concerns long wave measurements inside the outer harbor. After calibrating and validating the model, it was concluded that the model runs are consistent with the measured data.

5.3.2 Model grids

Before working with the PHAROS models the existing harbor layout grids have been adjusted. The new basin layout as dimensioned in chapter 3.2.2 is added to the model bathymetry. The new harbor layout is integrated into both models as a new grid file. The grid of the new basin has been chosen in such a way that its resolution is the same or even finer than the existing grid of the outer harbor. Figures E.1 and E.2 in appendix E.1 show the harbor grids with and without the implementation of the new basin for the long wave model. Figures E.3 and E.4 show a close up of the resolution of the grids of the new basin for the short and long wave model.

5.4 Modeling approach

Before the results of the PHAROS model runs will be discussed it is explained what calculations have been performed. The following sections explain the model parameters that have been used and which output locations have been chosen.

5.4.1 Model parameters

PHAROS enables the user to adjust several parameters for model calculations. Appendix E.2 provides an explanation concerning the most important Pharos model parameters.
The parameters used for the long wave model compilations are shown in table 5.1.

Table 5.1: Input parameters for the long wave model

Type of parameter	parameter value
Significant wave height (m)	0.05
Main wave direction (degrees)	285
Water level (m)	0.00
Frequency range	0.004 - 0.033 Hz
Frequency increment	0.0001 Hz
Boundary reflection	100%
Nikuradse roughness (m)	0.1

For the wave height input a significant wave height of 0.05 meter is chosen. Earlier studies [5] have indicated that a wave height of this value is representative for long waves arriving at the IJmuiden harbor. This value has been determined by dividing long wave amplified wave heights measured inside the outer harbor by their amplification factors.
It has to be realized that the model treats the incoming wave energy stationary for all frequencies. The model calculates wave agitation in the expectation that wave energy is present for all wave periods. Therefore it has to be determined by examining the results of chapter 4 whether the wave periods showing high wave height amplification do posses a significant amount of wave energy in the the incoming wave spectrum to trigger the wave agitation that results out of the model.
To obtain the amplification of the resulting wave heights inside the outer harbor the results

of the wave heights inside the basin have been translated to a dimensionless wave amplification factor by dividing all results through the incoming wave height.

In the long wave model all the element groups that form the boundaries of the harbor have been submitted a reflection coefficient of 100% as is it is assumed that long waves do not break at the shoreline or quays but will reflect back to continue their path. Wave breaking is not simulated in the long wave model, assuming that the long waves will not break.

The parameters used for the short wave model compilations are shown in table 5.2 and 5.3.

Table 5.2: Input parameters for the short wave model

Type of parameter	parameter value
Significant wave height (m)	0.05
Main wave direction (degrees)	285
Water level (m)	0.00
Wave period range (s)	10 - 0.30
Wave period increment (sec)	1
Boundary reflection	depends on boundary
Nikuradse roughness (m)	0.1

In the short wave model all the element groups that form the boundaries of the harbor have been submitted different reflection coefficients. The coefficients were available with the model and both the values of these coefficients as a controlling study to verify these values are added in appendix E.3. Apart from determining the right reflection coefficients it is important to determine the right angle of approach of incoming waves in the model as the results of the reflecting wave can provide surreal outcomes when the incoming wave has been given a wrong incoming wave angle α. The incoming wave angles α for the existing harbor elements provided with the model have not been changed. For the new basin angles have been determined in cooperation with DHV hydraulic experts. Appendix E.4 provides a short explanation concerning the sensitivity of wave reflection concerning the incoming wave angle.
As the new basin consists of sloping shore lines it is chosen to use the same reflection coefficients for the basin as for the other sloping shorelines inside the outer harbor provided with the model.

It is assumed that wave breaking could occur for waves modeled in the short wave model, therefore wave breaking has been included in the short wave model (see table 5.3). The wave breaking parameters are based on general determined values [6].

Table 5.3: Wavebreaking parameters

Type of parameter	parameter value
Breaking index γ_{br}	0.80
Maximum wave steepness coefficient γ_{st}	0.14

5.4.2 Modeling resonance periods of the new basin

The first approach is to model the frequency of 0.004 to 0.034 Hz (wave periods of 31 to 250 seconds) in the long wave model. As stated this model is accurate for wave periods bigger than 30 seconds. Therefore the 10 to 30 seconds wave periods will be modeled using the short wave model.
It is possible to create dedicated output locations in the PHAROS models. For these locations graphs can be configured showing the wave agitation for every wave frequency modeled. The exact positions of these output locations will be described in chapter 5.6 together with the results of the analysis. The position of the output locations are determined considering the exact mooring location of the bulk vessel. This way modeled peak agitation frequencies at the bulk carrier mooring location can be compared to the ship resonance frequencies.
After the model calculations are carried out, results can be compared to the earlier derived basin resonance frequencies (see chapter 4) and conclusions concerning basin resonance can be drawn.
An extra calculation concerning changes in the dimensions of the new basin will be compared to obtained results. This way conclusions can be drawn whether the basin dimensions could be improved.

5.4.3 Modeling the effects of the new basin on the outer harbor

It is not sufficient to determine whether the hydraulic design of the new basin itself will satisfy its design criteria concerning wave action and basin resonance. The effects on the existing harbor layout due to the implementation of the new basin also have to be investigated.
In the current situation the existing basins show resonance for certain incoming wave periods. However, as the layout of the outer harbor changes due to the implementation of the new basin, it could be that resonance of the existing basins will appear for different incoming wave periods. A possible result is that the implementation of the new basin causes standing wave patters to arise in the outer harbor that are not present in the current harbor situation. Whether these changes in resonance periods can be interpreted positively or negatively has to be determined.
To provide answers to these questions two model runs will be carried out and analyzed. The first run concerns the PHAROS grid for the existing harbor layout. The second run concerns the grid with the new basin. In this run exactly the same parameters will be implemented and the same output locations will be analyzed for the harbor layout. After the two runs have been computed, the results for the output locations can be compared and it can be determined whether changes in wave agitation peaks arise.
Again the results will be compared to an extra PHAROS run concerning changes in the new basin dimensions mentioned in chapter 5.4.2. After comparing results of the two basin layouts conclusions can be drawn about the determined shape of the new basin.

5.5 Results of PHAROS calculations concerning the new basin

5.5.1 Resonance in the new basin

To analyze whether resonance occurs in the new basin a run has been carried in the long wave model concerning incoming waves between 30 and 250 seconds and runs in the short wave model concerning wave periods between 10 and 30 seconds. For the runs several output locations in the new basin have been created. Figure 5.3 shows the exact locations.

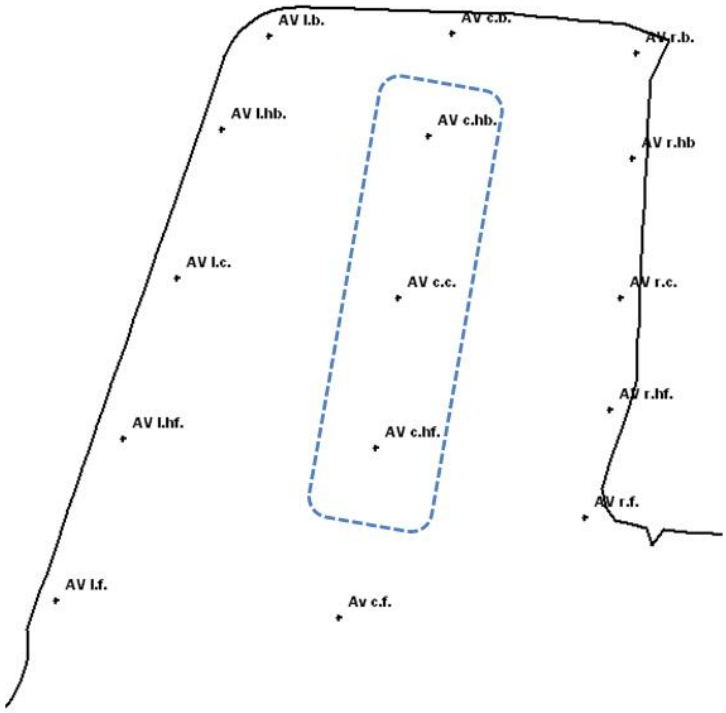

Figure 5.3: Output locations providing the wave agitation in the new basin

Locations "AV c.hb.," "AV c.c." and "AV c.hf." (see figure 5.3) are situated at the mooring location of the bulk carrier.
Figure 5.4 shows the wave amplification at the location "AV c.hb." situated at the front in the center of the bulk carrier mooring location. It is chosen to use this output location for the analysis as the wave amplification at this location is highest and therefore normative for the bulk carrier down time criteria.
Appendix F.1 shows the amplification factors for wave periods between 30 and 250 seconds for all the output locations inside the new basin. After analyzing the wave periods belonging to the amplification peaks in all the output locations, it can be concluded that there is a strong correlation between the results for all the output locations in the new basin. This indicates that the basin as a whole reacts to a standing wave with only one node and one anti node in the basin area. This phenomenon could be explained as a first mode standing wave. However, it could also be interpreted as the last part of a standing wave that arises over a larger area and ends with its last node and anti node inside the new basin.

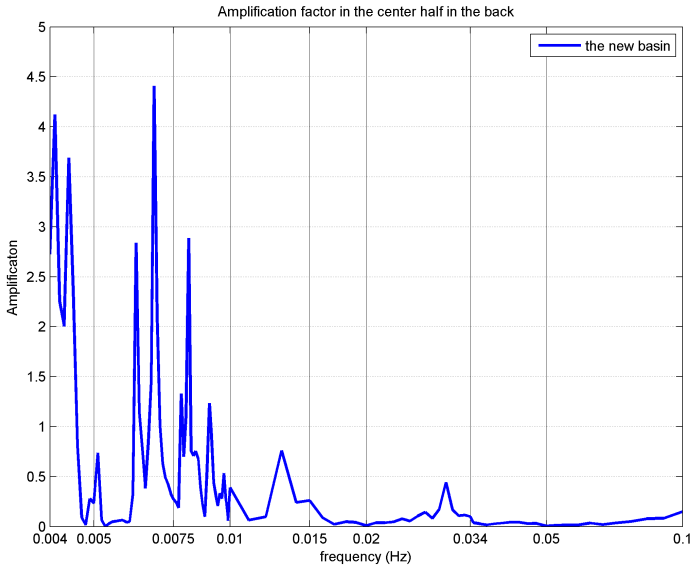

Figure 5.4: Wave amplification at the "AV c.hb." output location for wave periods between 10 and 250 seconds (0.004 to 0.1 Hz)

Table 5.4 provides the wave periods belonging to the highest amplification peak values.

Table 5.4: Amplification peaks at the "AV c.hb." output location for wave periods between 10 and 250 seconds (0.004 to 0.1 Hz)

Frequency (Hz)	Wave period (s)	Amplification (-)
0.0041	244	4.1
0.0044	227	3.7
0.0051	196	0.7
0.0062	161	2.8
0.0068	147	4.4
0.0081	123	2.9
0.0090	111	1.2
0.0130	77	0.8
0.0300	33	0.4

To understand the mode standing wave that arises in the basin for wave periods belonging to the resulting amplification peaks, not only the wave amplification graphs are studied but also the figures showing the wave images in the basin belonging to these wave periods. This way the arising wave pattern for these wave periods can be determined. Appendix F.2 provides the figures of the wave image plots belonging to the amplification peaks in table 5.4. The calculations belonging to a number of the standing wave modes have been added to show the resemblance of the PHAROS results and theoretical resonance calculations.
After analyzing the plots, the wave periods of table 5.4 have been arranged by their mode standing waves in tables 5.5 to 5.8. Better insight can now be obtained of the standing wave

patterns that arise in the new basin.

Table 5.5: Model results for wave frequencies belonging to first mode standing waves between the new basin and the IJmond harbor

1^{st} mode standing wave between IJmond harbor and new basin	
Wave frequency (Hz)	Coinciding wave period (s)
0.0044	227

Table 5.6: Model results for wave frequencies belonging to higher mode standing waves covering the whole outer harbor

Higher mode standing waves covering the whole outer harbor	
Wave frequency (Hz)	Coinciding wave period (s)
0.0041	244
0.0051	196
0.0068	147
0.0081	123

Table 5.7: Model results for wave frequencies belonging to higher mode standing waves between the new basin and the outer harbor entrance

Higher mode standing waves involving the new basin and harbor entrance	
Wave frequency (Hz)	Coinciding wave period (s)
0.0062	161
0.0090	111
0.0130	77

Table 5.8: Model results for wave frequencies belonging to local random wave agitation in the new basin

Local random wave agitation in the new basin	
Wave frequency (Hz)	Coinciding wave period (s)
0.030	31

In chapter 3.4.1 the theoretical resonance frequencies of the new basin have been calculated. The calculated value of a first mode standing wave was 103 seconds (frequency of 0.0097 Hz). The results out of the PHAROS model do show a wave amplification peak at this wave period (see figure 5.4). However it appears that the wave amplification of different mode standing waves are far more dominant concerning wave agitation.

It is interesting to see that amplified wave heights inside the new basin are triggered by standing wave patterns covering larger areas than only the basin itself. This chapter only analyses wave amplification inside the new basin and will therefore not go into detail on these wave patterns outside the basin. Chapter 5.6 will discuss these waves in further detail.

It is concluded in chapter 3.2.9 that the critical significant wave height for the unloading of a bulk carrier is 0.80 meter, concerning a worst case incoming wave angle. When looking at table 5.4, the highest wave amplification is almost 4.5 times the incoming wave height for an incoming wave period of 147 seconds. If it is assumed that for this incoming wave period, enough energy in the incoming wave spectrum is present to generate a wave height of 0.05 meter outside the harbor [6], it would result into an amplified wave height of 0.23 meter at the bulk carrier mooring location.
Therefore only considering the vertical wave movement, the waves in the range between 10 and 250 seconds will not cause downtime to the basin as they do not exceed the critical wave height of 0.80 meter. The measured wave heights belonging to long wave periods between 2 and 8 minutes in chapter 4.2.5 agree with these conclusions as amplified wave heights higher than 0.10 meter have a very low probability of occurrence according to the Alkyon report [5].
Another argument substantiating this conclusion is that (as explained in chapter 5.4.1) PHAROS treats the input of wave energy uniform over all wave frequencies. It is uncertain in the real harbor situation whether the intensity of the energy level can reach a sufficient level to even get to wave heights of 0.23 meter inside the outer harbor.

5.5.2 Effects of changing the basin

Changing the new basin layout could possibly improve the effect of incoming waves on basin resonance. When changing the basin layout it should be kept in mind that the basin cannot be extended in width and length due to restrictions demanded by several stakeholders in the design process. Therefore changes in basin layout should be implemented in adapting the basin depths or changing the slopes.
As the analysis is about long waves it is explained in chapter 5.4.1 that all reflection parameters are set at 100% for the harbor boudaries. Therefore changing the characteristics of the slopes in order to change the absorbtion of wave energy is not an option. However changing the shorelines into slopes with steeper angles will decrease the total width of the basin.
As explained in appendix C.1 decreasing the basin width will cause resonance in the basin for waves with lower wave periods as the wave number k of the waves will increase (for further explanation see appendix C.1). The objective of changing the basin layout is to determine whether the standing wave patterns will change due to other dimensions of the basin. As most of the standing wave patterns cover a larger area than only the new basin it is interesting to investigate whether changing the basin layout can influence these standing waves patterns.

It is chosen to change the slopes of the basin (the original dimensions are explained in chapter 3.2.2) into 1:3 slopes from top to toe. This adjustment decreases the width of the basin with a distance of 40 meter and the length of the basin with 20 meter. Theoretically the basin could even be decreased to smaller dimensions in width by implementing a sheet pile construction. However, this decreasing of the basin width would interfere with the objectives set for the functions of the basin explained in chapter 3.2.
Figures 5.5 to 5.8 shows the new adjusted basin layout in comparison to the original new basin layout.

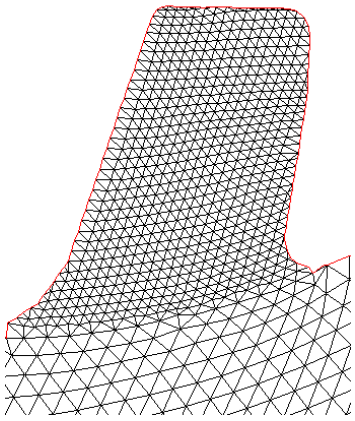

Figure 5.5: Model grid of the new basin with the adjusted 1:3 dimensions

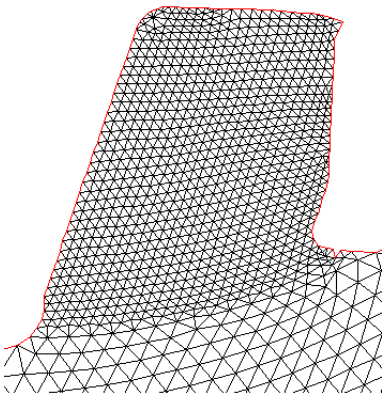

Figure 5.6: Model grid of the new basin with original layout dimensions)

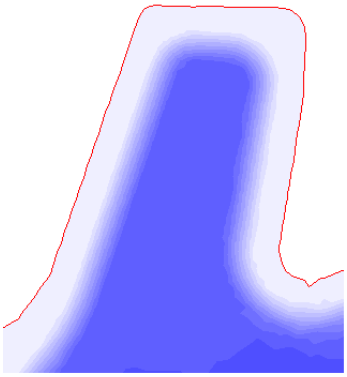

Figure 5.7: Depth contours of the new basin with the adjusted 1:3 slope dimensions

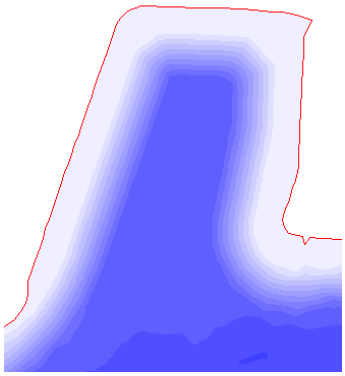

Figure 5.8: Depth contours of the new basin with original layout dimensions

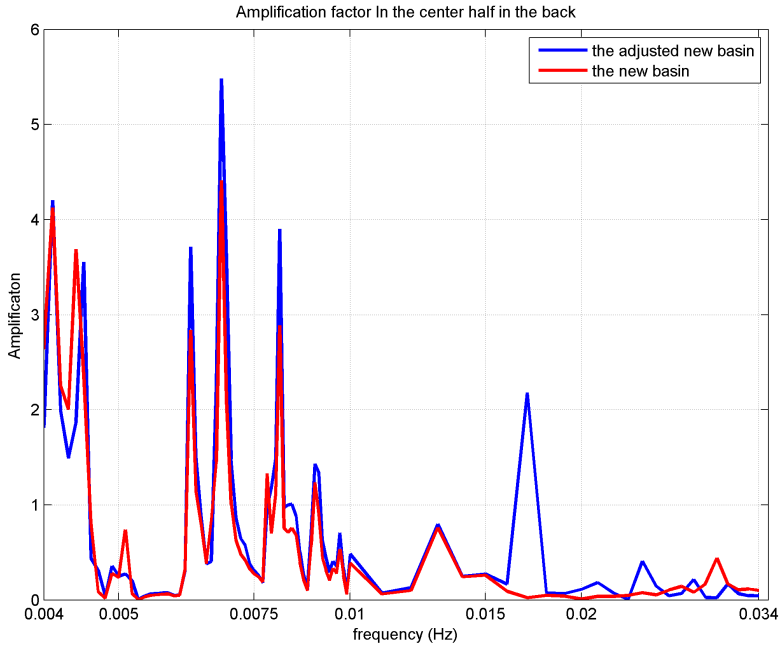

Figure 5.9: Comparing wave amplification at the bulk carrier mooring location between the original and the adjusted new basin

Figure 5.9 shows the wave amplification for location "AV c.hb." for the original new basin layout (blue) in comparison to the adjusted new basin (red). The figure shows minimal change in wave amplification for incoming wave periods. However, it can be concluded that overall amplification peaks increase when decreasing the basin dimensions. Furthermore, an amplification peak arises around a wave period of 60 seconds (0.017 Hz). When looking at the wave pattern for this situation (see figure 5.10) a standing wave pattern can be seen between the Fort island and the end of the adjusted new basin.

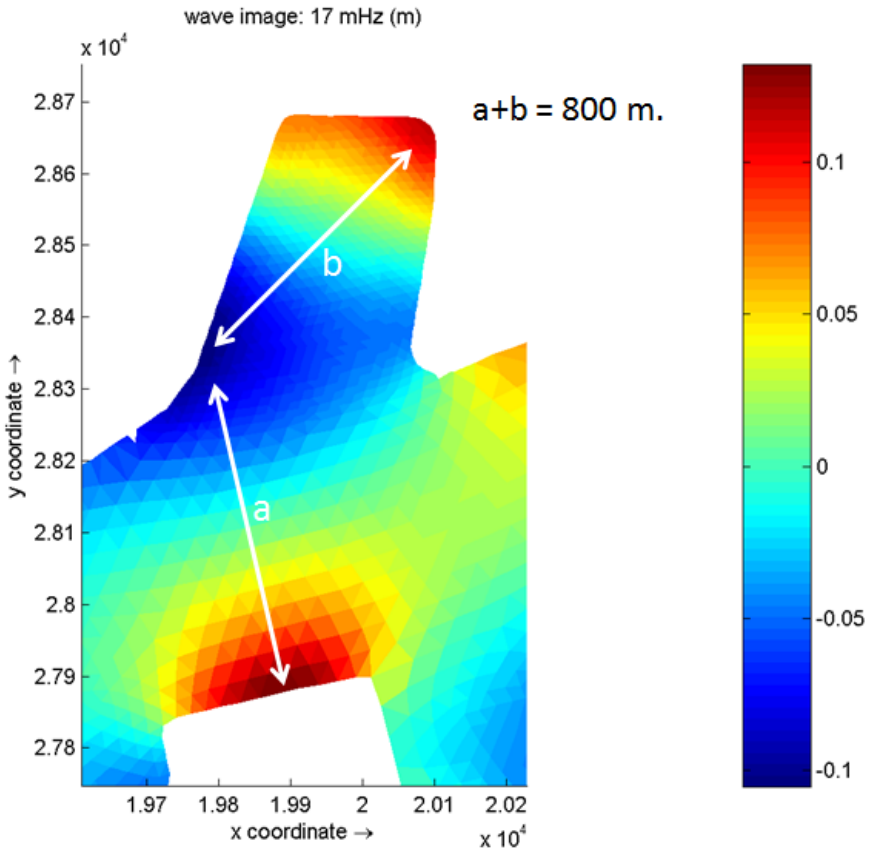

Figure 5.10: Wave image of the agitation (m) of a second mode standing wave between the adjusted new basin and the Fort island

The wave image shows a second mode standing wave that arises with wave amplification peaks at the reflecting shorelines. It seems that the standing wave is positioned between the three reflecting shorelines with two positive water level anti nodes at the Fort island and the end of the new basin and a negative water level anti node at the left front of shoreline of the new basin (complying with the image of a second mode standing wave).
When calculating the theoretical wave period belonging to a second mode standing wave over a length of around 800 meter (distance between the Fort island and the opposing end of the new basin, see figure 5.10) and a depth of 20 meter following the theory explained in appendix C.1, it results in a wave period of 57 seconds (a wave frequency of 0.018 Hz) which is very close to the calculated wave period provided by the model.

Overall it can be concluded that effects of decreasing the dimensions of the new basin are very little. However, the changes that do occur turn out to be negative concerning basin resonance in comparison to the results obtained from the analyses concerning the original dimensions of the new basin.

5.6 Effects of the new basin on the outer harbor

To investigate the effect of the implementation of the new basin on the existing harbor basins, model runs of the existing situation (without the new basin) are compared to model runs including the new basin. To analyze the possible differences in wave agitation, output locations have been created in both model runs for the exact same locations. These locations have been chosen in the far ends of all the existing basins, see figure 5.11.

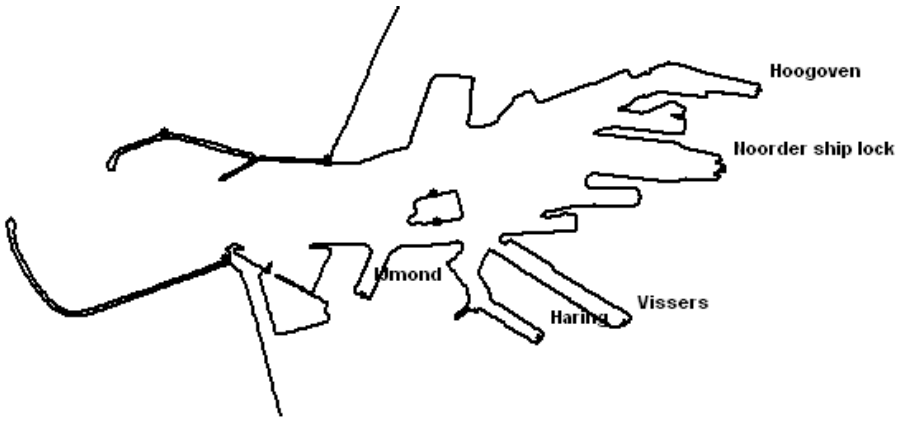

Figure 5.11: Output locations used to define wave amplification in the outer harbor

As explained in appendix C.1 highest wave amplification occurs in the anti nodes of a standing wave. Depending on the mode of a standing wave, anti nodes arise in different locations in a basin. However at the far end of the basin an anti node will always occur. To test the sensitivity of this conclusion appendix F.3 shows the difference in wave agitation for the output location at the far end of an existing basin (as used in the analysis) with the output locations located a little more away from the basin end. After analyzing the results it can be concluded that indeed the highest wave agitation is shown in the far end of the basins.

In chapter 5.5.1 it was already mentioned that most of the standing wave patterns arising in the new basin did not only appear in the new basin itself but seemed to originate further away in the mouth of the outer harbor. In the following chapters the origin of these standing waves will be analyzed together with the effects on the existing basins due to the implementation of the new basin.

5.6.1 Effect of swell waves in the outer harbor

Figure 5.4 shows that for the new basin wave periods lower than 100 seconds do not cause an enforced amplification of incoming waves. When looking at waves with wave periods between 10 and 30 seconds (swell) it can be concluded that no significant amplification peaks arise in the new basin. After investigating the other basins in the outer harbor, this same conclusion can be drawn. Figure 5.12 shows the amplification of incoming waves in the outer harbor with a wave period of 20 seconds.

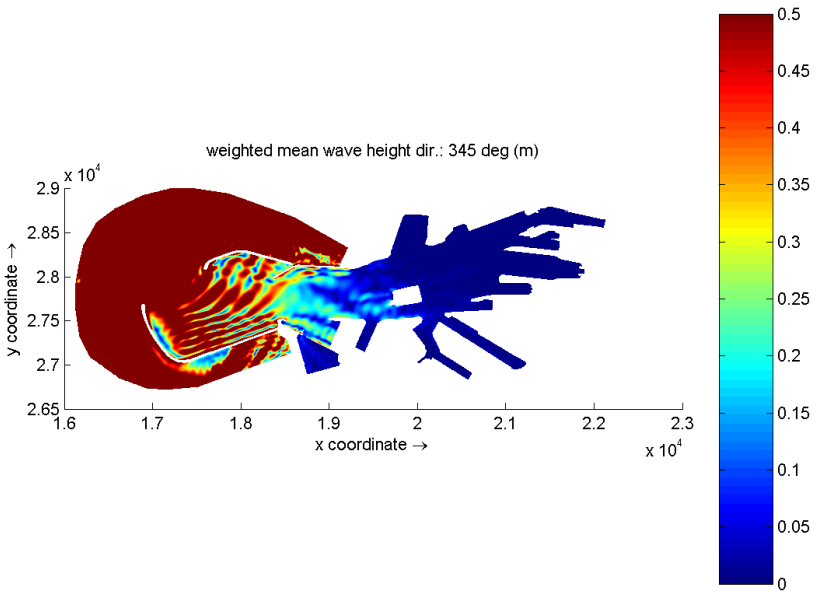

Figure 5.12: Wave amplification in the outer harbor for an incoming wave period of 20 seconds and a nautical direction of 285°

It can clearly be seen that wave energy and wave heights have strongly decreased when waves propagate further into the harbor. Appendix F.4 shows the results of wave amplification of all the wave periods between 10 and 30 seconds. All results agree with the result shown in figure 5.12. The modeled results are substantiated by the the measured wave heights of swell waves inside the outer harbor [29] (see chapter 4.6.3). As waves between 10 and 30 seconds show minimal amplification in the outer harbor, it is chosen not to include these waves in the analyses considering the effects of the new basin on the outer harbor.

5.6.2 Standing waves in the outer harbor

When looking at the outer harbor as a whole the implementation of the new harbor basin has significant influence on changes in standing wave patterns concerning the whole outer harbor. It can be concluded that especially for high wave agitation in the far end of the outer harbor (considering the Hoogoven harbor and the connecting ship locks to the North Sea channel) the new basin has a positive influence. Figures 5.13 and 5.14 show wave images in the outer harbor for the current and the new situation considering a wave period of 125 seconds. The figures show clear examples of the changes in standing wave patterns due to the implementation of the new basin.

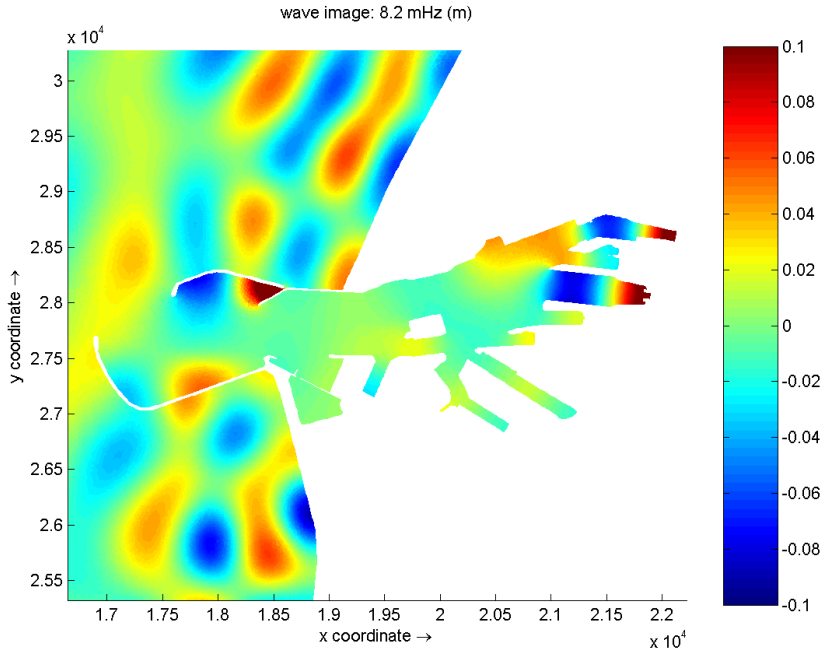

Figure 5.13: Standing wave pattern in the current situation for a wave period of 125 seconds causing high wave agitation (m) at the Noorder ship lock

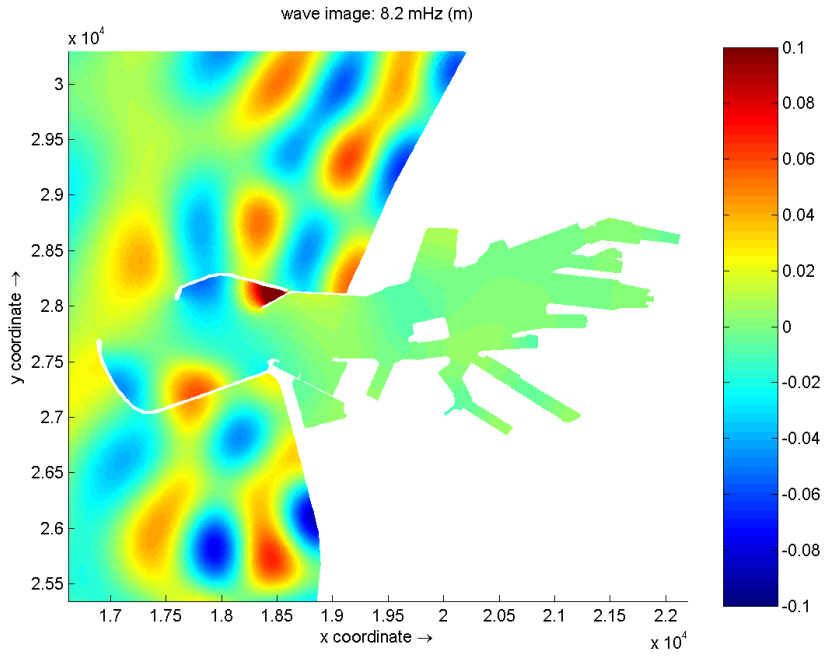

Figure 5.14: Standing wave pattern in the new situation for a wave period of 125 seconds. The high wave agitation (m) at the Noorder ship lock has decreased significantly

It can be seen that in the current situation a standing wave pattern arises that shows wave

agitation all the way to the far end of the outer harbor. In the new situation the agitation at the end of the outer harbor has decreased significantly which can be concluded as a positive effect concerning wave action.
It appears that the wave energy propagates into the new basin instead of to the end of the harbor in the new situation. This effect can be explained by the fact that the new basin is wide and deep. Therefore the path followed by the wave experiences less friction when it diffracts into the new basin.

This is a first observation concerning the entire outer harbor as a whole. In the next sections of this chapter a more detailed approach of the existing harbor basins will be provided. These sections will show and explain the main differences in basin resonance due to the implementation of the new basin as it is has to be defined whether this change in standing wave patterns also appears to be of positive effect for the other existing basins.

5.6.3 Effects on the IJmond harbor

Figure 5.15 shows the wave amplification in the end of the IJmond harbor before and after the implementation of the new basin. The red graph signifies the existing situation and the blue graph shows the situation after the implementation of the new basin.

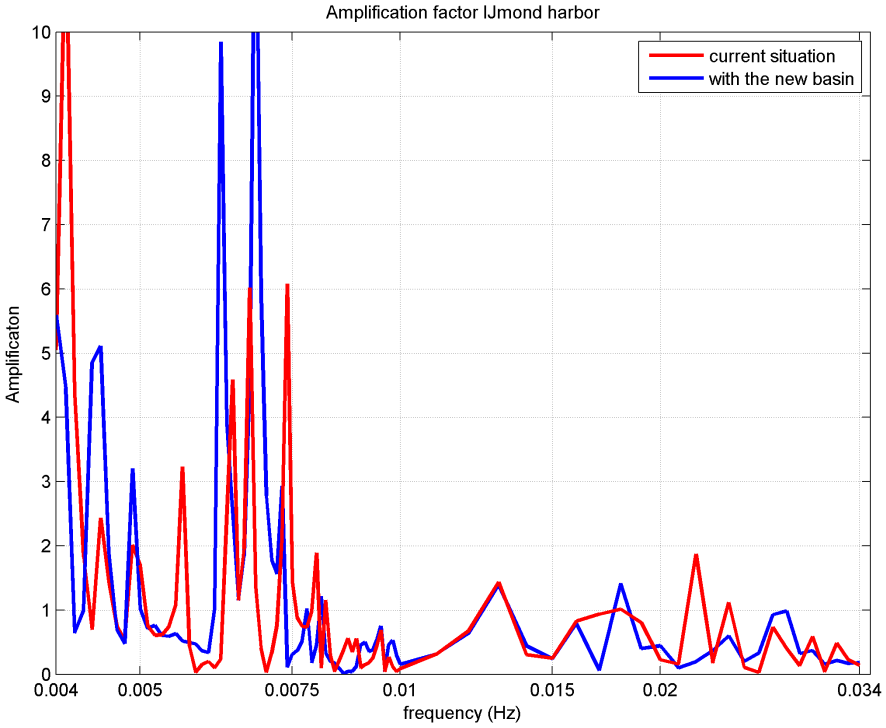

Figure 5.15: Wave amplification at the end of the IJmond harbor for wave periods between 30 and 250 seconds

In chapter 3.4.1 it is concluded that a first mode standing wave in the IJmond harbor would occur for a period of 149 seconds (0.0067 Hz). When looking at the results derived from

PHAROS a first mode standing wave image can be seen for a wave period of 151 seconds (0.0066Hz), the calculated results in chapter 3.4.1 and the modeled results coincide.
Figure 5.15 does also show an amplification peak for the exact wave period of 149 seconds (0.0067 Hz). However, this peak does not belong to the first mode but to a higher mode standing wave. Similarly to the new basin, the modeled amplification factor belonging to the first mode standing wave in the IJmond harbor is also small in comparison to higher mode standing waves modeled for the IJmond harbor. When energy is present in the wave spectrum for the wave periods beloning to the higher mode standing waves, they may cause operational problems and will therefore be discussed in this chapter.

After the implementation of the new basin a small shift in agitation peaks occurs for the IJmond harbor (see figure 5.15. The amplification peak at a wave period of 244 seconds (frequency of 0.0041 Hz) is decreased, the amplification peak for a wave period of 227 seconds (frequency of 0.0044 Hz) is enforced and two amplification peaks peaks arise for wave periods of 161 and 147 seconds (0.0062 and 0.0068 Hz). Figure 5.16 shows the wave image of the standing wave pattern for the outer harbor for a wave period of 227 seconds for the new harbor situation.

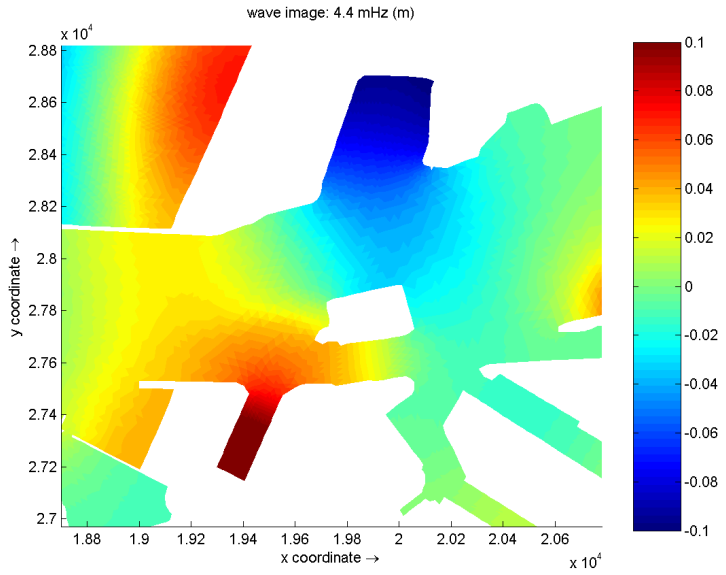

Figure 5.16: Wave image (m) between the new basin and the IJmond harbor showing a first mode standing wave for a wave period of 244 seconds

The figure shows that after the new basin is implemented the occurrence of a first mode standing wave pattern may arise between the new harbor basin and the IJmond harbor. Table 5.5 shows that the amplification peak measured in figure 5.15 coincides with the peak measured in the new basin. The calculation in appendix F.2 belonging to figure F.17 confirms that following the basin resonance calculations in chapter 3.4 a first mode standing wave fits between these two basins for a wave period very close to 227 seconds.

Figure 5.17 and 5.18 show the wave image in the harbor for the wave periods of 147 and 161 seconds.

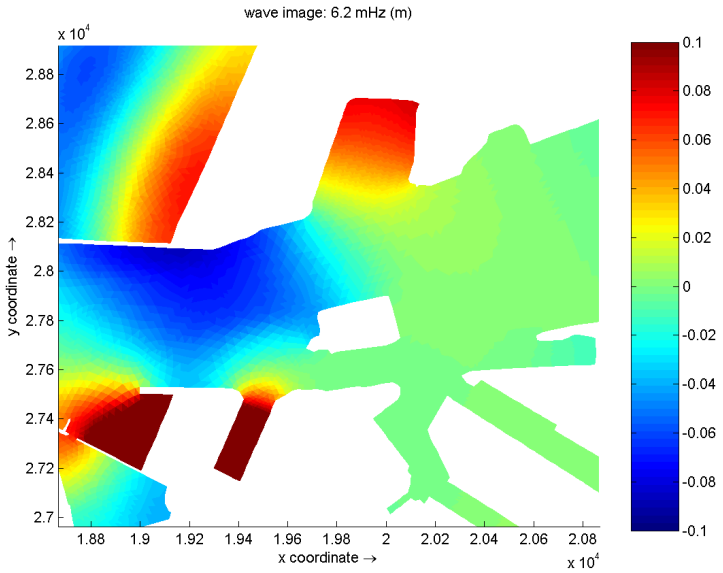

Figure 5.17: A combination of standing wave patterns between the harbor entrance, the IJmond harbor and the new basin arising for a wave period of 161 seconds

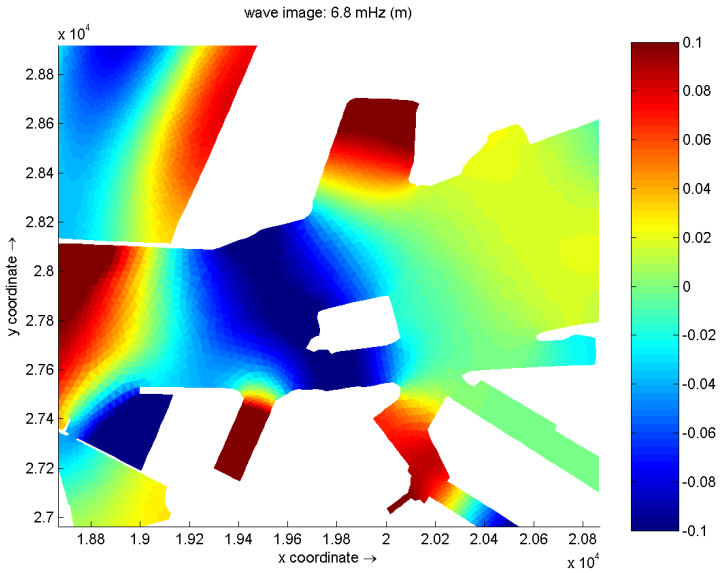

Figure 5.18: A combination of standing wave patterns between the harbor entrance, the IJmond harbor and the new basin arising for a wave period of 147 seconds

It seems that two phenomena occur. Firstly a standing wave pattern arises between the harbor entrance and the end of the new basin. Secondly a standing wave arises between the new basin and the IJmond basin. This second conclusion is enforced by the presence of

agitation peaks at 6.2 and 6.8 mHz in the end of the IJmond basin as well as at the end of the new basin indicating two anti nodes of a standing wave at both basin ends.
It is unclear whether the wave agitation in the middle of the approach channel is also a contribution of the standing wave between the IJmond harbor and the new basin, if this is the case it can be interpreted as a second mode standing wave. The simplified calculations in table 3.8 suggest that a second order standing wave between the IJmond harbor and the new basin would occur for a wave period of 141 seconds (frequency of 0.0071 Hz). The wave periods of 161 and 147 seconds (frequencies of 0.0062 and 0.0068 Hz), showing the standing wave images in figures 5.17 and 5.18, are close to this calculated value making this assumption plausible.

In the current situation ships inside the IJmond harbor do not seem to experience mooring problem due to basin resonance [27]. This could indicate that wave periods propagating into the IJmond harbor do not affect the moored ship response or that the magnitude of the wave energy level is not sufficient enough to trigger the modeled wave action for the determined wave periods.
As the amplification peaks in the new situation are very close to amplification peaks arising in the current situation it should be questioned whether these new peaks will cause additional effects to moored ships in the IJmond harbor. Furthermore nothing is known about the mooring facilities in the IJmond basin, therefore it cannot be concluded whether ships will suffer critical movement for these long wave periods.

5.6.4 Effect on the Noorder ship lock

Figure 5.19 shows the wave amplification peaks at the Noorder ship lock before and after the implementation of the new basin. The red graph signifies the existing situation and the blue graph shows the wave agitation after the implementation of the new basin.

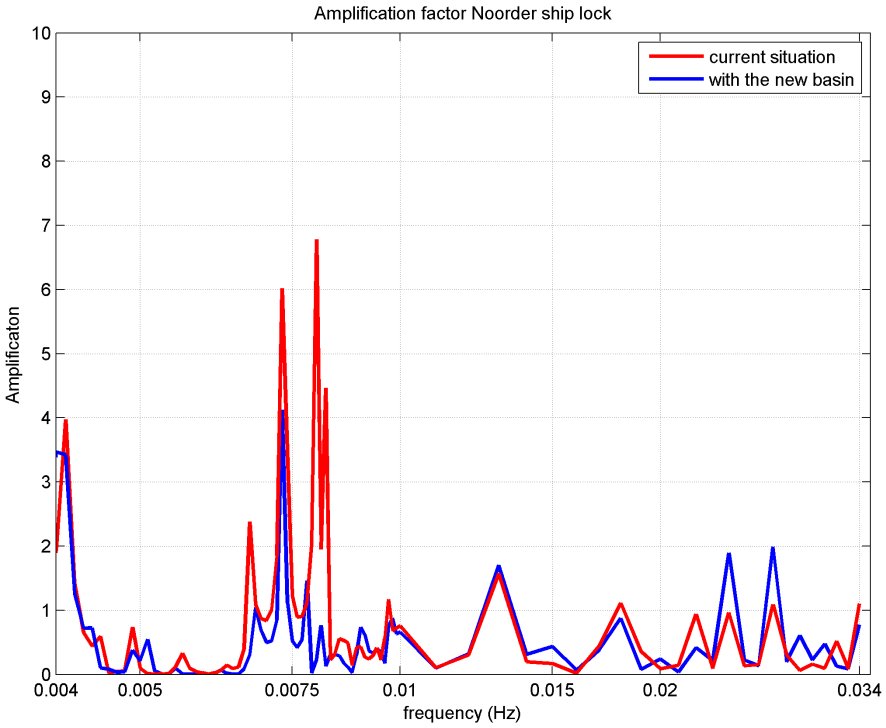

Figure 5.19: Wave amplification at the end of the Noorder ship lock for wave periods between 20 and 250 seconds

It can be seen that the conclusion derived in chapter 5.6.2 remarking that the new basin reduces the wave agitation in the harbor area behind the Fort island is clearly the case for the Noorder ship lock for long waves between 250 and 100 seconds. More important there are very few shifts in wave peak frequencies, indicating that the resonance occurring in the Noorder ship lock will not change due to the implementation of the new basin. In general the new basin decreases the resonance effect in the Noorder ship lock. However, two changes in the agitation graphs should be mentioned. Although the peak is small, an agitation peak arises at an incoming wave period of 196 seconds (coinciding with a wave frequency of 0.0051 Hz). The other change in the agitation graph is the shift of the two agitation peaks around 125 seconds (0.008 Hz). These two peaks shift to lower wave frequencies. Although the strength of the wave agitation decreases significantly, peaks still arise. The peaks arise around wave periods of 130 seconds (frequencies of 0.0077 and 0.0081 Hz). At the shorter wave periods around 40 seconds (0.025 Hz) the two existing amplification peaks are enforced because of the implementation of the new basin.

5.6.5 Effect on the other basins

In Appendix F.5 all graphs concerning wave agitation measured in the far ends of the basins are showed. It can be concluded for the Haring harbor, Vissers harbor and Hoogoven harbor that the implementation of the new basin does not have significant effects on the wave agitation peaks of these basins. For the Hoogoven harbor the implementation of the new basin has a positive effect for wave agitation concerning wave periods between 140 and 170 seconds. Wave agitation peaks decrease significantly in the Hoogoven harbor as the new basin decreases the propagating wave energy in the far end of the outer harbor.
The Vissers harbor and Haring harbor experience the most positive influence for the long waves with periods between 250 and 200 seconds. Due to the implementation of the new basin wave amplification decreases significantly for those wave periods.

5.6.6 Effects of changing the basin on the outer harbor

Changing the dimensions of the new basin will not only affect wave amplification inside the basin itself but can also influence wave agitation in the entire outer harbor. As chapter 5.5.2 already discussed the effects inside the new basin, this chapter emphasis on the effects on the other harbor basins.
To determine whether changes occur due to the new basin adjustments, amplification graphs for exactly the same output locations as shown in figure 5.11 have been created for the adjusted basin PHAROS runs. The amplification at these output location, considering the new basin and of the adjusted new basin, have been combined in one figure to show the differences in wave amplification per wave frequency. Appendix F.6 shows the results for all harbor basins.
Overall it can be stated that the results considering the adjusted new basin do not differ significantly from the already analyzed results concerning the normal dimensions of the new basin. Amplification peaks arise for the same wave periods. For the adjusted new basin dimensions results tend to show slightly more negative effects.
However, for the situation in the IJmond harbor results are significantly more negative when looking at the adjusted basin (see figure 5.20).

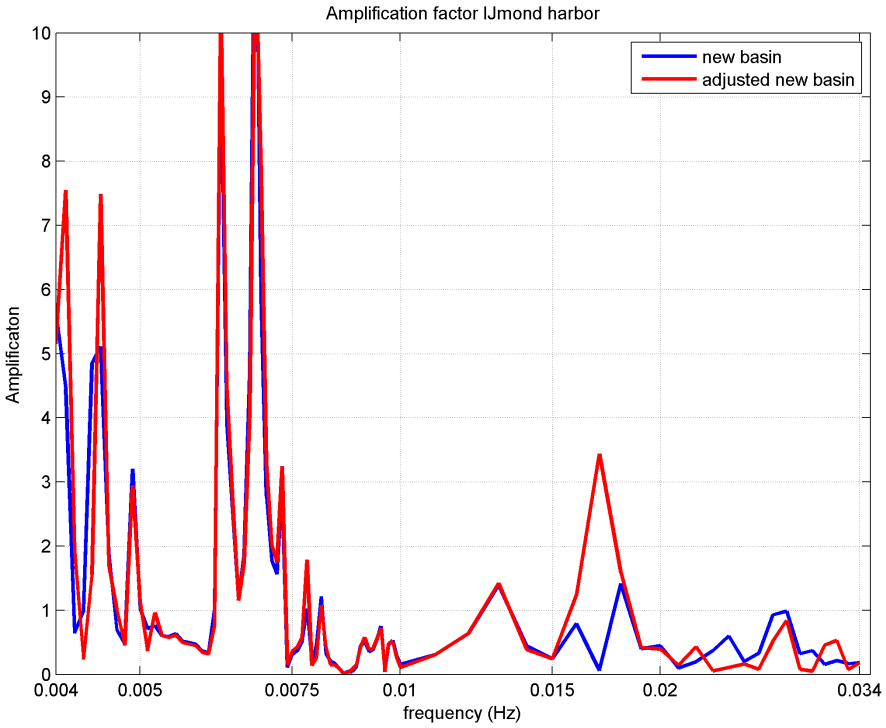

Figure 5.20: Comparing wave amplification in the IJmond harbor for the new basin (blue) and the adjusted new basin (red)

As expected amplification peaks shift a little to higher wave frequencies (lower wave periods) as the wave number k increases. This can be seen for the shift in amplification peaks around 220 seconds (frequency of 0.044 Hz). However the amplification peaks for these wave periods also increase with 40% in comparison to the results concerning the original new basin dimensions. At a wave period of 60 seconds (frequency of 0.017 Hz) an amplification peak arises that does not exist for the original new basin situation. This amplification arises for the same wave period as for the situation inside the new basin in chapter 5.5.2. However the reason for the IJmond harbor to react is unclear as the wave image does not seem to affiliate with a standing wave occurrence between the new basin and the Fort island. The wave image shows a second mode standing wave in the IJmond harbor while in theory the basin should not react.

5.7 Conclusions

Results out of the PHAROS runs comply with the calculated first mode standing waves in chapter 3.4.1. However higher mode standing waves covering larger areas than single basins are normative for high wave amplification. The PHAROS results assume that the wave energy is uniformly distributed over all modeled wave periods. Outcomes are purely theoretically and it should be investigated whether wave energy in the outer harbor for long wave periods is of a sufficient level to trigger the modeled basin resonance.

The new basin shows resonance for several wave periods. The different standing wave patterns only consist of one anti node in the basin, making the new basin as a whole react to high wave agitation peaks. The highest wave amplification at the location where the bulk carrier will be moored is around 4.5 times the incoming wave at sea. This long wave amplification will not contribute to down time conditions considering vertical ship movement.
Decreasing the width of the basin with 40 meter by changing the shoreline into 1:3 slopes does not result into positive effects concerning wave agitation. Existing amplification peaks increase and an extra amplification peak arises for a wave period of around 60 seconds.

When looking at the interaction between the new basin and the existing harbor basins the conclusion can be drawn that the basin has a positive decreasing effect on wave agitation in the end of the outer harbor. Standing wave patterns that arise all the way to the ship locks and Hoogoven harbor in the current situation disappear due to the implementation of the new basin. This can be explained by the fact that the standing waves diffract into the new basin instead of the end of the outer harbor because of the lack of friction forces due to the deeper bottom contours and disappearance of the shoreline.
Due to the implementation of the new basin amplification peaks of standing waves shift to different wave frequencies for the IJmond harbor. However, as the amplification peaks in the new situation are very close to amplification peaks arising in the current situation it should be questioned whether these new peaks will cause additional effects to moored ships in the IJmond harbor. In the current situation it appears that energy levels belonging to long waves are not of proportions to cause basin resonance to interfere with the mooring operations.

When analyzing the results concerning the outer harbor in general after changing the new basin dimensions with 40 meters, it can be concluded that effects are small and do not show significant positive effects.

As statistics about long wave action near the IJmuiden harbor are barely available, it cannot be determined whether energy is present in the wave spectra for the wave periods showing high amplification peaks. The bit of data available shows that measured wave spectra do show that energy can be present for long waves around 200 seconds. However nothing is known about the probability of occurrence of these waves. Measurements also show that wave heights belonging to these long waves inside the outer harbor are smaller than the 0.80 meter critical wave height for vertical ship movement.

Chapter 6

Basin and moored ship response system

In the previous chapters it has been analyzed which wave periods cause a bulk carrier to react. It has also been modeled whether standing waves may theoretically occur in the outer harbor and it is determined that standing waves may arise in the new basin for a number of incoming wave periods. However, it has been concluded that the amplification of the vertical movement of the long waves inside the new basin will not contribute to the 5% operating down time per year.
Thus far, basin resonance and ship response to incoming wave periods have been analyzed separately. However, the two systems could act as a coupled system. This chapter analyzes whether for certain incoming wave periods, basin resonance and ship response will enforce each other in such a way that down time criteria could be exceeded.

6.1 Calculating the coupled system

To investigate whether a moored bulk carrier will react to basin resonance periods, the output locations located at the ship mooring facility (see figure 5.3) have been investigated in further detail. As the most sensitive output location is normative for the down time criteria exceedence, location "AV c.hb" (as explained in chapter 5.5.1) will be used for the representation of the basin resonance for the analysis of the coupled system.

To determine whether the basin peak resonance frequencies coincide with the bulk carrier resonance frequencies, the bulk carrier's RAO's for the vertical degrees of freedom of ship movement, obtained in appendix B.2, have been multiplied with the amplification graph concerning the "AV c.hb." output location.
As the RAO's show the ship's reaction for four incoming wave angles (see appendix B.2), the results showing the highest ship response outcomes have been chosen for every free motion. It has to be taken into account that the results for the bulk carrier RAO's are based on the ship positioned in open water instead of at the mooring location inside the basin. Therefore results of the coupled system will be analyzed to determine whether the outcomes are realistic.

6.1.1 Results for the coupled system of basin resonance and ship heave

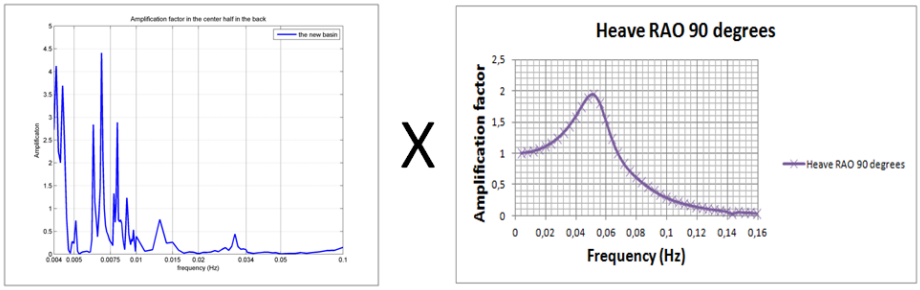

Figure 6.1: The coupled system is modeled by multiplying the basin resonance with the ship RAO over the same frequencies

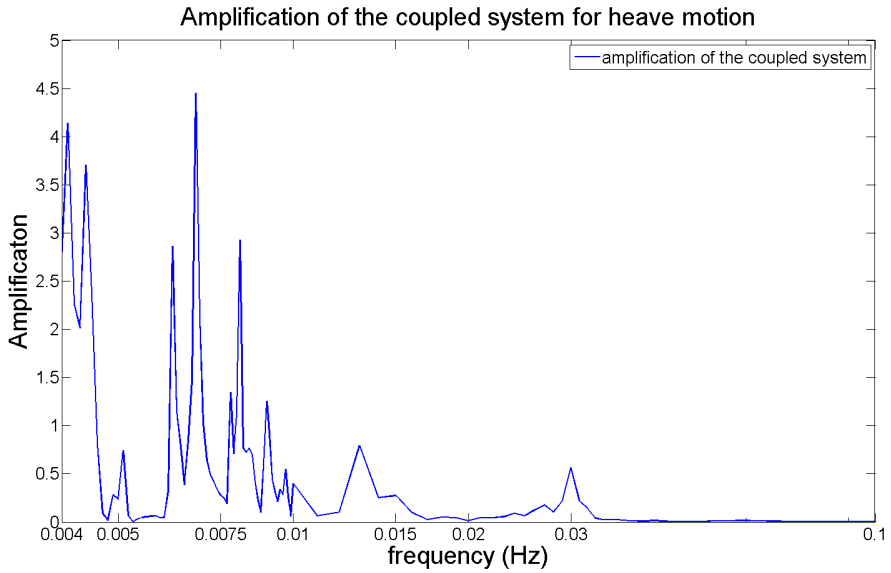

Figure 6.2: Amplification of the incoming wave for the coupled system of basin resonance and ship heave motion

Table 6.1: Amplification peaks for the coupled system of basin resonance and the ship's heave motion

Frequency (Hz)	Wave period (s)	Amplification (-)
0.0041	244	4.1
0.0044	227	3.7
0.0051	196	0.7
0.0062	161	2.9
0.0068	147	4.5
0.0081	123	2.9
0.0090	111	1.3
0.0130	77	0.8
0.0300	33	0.6

Chapter 3.3.2 indicated that wave periods causing vertical ship movement enforcement are lower than the wave periods responsible for the horizontal enforcements. The coupled system is derived through a multiplication of two amplification factors. In case the basin amplification is very little (close to zero), the multiplication of this amplification with a ship's RAO will also result into a small amplification factor for the coupled system.
As the peak of the ship's amplification is around 0.05 Hz (see figure 6.1) and basin amplification is very little for that wave frequency the result of the coupled system seems barely changed by the contribution of the heave RAO. The amplification of the coupled system is almost identical to the amplification of the incoming waves in the new basin. Especially since the heave RAO amplification factor is around 1 for the wave periods between 250 and 50 seconds.

The same conclusion can be drawn as for the results derived out the basin resonance analyses. Table 6.1 shows that especially wave periods of 244, 227 and 147 seconds can cause amplification of incoming waves. It should be taken into mind that the heave RAO has been obtained by means of modeling the bulk carrier in open water. The mooring facility in the new basin will damp the vertical ship movement. However, even taking the obtained open water results into account it can be concluded that the contribution to the down time of the lightering process due to heave movement is almost nigligable. Incoming wave heights outside the harbor belonging to the long waves with a 147 second wave period should be higher than 0.18 meter to cause a 0.80 meter vertical movement for the highest amplification value of 4.5 times the incoming wave height (see table 6.1). When looking at earlier investigations on long wave penetration and seiches in the harbor [5] it can be concluded that these wave heights have almost no probability of occurrence. As earlier reports [5], [6] state that incoming waves with wave periods between 2 and 8 minutes result in amplified wave heights of 0.10 meter at the end of the outer harbor have a probability of occurrence of 0.02% per year, it can be assumed that a wave height of 0.17 meter outside the harbor for waves with a wave period of 147 seconds is very unlikely to occur.

6.1.2 Results for the coupled system of basin resonance and ship roll

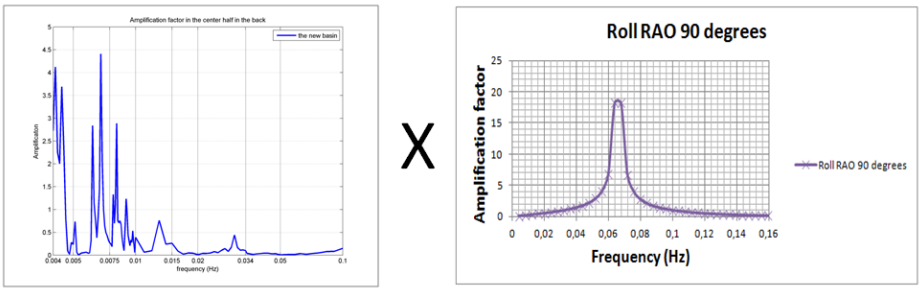

Figure 6.3: The coupled system is modeled by multiplying the basin resonance with the ship RAO over the same frequencies

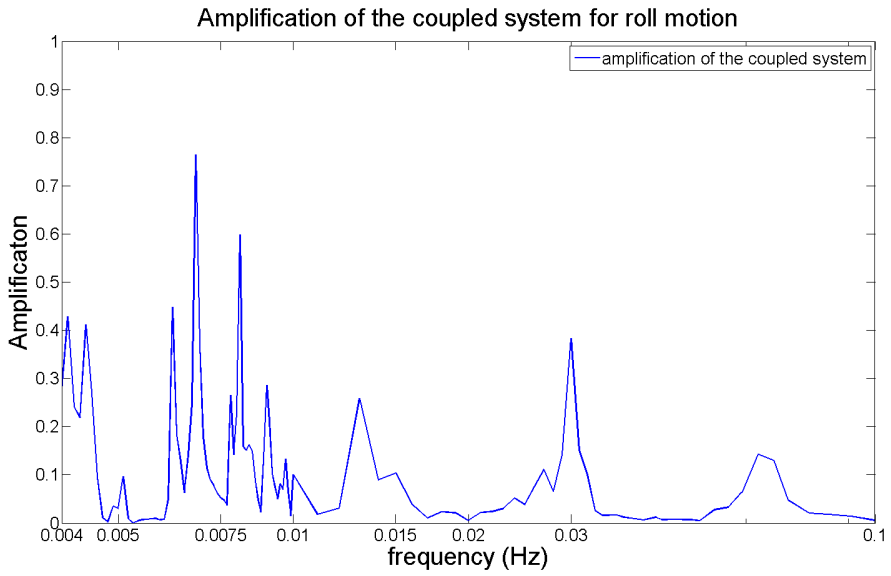

Figure 6.4: Amplification of the incoming wave for the coupled system of basin resonance and ship roll motion

Table 6.2: Amplification peaks for the coupled system of basin resonance and the ship's roll motion

Frequency (Hz)	Wave period (s)	Amplification (-)
0.0041	244	0.4
0.0044	227	0.4
0.0051	196	0.1
0.0062	161	0.4
0.0068	147	0.8
0.0081	123	0.6
0.0090	111	0.3
0.0130	77	0.3
0.0300	33	0.4

The coupled system of basin resonance and ship roll is maybe the best example of showing the weight of the basin resonance factor in the calculation. Figure 6.3 shows that the amplification peak for the bulk carrier's roll motion is around 20 times the incoming wave height for a frequency of 0.06 Hz, coinciding with a wave period of around 15 seconds (figure B.14 in appendix B.2 provides a bigger image). This is a significant value that could enforce the roll motion. However, after multiplying the RAO with the basin resonance amplification, the original amplification peak in figure 6.4 reduces this peak to a amplification of less than 0.2 times the incoming wave height for the coupled system. The basin's response to wave periods smaller than 100 seconds decreases all ship's responses to minimal amplification factors in the coupled system for vertical ship motions.
Table 6.2 shows that as ship response factors on long waves are minimal for roll the coupled system's reaction on incoming waves is strongly reduced in comparison to the reaction of the two individual resonance systems.
It can be concluded that the coupled system for roll will not negatively effect the unloading operations in the new basin and therefore will not contribute to the down time conditions of the new basin.

6.1.3 Results for the coupled system of basin resonance and ship pitch

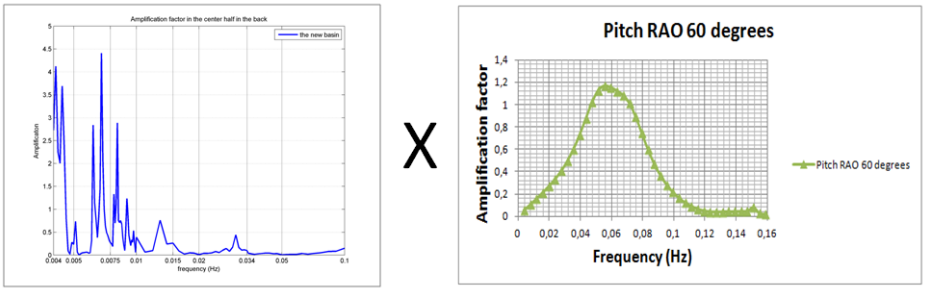

Figure 6.5: The coupled system is modeled by multiplying the basin resonance with the ship RAO over the same frequencies

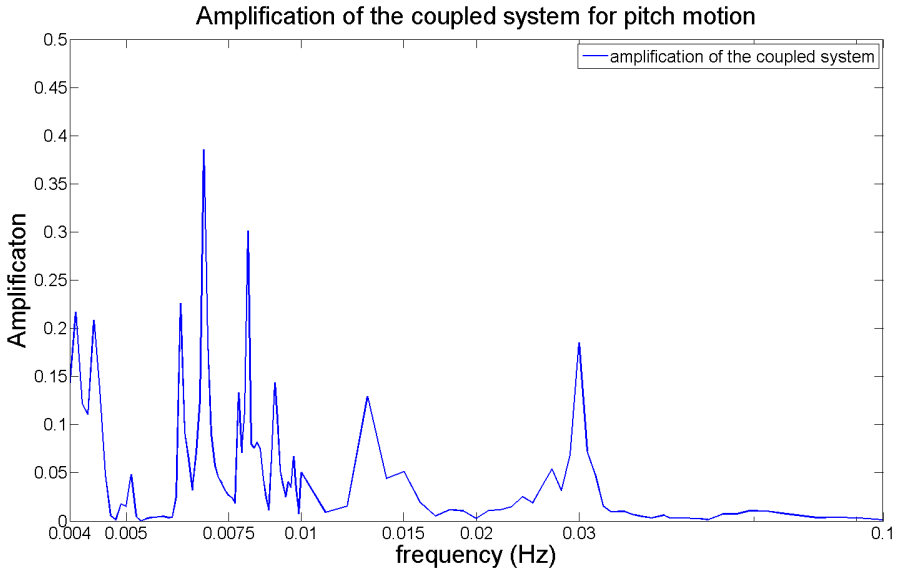

Figure 6.6: Amplification of the incoming wave for the coupled system of basin resonance and ship pitch motion

Table 6.3: Amplification peaks for the coupled system of basin resonance and the ship's pitch motion

Frequency (Hz)	Wave period (s)	Amplification (-)
0.0041	244	0.2
0.0044	227	0.2
0.0051	196	0.0
0.0062	161	0.2
0.0068	147	0.4
0.0081	123	0.3
0.0090	111	0.1
0.0130	77	0.1
0.0300	33	0.2

When looking at pitch the same conclusions can be drawn as for roll. The difference is that the pitch RAO has amplification factors that are much smaller than the roll RAO. Therefore table 6.3 shows even smaller amplification factors for the coupled system concerning pitch. Overall conclusion is that the coupled system of basin resonance and the bulk carrier pitch motion will not cause down time to the unloading operations.

6.1.4 Coupled system of basin resonance and the ship's horizontal motions

As the ship is situated in shallow water the orbital motion of the water particles is elliptical. Therefore the radius of the horizontal water motion is different from the vertical water motion. As it is not known what the amplitude of the horizontal water motion is, the coupled system for horizontal basin and ship motion cannot not be calculated. The obtained

RAO's in chapter 3.3.2 are not representative for the new basin situation as horizontal ship movement in the new basin will be damped by the mooring system.

6.1.5 Conclusion

The coupled system of basin resonance and vertical bulk carrier RAO results into peak amplification factors of incoming waves for a number of wave periods in the range of 100 to 250 seconds. The obtained results have been modeled for a ship in open water. As the ship movements will be damped by the mooring system these results are not representative for the lightering situation in the new basin.
However, the undamped couple system for vertical ship movement results into ship displacement values that have little chance of probability of occurrence. It can be assumed that the damped system will experience less movement as the mooring facility will decrease the vertical movement. Furthermore, it is questioned whether the duration of the long waves penetrating the harbor is long enough to trigger the basin resonance system. Therefore it can be concluded that the coupled system for vertical ship movement has very little contribution to the 5% downtime criterium of the new basin.
To draw conclusions on the horizontal effects of the coupled system amplification of the horizontal wave movement in the basin is needed. As the RAO's obtained for horizontal bulk carrier movement are obtained for an open water situation, these values are not representative to investigate the coupled basin ship horizontal movement in the new basin.

Chapter 7

Conclusions and recommendations

This final chapter describes the conclusions and recommendations of the analysis of the impact of the new basin on the current outer harbor of IJmuiden and the influence of long waves and basin resonance on a moored bulk carrier situated in the new basin.

7.1 Conclusions

This thesis concludes that long waves with wave periods between 10 and 250 seconds have minimal impact on the vertical movement of the moored bulk carrier. Contribution to the new basin down time criteria is negligible in comparison to other down time factors.

- Wave measurements in and outside the outer harbor indicate that waves with periods between 10 and 250 seconds penetrate the outer harbor. However, as the percentage of the wave energy penetrating the outer harbor is only a few percent of the energy measured for the waves just outside the outer harbor, it is questionable whether the energy values are sufficient to trigger the new basin resonance system, especially as no resonance incidents are reported in the current situation for the other harbor basins.
- Modeling the new basin in a PHAROS model of the outer harbor, based on uniform distribution of energy over all wave periods, results in standing wave patterns for wave periods between 100 and 250 seconds. However, for a typical incoming wave height measured at sea for long waves just outside of the outer harbor, resulting amplified wave heights at the bulk carrier mooring location are below critical wave heights.
- Modeled resonant wave periods in the PHAROS model coincide with results obtained by means of hand calculations based on standing wave formulas for harbor basins. The resulting standing wave patterns for the new basin show that the highest wave amplification in the new basin is caused by the potential occurrence of a standing wave between the end of the new basin and the end of the IJmond harbor situated opposite of the new basin.
- It is possible that basin amplification and ship response occur for the same wave period. Therefore the coupled ship response and basin resonance system is analyzed for the wave period range between 10 and 250 seconds. The Response Amplitude Operators have been calculated for the bulk carrier in a shallow open water situation to analyze the resonance periods for ship movement. The coupled response system does not result in further amplification of the vertical ship motion.

- The only possible change to the geometry of the new basin is decreasing the basin's width by 40 meter by changing the basin's slopes into steeper slopes. The change in geometry does not result into positive effects concerning resonance of the new basin and the other harbor basins.
- The PHAROS runs show a decrease of wave amplification in the harbor ship locks and the Hoogoven harbor situated in the end of the outer harbor.
- The implementation of the new basin can potentially cause standing waves to occur between the end of IJmond harbor and the end of the new basin. However, the amplification peaks concerning these standing waves are close to the modeled amplification peaks in the current situation. Although these peaks are calculated for the existing situation, there are no incident reports related to long wave amplification occurrences. This in combination with the little amount of energy measured in the outer harbor for long waves makes it questionable whether the standing wave will occur in the real situation.
- Data on ship resonance periods are limited. Therefore it is difficult to draw conclusions on moored ship response based on only a numerical wave study.

7.2 Recommendations

To improve study results the following actions are recommended.

- There is very little data available on long waves (periods larger than 50 seconds) near and inside the outer harbor of IJmuiden. More data should be generated on long waves by means of pressure box measurements to establish strong conclusions on the incoming wave climate and the probability of occurrence of certain long waves.
- RWS has just started AWAC measurements inside the outer harbor. Therefore the data used for the investigation of wave period sup to 30 seconds only concern several weeks of measurements. As the AWAC installations are permanently situated in the harbor more data will be available in the future and analyses concerning this broader range of data should be carried out to determine whether conclusions drawn in this thesis still apply for a broader dataset.
- To analyze the ship response in the IJmond harbor the future use of the IJmond harbor, the type of ships berthing inside the basin and the properties of the mooring facility should be analyzed. By use of a numerical wave model in combination with a ship response model it should be analyzed for the IJmond harbor what the effects on ship movement for the measured incoming wave climate are.
- During this thesis investigation it came to attention that it is difficult to obtain resonant periods for all six degrees of freedom for different types of ships. A database should be formed collecting all results on earlier RAO and ship resonance studies. The database can be used when similar cases of ship response are investigated in the future.

Bibliography

[1] *Deltares website*. http://www.deltares.nl/nl/software/919484/pharos.

[2] *Development plan ijmond harbor*. http://www.weekbladhuisaanhuis.nl/nieuws/194930-ijmondhaven-klaar-om-grootste-cruiseschepen-te-ontvangen.

[3] *Noordzee atlas*. http://www.noordzeeatlas.nl.

[4] *Wikipedia*. http://www.wikipedia.nl.

[5] Alkyon, *Seiches (of halingen) in de buitenhaven van ijmuiden*, A679, (2001).

[6] Arcadis and Deltares, *Opzet en calibratie modelinstrumentarium ijmuiden*, tech. report, Deltares.

[7] J. Battjes, *Stroming in waterlopen*, TU Delft, 2002.

[8] H. Bingham, *A hybrid boussinesq-panel method for predicting the motion of a moored ship*, Coastal Engineering, 40 (2000), pp. 21–38.

[9] J. Boeyinga, *Boussinesq-type wave modelling in port applications, workability assessment with triton, a boussinesq-type wave model*, MSc thesis, Delft University of Technology, Delft, (2010).

[10] K. d'Angremond, *Inleiding waterbouwkunde*, TU Delft, 2003.

[11] T. de Boer, *Voorstel variantkeuze planstudie lichteren*, tech. report, DHV.

[12] J. de Bont, W. van der Molen, J. van der Lem, H. Ligteringen, D. Mühlestein, and M. Howie, *Calculations of the motions of a ship moored with moormaster units*, (2010).

[13] M. de Jong, *Origin and prediction of seiches in rotterdam harbour basins*, Delft University of Technology, Delft, (2004).

[14] D. H. de Koning Gans, *Bulk carrier response amlitude operators*, (Personal consult 09-11-2011).

[15] A. de Kruif and A. Keijer, *Evenwichtsligging kennemerstrand en aanzanding havenmond ijmuiden*, tech. report, Rijkswaterstaat.

[16] Deltares, *Pharos manual version 9.10*, tech. report, Deltares.

[17] ——, *Planstudie lichteren ijmuiden*, (2009).

[18] DHV, *Ontwerpnota varianten*, tech. report, DHV.

[19] ——, *Concept afweging voorkeursvarianten planstudie lichteren*, BA1469, LW-AF20111272, (2010).

[20] ——, *Hydraulica en morfologie lichteren ijmuiden, fase 2: berekeningen en analyses met het detail model instrumentarium*, BA1469, LW-AF20112024, (2010).

[21] ——, *Memo, seiches in de buitenhaven van ijmuiden*, BA1469, (2010).

[22] ——, *Planstudie lichteren ijmuiden, analyse hydraulische condities fase 1*, BA1469, LW-AF20110853, (2010).

[23] EM. PROF. DR. IR. PINKSTER, *Calculating the rao's of a 200.000dwt bulk carrier*, (Personal consult 08-08-2011).

[24] L. HOLTHUYSEN, *Waves in oceanic and coastal waters*, Cambridge university press, New York, 2007.

[25] KNMI, *Wind data*. http://www.knmi.nl.

[26] H. LIGTERINGEN AND J. MOES, *Motions of moored ships in long waves*, in Int. Conf. on Port and Maritime R&D and Technology, 2001.

[27] MANAGING DIRECTOR AND HEAD TECHNICAL AFFAIRES, *Sea port ijmuiden*, (Meeting 29-03-2011).

[28] NORTEK, *Nortek as*. http://www.nortekusa.coml.

[29] NORTEK OCEANOGRAFISCHE INSTRUMENTEN EN DIENSTEN B.V., *Golf- en stromingsmetingen ijmuiden, averijhaven*, tech. report, Rijkswaterstaat Noord-Holland.

[30] RIJKSWATERSTAAT, *Waterbase*. http://www.waterbase.nl.

[31] ——, *Waternormalen*. http://www.waternormalen.nl.

[32] RIJKSWATERSTAAT AND DIRECTIE NOORD-HOLLAND, *Golfdoordringing in de haven van ijmuiden*, H0542, (1987).

[33] RIJKSWATERSTAAT NOORD-HOLLAND, *Systeemspecificatie insteekhaven,varianten planstudie lichteren*, tech. report, DHV.

[34] RIJKSWATERSTAAT NOORD-HOLLAND AND DIRECTIE WATER SCHEEPVAART EN REALISATIE INFRASTRUCTUUR, *Startnotitie lichteren buitenhaven ijmuiden*, (2010).

[35] ROM 3.1-99, *Design of the maritime configuration of ports, approach channels and harbour basins*, tech. report, Puertos del Estado.

[36] C. THORESEN, *Port Designer's Handbook: Recommendations and Guidelines*, Thomas Telford publishing, London, 2006.

[37] G. VAN DEN BRENK, *Wave measurements ijmuiden*, (Personal consult 14-04-2011).

[38] W. van der Molen, H. Ligteringen, J. van der Lem, and J. de Waal, *Behavior of a moored lng ship in swell waves*, Journal of waterway, port, coastal, and ocean engineering, 129 (2003), p. 15.

[39] W. Van der Molen and H. Moes, *General characteristics of south african ports and the safe mooring of ships*, SATC 2009, (2009).

[40] W. Van Der Molen, P. Monardez, and A. Van Dongeren, *Numerical simulation of long-period waves and ship motions in tomakomai port, japan*, Coastal Engineering Journal, 48 (2006), pp. 59–79.

[41] J. van Os, *Investigating the deltares pharos models*, (Personal consult 02-08-2011).

[42] working group no. 24 of the Permanent Technical Committee, *Criteria for movements of moored ships in harbors*, tech. report, PIANC.

[43] WSP, *Methods for determining the wave reflection coefficients of structures in a port, research summary*, (2009).

Appendices

Appendix A

Hydraulic conditions

A.1 Locations of measurement stations

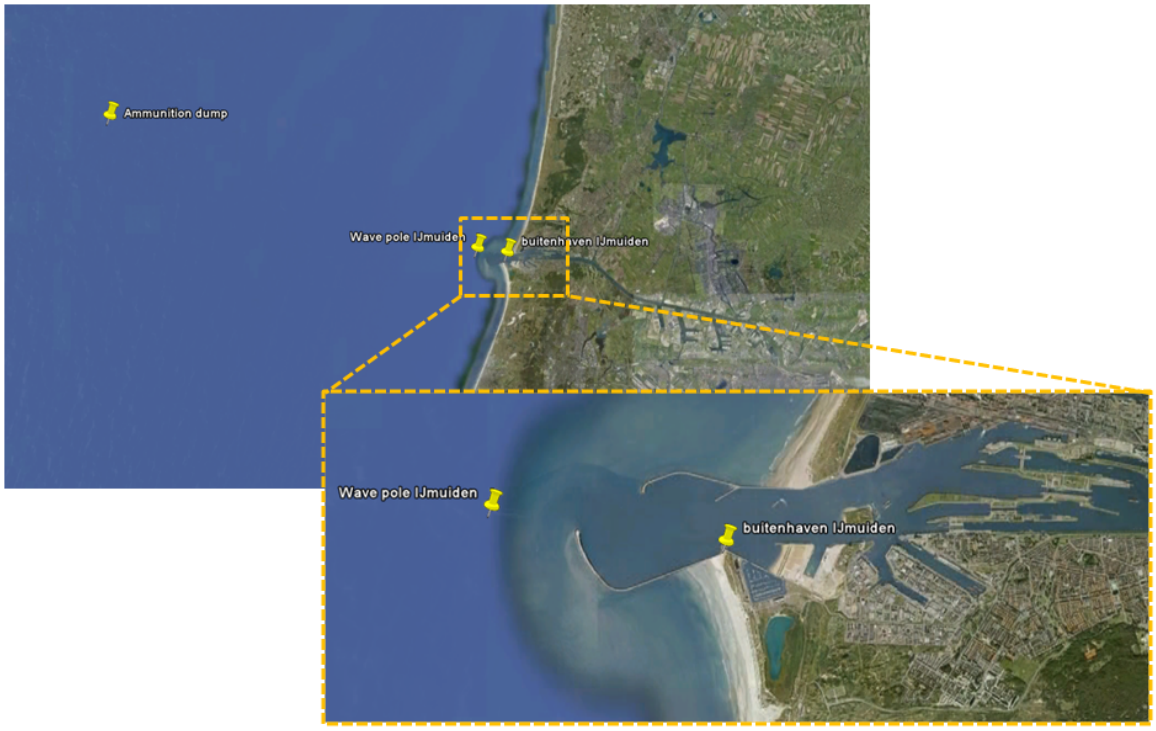

Figure A.1: Overview of the locations of the measurement stations around the harbor of IJmuiden

A.2 General characteristics of water levels in the port of IJmuiden

IJmuiden buitenhaven (Noordzee) Slotgemiddelden 1991.0

Algemene gegevens

1871	Aanvang waarnemingen
1 sep 1883	Peilschrijver geplaatst
14 jan 1988	DNM geplaatst

Gemiddelde waterstanden

type tij	HW-stand cm + NAP	LW-stand cm + NAP	tijverschil cm
gemiddeld tij	**97**	**-73**	**170**
springtij	**115**	**-75**	**190**
doodtij	**75**	**-64**	**139**
gem. waterstand		**2**	

Gemiddelde havengetallen waarden maansverloop

type tij cq grootheid	HW-tijd u:min	tijd u:min	LW-tijd u:min
gemiddeld tij	**2:37**		**10:37**
springtij	**2:38**		**10:44**
doodtij	**2:37**		**10:34**
duur rijzing		**4:25**	
duur daling		**8:00**	

Gemiddelde over- en onderschrijdings frequentie per jaar geldig voor de toestand 1985

overschrijding hoogwaterstanden		onderschrijding laagwaterstanden	
frequentie	stand in cm + NAP	frequentie	stand in cm + NAP
1x per 10.000 jaar	**515**	1x per 10 jaar	**-205**
1x per 1.000 jaar	**435**	1 x per jaar	**-170**
1x per 100 jaar	**360**		
1x per 50 jaar	**340**	LLWS 1985.0	**-95**
1x per 20 jaar	**310**		
1x per 10 jaar	**290**		
1x per 5 jaar	**270**		
1x per 2 jaar (grenspeil)	**250**		
1x per jaar	**235**		
2x per jaar	**210**		
5x per jaar	**190**		
basispeil	**515**		
ontwerppeil	**515**		

Bijzonderheden:

Datum	stand cm + NAP	kenmerkende waarden	periode
1 feb 1953	**385**	hoogst bekende waarde	(periode 1951...1990)
15 mrt 1964	**-240**	laagst bekende waarde	(periode 1951...1990)
2 apr 1973	**320**	maximale rijzing	(periode 1971...1990)
4 jan 1976	**317**	maximale daling	(periode 1971...1990)

A.3 Wind distributions at IJmuiden obtained from KNMI website

Return level (m/s)
Location: 225 IJmuiden, Season: Year
Wind direction (x 10 degrees)

T (year)	20-40	50-70	80-100	110-130	140-160	170-190	200-220	230-250	260-280	290-310	320-340	350-10	omni
0,5	12,8	11,9	10,7	10,4	11,8	14,5	17	18	17,5	15,9	14,4	13,4	19
1	13,9	12,8	11,6	11,4	12,8	15,5	18,1	19,2	18,7	17,3	15,8	14,8	20,1
2	15,1	13,7	12,5	12,2	13,8	16,5	19,1	20,2	19,8	18,4	17,2	16	21,2
5	16,4	14,9	13,4	13,2	14,9	17,6	20,2	21,5	21,2	19,9	18,7	17,6	22,4
10	17,4	15,7	14,1	13,9	15,6	18,4	21	22,4	22,2	21	19,8	18,7	23,3
20	18,4	16,5	14,8	14,5	16,2	19,1	21,8	23,2	23,1	22	20,9	19,8	24,2
50	19,6	17,5	15,6	15,2	17	20	22,7	24,3	24,3	23,3	22,3	21,2	25,2
100	20,5	18,1	16,1	15,7	17,6	20,7	23,4	25	25,1	24,2	23,3	22,3	26
200	21,4	18,8	16,6	16,1	18,1	21,3	24	25,8	25,9	25	24,2	23,3	26,7
500	22,5	19,7	17,3	16,7	18,9	22,1	24,7	26,6	26,9	26,1	25,4	24,5	27,6
1000	23,4	20,3	17,7	17,1	19,4	22,7	25,3	27,2	27,5	26,8	26,2	25,4	28,3
2000	24,2	20,9	18,1	17,5	19,9	23,3	25,8	27,8	28,2	27,5	27	26,2	28,9
5000	25,2	21,7	18,7	18	20,6	24	26,5	28,5	28,9	28,5	28	27,2	29,6
10000	25,9	22,3	19,1	18,3	21,2	24,5	27	29	29,4	29,1	28,7	27,9	30,2

FREQUENCY TABLE OF POTENTIAL WIND SPEED - CUMULATIVE RELATIVE

225 Ijmuiden, Year 1971-2000

Windspeed [m/s]	Var/ Calm	350-10	20-40	50-70	80-100	110-130	140-160	170-190	200-220	230-250	260-280	290-310	320-340	Cum.
0.0 - 0.9	0,1	0,06	0,06	0,04	0,06	0,07	0,09	0,09	0,07	0,07	0,06	0,05	0,06	0,88
1.0 - 1.9	0,69	0,31	0,29	0,16	0,39	0,48	0,45	0,43	0,34	0,32	0,34	0,31	0,35	4,87
2.0 - 2.9	1,05	0,81	0,81	0,35	1,23	1,32	1,2	1,02	0,8	0,8	0,85	0,8	0,88	11,91
3.0 - 3.9	1,09	1,56	1,75	0,66	2,54	2,35	2,28	1,87	1,58	1,77	1,76	1,5	1,53	22,22
4.0 - 4.9	1,09	2,36	2,92	1,12	4,2	3,28	3,46	2,93	2,43	2,75	2,52	2,25	2,35	33,67
5.0 - 5.9	1,09	3,42	4,27	1,79	6,22	3,93	4,47	4,1	3,46	3,79	3,31	2,95	3,29	46,09
6.0 - 6.9	1,1	4,28	5,12	2,68	7,57	4,52	5,37	5,34	4,8	5,36	4,28	3,66	3,99	58,07
7.0 - 7.9	1,1	5,09	5,71	3,47	8,61	4,82	5,85	6,25	6,21	6,79	5,33	4,41	4,69	68,33
8.0 - 8.9	-	5,68	6,13	4,09	9,25	4,96	6,15	6,95	7,4	8,04	6,1	5,14	5,35	76,33
9.0 - 9.9	-	6,11	6,47	4,61	9,8	5,03	6,36	7,46	8,67	9,36	6,85	5,68	5,93	83,42
10.0 - 10.9	-	6,32	6,66	4,92	10,03	5,06	6,47	7,82	9,67	10,33	7,49	6,06	6,32	88,26
11.0 - 11.9	-	6,44	6,75	5,11	10,17	5,07	6,52	8,08	10,75	11,13	8,1	6,38	6,58	92,16
12.0 - 12.9	-	6,52	6,79	5,2	10,25	5,07	6,54	8,27	11,59	11,9	8,53	6,65	6,77	95,2
13.0 - 13.9	-	6,57	6,81	5,27	10,31	5,07	6,56	8,39	12,19	12,29	8,83	6,81	6,88	97,09
14.0 - 14.9	-	6,59	6,83	5,29	10,34	5,07	6,56	8,45	12,65	12,55	9,11	6,93	6,93	98,4
15.0 - 15.9	-	6,61	6,84	5,29	10,35	-	6,56	8,48	12,89	12,68	9,26	7,01	6,97	99,12
16.0 - 16.9	-	6,62	6,84	5,29	10,35	-	-	8,5	13,04	12,76	9,36	7,05	6,99	99,53
17.0 - 17.9	-	6,62	6,84	5,3	-	-	-	8,51	13,1	12,8	9,42	7,08	7	99,76
18.0 - 18.9	-	6,62	6,84	-	-	-	-	8,51	13,14	12,83	9,46	7,09	7	99,89
19.0 - 19.9	-	6,62	-	-	-	-	-	8,52	13,16	12,85	9,48	7,09	7,01	99,95
20.0 - 20.9	-	6,62	-	-	-	-	-	8,52	13,17	12,85	9,49	7,1	7,01	99,98
21.0 - 21.9	-	-	-	-	-	-	-	-	13,17	12,86	9,49	7,1	7,01	99,99
22.0 - 22.9	-	-	-	-	-	-	-	-	13,17	12,86	9,49	7,1	7,01	99,99
23.0 - 23.9	-	-	-	-	-	-	-	-	13,17	12,86	9,49	7,1	-	100
24.0 - 24.9	-	-	-	-	-	-	-	-	13,18	12,86	9,49	7,1	-	100
25.0 - 25.9	-	-	-	-	-	-	-	-	-	12,86	-	7,1	-	100
26.0 - 26.9	-	-	-	-	-	-	-	-	-	-	-	-	-	-
27.0 - 27.9	-	-	-	-	-	-	-	-	-	-	-	-	-	-
28 and higher	-	-	-	-	-	-	-	-	-	-	-	-	-	-

Figure A.2: Extreme value distribution and normal wind distribution for the IJmuiden harbor (Source: KNMI [25])

A.4 Summary of normal wave conditions at IJmuiden

	DIR					IJmuiden Munitiestortplaats							
	van	0	30	60	90	120	150	180	210	240	270	300	330
HS	tot	30	60	90	120	150	180	210	240	270	300	330	360
van	tot												
0	50	0,02	0,00	0,00	0,00	0,00	0,00	0,00	0,01	0,02	0,02	0,03	0,04
50	100	0,05	0,01	0,01	0,01	0,01	0,01	0,01	0,04	0,03	0,02	0,04	0,07
100	150	0,03	0,01	0,00	0,00	0,02	0,00	0,01	0,05	0,02	0,02	0,03	0,05
150	200	0,01	0,00	0,00	0,00	0,00	0,00	0,01	0,04	0,01	0,02	0,02	0,03
200	250	0,00	0,00	0,00	0,00	0,00	0,00	0,00	0,03	0,01	0,01	0,01	0,01
250	300	0,00	0,00	0,00	0,00	0,00	0,00	0,00	0,02	0,01	0,00	0,01	0,01
300	350	0,00	0,00	0,00	0,00	0,00	0,00	0,00	0,01	0,00	0,00	0,01	0,00
350	400	0,00	0,00	0,00	0,00	0,00	0,00	0,00	0,00	0,00	0,00	0,00	0,00
400	450	0,00	0,00	0,00	0,00	0,00	0,00	0,00	0,00	0,00	0,00	0,00	0,00
450	500	0,00	0,00	0,00	0,00	0,00	0,00	0,00	0,00	0,00	0,00	0,00	0,00
		0,11	0,03	0,02	0,01	0,03	0,02	0,03	0,20	0,10	0,09	0,14	0,21

	DIR					IJmuiden Munitiestortplaats							
	van	0	30	60	90	120	150	180	210	240	270	300	330
Tmean	tot	30	60	90	120	150	180	210	240	270	300	330	360
van	tot												
0	1	0,00	0,00	0,00	0,00	0,00	0,00	0,00	0,00	0,00	0,00	0,00	0,00
1	2	0,00	0,00	0,00	0,00	0,00	0,00	0,00	0,00	0,00	0,00	0,00	0,00
2	3	0,00	0,00	0,00	0,00	0,00	0,00	0,00	0,00	0,00	0,00	0,00	0,00
3	4	0,04	0,02	0,01	0,01	0,01	0,01	0,02	0,05	0,03	0,03	0,03	0,03
4	5	0,05	0,01	0,00	0,00	0,02	0,01	0,01	0,09	0,04	0,04	0,06	0,08
5	6	0,01	0,00	0,00	0,00	0,00	0,00	0,00	0,05	0,02	0,02	0,04	0,07
6	7	0,00	0,00	0,00	0,00	0,00	0,00	0,00	0,01	0,00	0,01	0,01	0,02
7	8	0,00	0,00	0,00	0,00	0,00	0,00	0,00	0,00	0,00	0,00	0,00	0,00
8	9	0,00	0,00	0,00	0,00	0,00	0,00	0,00	0,00	0,00	0,00	0,00	0,00
9	10	0,00	0,00	0,00	0,00	0,00	0,00	0,00	0,00	0,00	0,00	0,00	0,00
10		0,00	0,00	0,00	0,00	0,00	0,00	0,00	0,00	0,00	0,00	0,00	0,00
		0,11	0,03	0,02	0,01	0,03	0,02	0,03	0,20	0,10	0,09	0,14	0,21

	Tmean					IJmuiden Munitiestortplaats							
	van	0	1	2	3	4	5	6	7	8	9		
Hs	tot	1	2	3	4	5	6	7	8	9	10		
van	tot												
0	50	0,00	0,00	0,01	0,10	0,04	0,00	0,00	0,00	0,00	0,00	0,15	
50	100	0,00	0,00	0,00	0,15	0,12	0,03	0,00	0,00	0,00	0,00	0,31	
100	150	0,00	0,00	0,00	0,04	0,16	0,04	0,00	0,00	0,00	0,00	0,24	
150	200	0,00	0,00	0,00	0,00	0,09	0,04	0,00	0,00	0,00	0,00	0,14	
200	250	0,00	0,00	0,00	0,00	0,02	0,05	0,00	0,00	0,00	0,00	0,08	
250	300	0,00	0,00	0,00	0,00	0,00	0,03	0,01	0,00	0,00	0,00	0,04	
300	350	0,00	0,00	0,00	0,00	0,00	0,01	0,02	0,00	0,00	0,00	0,03	
350	400	0,00	0,00	0,00	0,00	0,00	0,00	0,01	0,00	0,00	0,00	0,01	
400	450	0,00	0,00	0,00	0,00	0,00	0,00	0,00	0,00	0,00	0,00	0,01	
450	500	0,00	0,00	0,00	0,00	0,00	0,00	0,00	0,00	0,00	0,00	0,00	
		0,00	0,00	0,02	0,29	0,42	0,21	0,05	0,01	0,00	0,00	1,00	

	Tmean					IJmuiden Stroommeetpaal							
	van	0	1	2	3	4	5	6	7	8	9		
Hs	tot	1	2	3	4	5	6	7	8	9	10		
van	tot												
0	50	0,00	0,00	0,03	0,17	0,04	0,01	0,00	0,00	0,00	0,00	0,26	
50	100	0,00	0,00	0,02	0,17	0,09	0,02	0,00	0,00	0,00	0,00	0,30	
100	150	0,00	0,00	0,00	0,10	0,09	0,01	0,00	0,00	0,00	0,00	0,20	
150	200	0,00	0,00	0,00	0,02	0,09	0,01	0,00	0,00	0,00	0,00	0,12	
200	250	0,00	0,00	0,00	0,00	0,05	0,01	0,00	0,00	0,00	0,00	0,06	
250	300	0,00	0,00	0,00	0,00	0,01	0,02	0,00	0,00	0,00	0,00	0,03	
300	350	0,00	0,00	0,00	0,00	0,00	0,01	0,00	0,00	0,00	0,00	0,02	
350	400	0,00	0,00	0,00	0,00	0,00	0,01	0,00	0,00	0,00	0,00	0,01	
400	450	0,00	0,00	0,00	0,00	0,00	0,00	0,00	0,00	0,00	0,00	0,00	
450	500	0,00	0,00	0,00	0,00	0,00	0,00	0,00	0,00	0,00	0,00	0,00	
		0,00	0,00	0,05	0,46	0,37	0,09	0,02	0,00	0,00	0,00	1,00	

A.5 Extreme value calculation considering the wave height near IJmuiden

As explained in chapter 2.6.1 figure A.3 shows a 1/1 per year probability of occurrence of a 5 meter wave height. This complies with the extreme wave heights considered by HR2006 in figure A.4

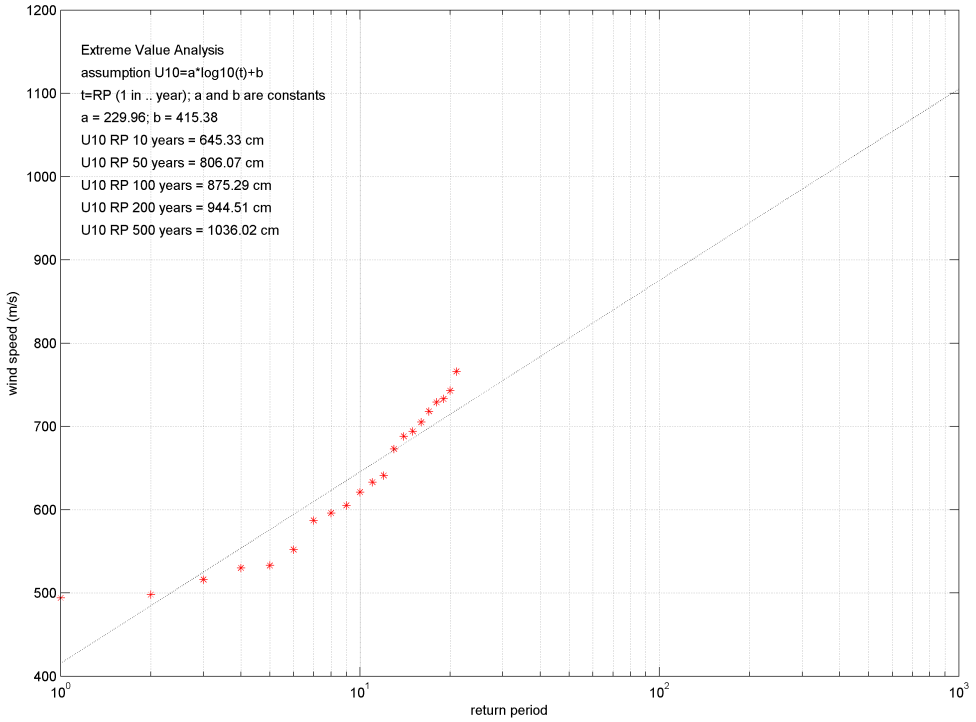

Figure A.3: Extreme value calculation of wave heights (source:DHV)

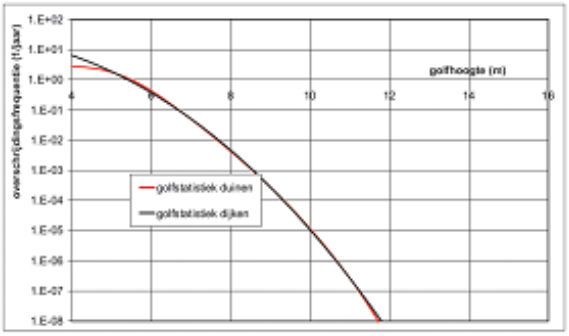

Figure A.4: Extreme wave heights considered by HR2006

A.6 One dimensional long wave spectra

The results for the long wave action in the outer harbor have been obtained from a technical report provided by Arcadis and Deltares [6]. For this research data was obtained from pressure box measurements. These pressure boxes were installed in the IJmond harbor, at the Midden sluice and in the Vissers harbor. The pressure boxes measured water levels at an interval of 2 Hz. The data has been average over periods of 15 seconds and transferred into continue signals without intervals. All results have been filtered with a high pass Butterworth filter to filter out the astronomical tide [6].
Spectral plots have been derived for eight selected moments in time. These moments have been chosen as the significant wave heights at the three location at those moments were highest in the obtained data.

The spectra include a frequency band between 0.0001 and 0.05 Hz (wave periods of 50 seconds up to 167 minutes). As horizontal ship movement is being investigated, the emphasis of the study lies on wave periods between 120 and 200 seconds. This concerns the frequency and between 0.005 and 0.008 Hz.
The figures provided in this appendix show two spectra for every graph. The blue colored spectra concerns the spectra measured at the provided location, the gray colored spectra signifies the spectrum measured at the wave pole just outside the outer harbor. The spectra derived at the wave pole for the graphs providing the data obtained at the first of April strike out in comparison to the other graphs. This is not a flaw in the analysis, the scale on the y axis is much smaller and therefore provides a different spectrum image.

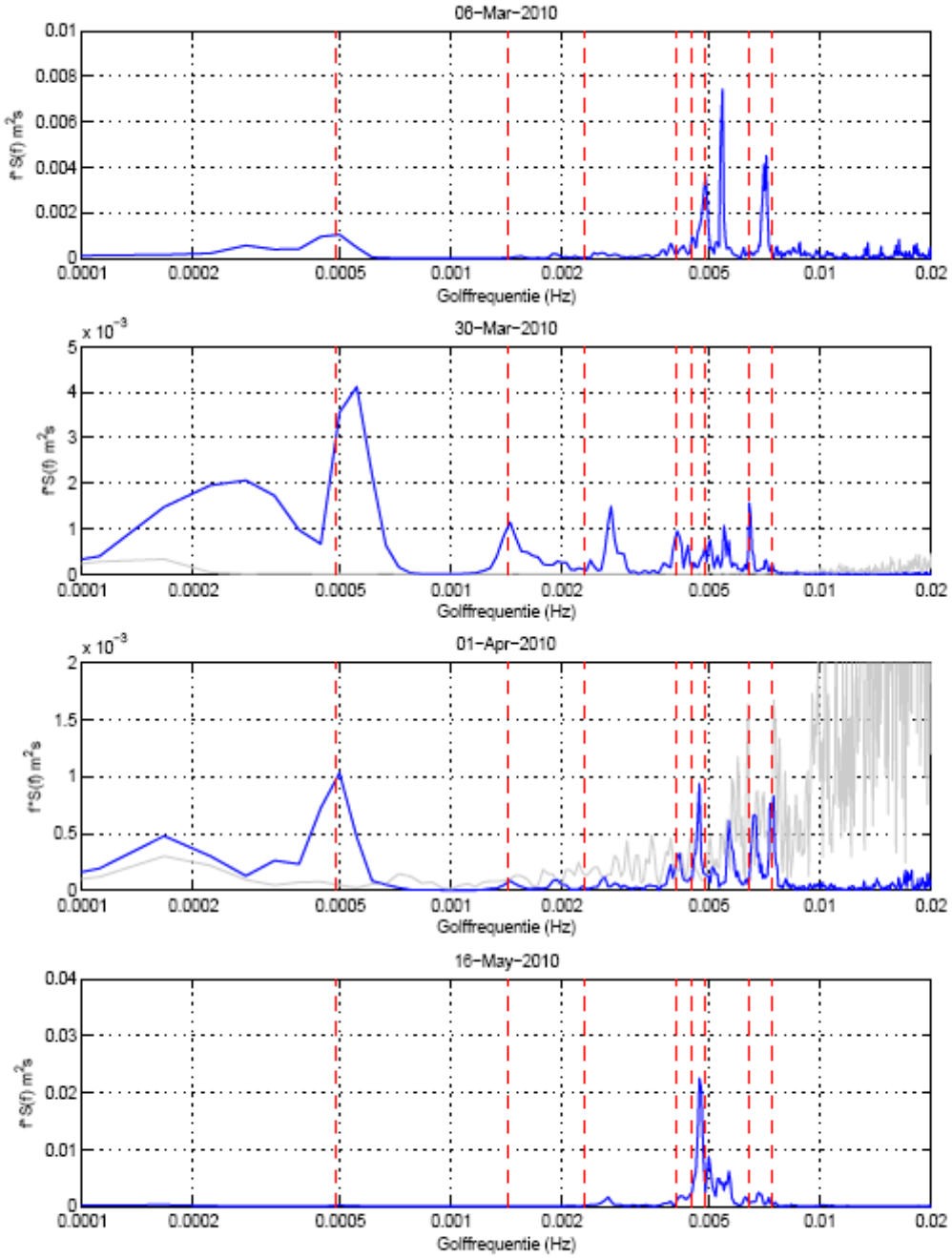

Figure A.5: One dimensional wave spectra derived at the IJmond harbor

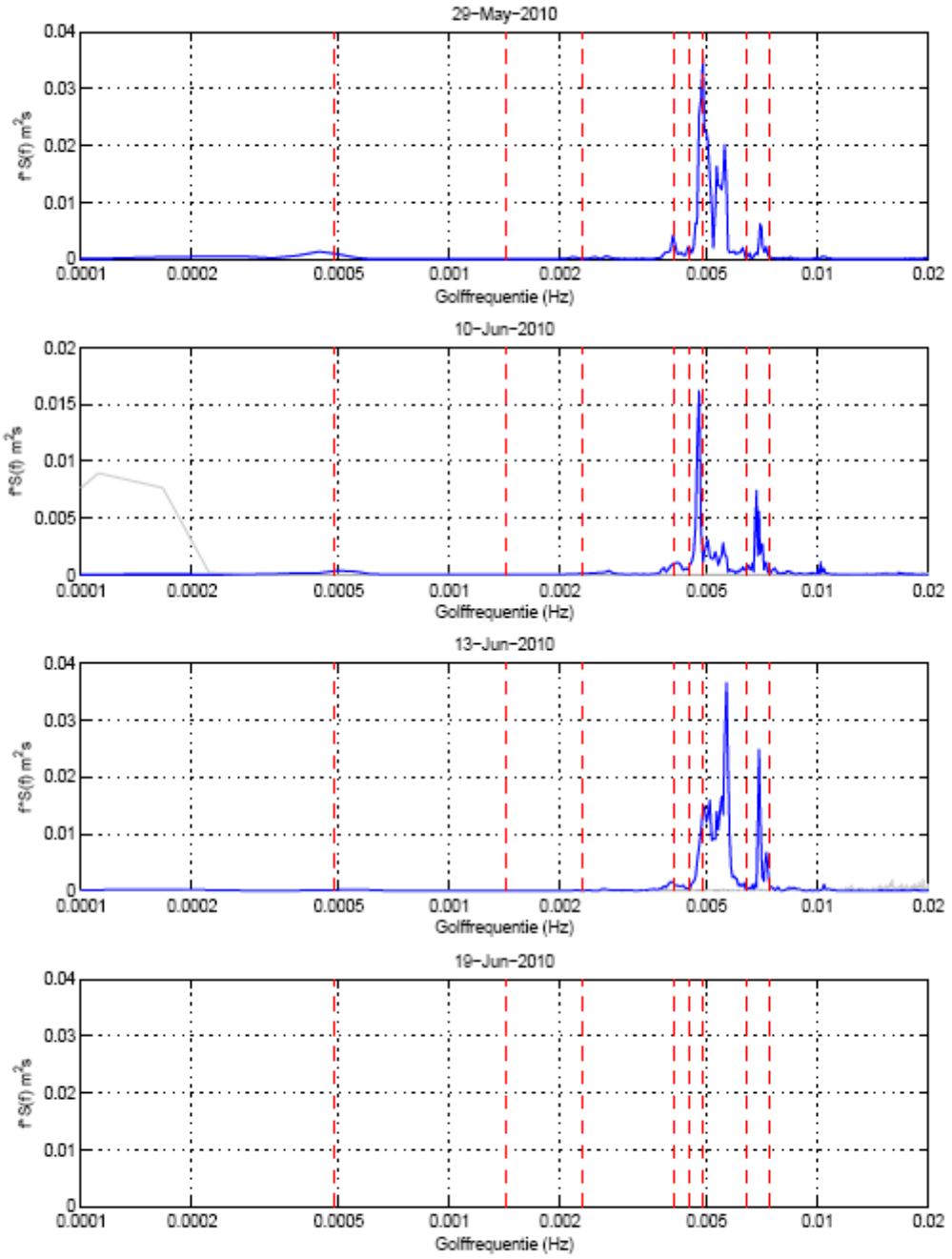

Figure A.6: One dimensional wave spectra derived at the IJmond harbor

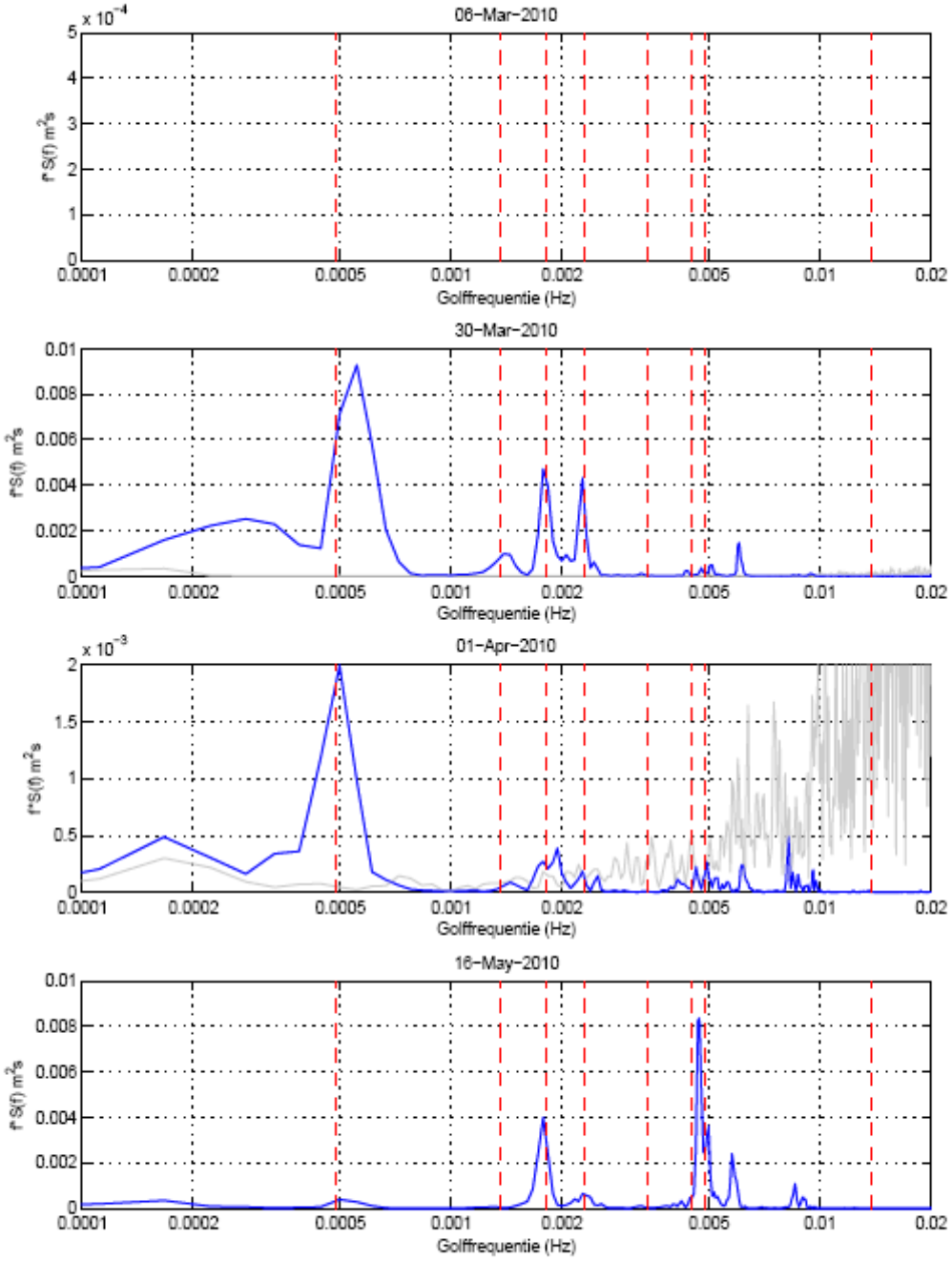

Figure A.7: One dimensional wave spectra derived at the Vissers harbor

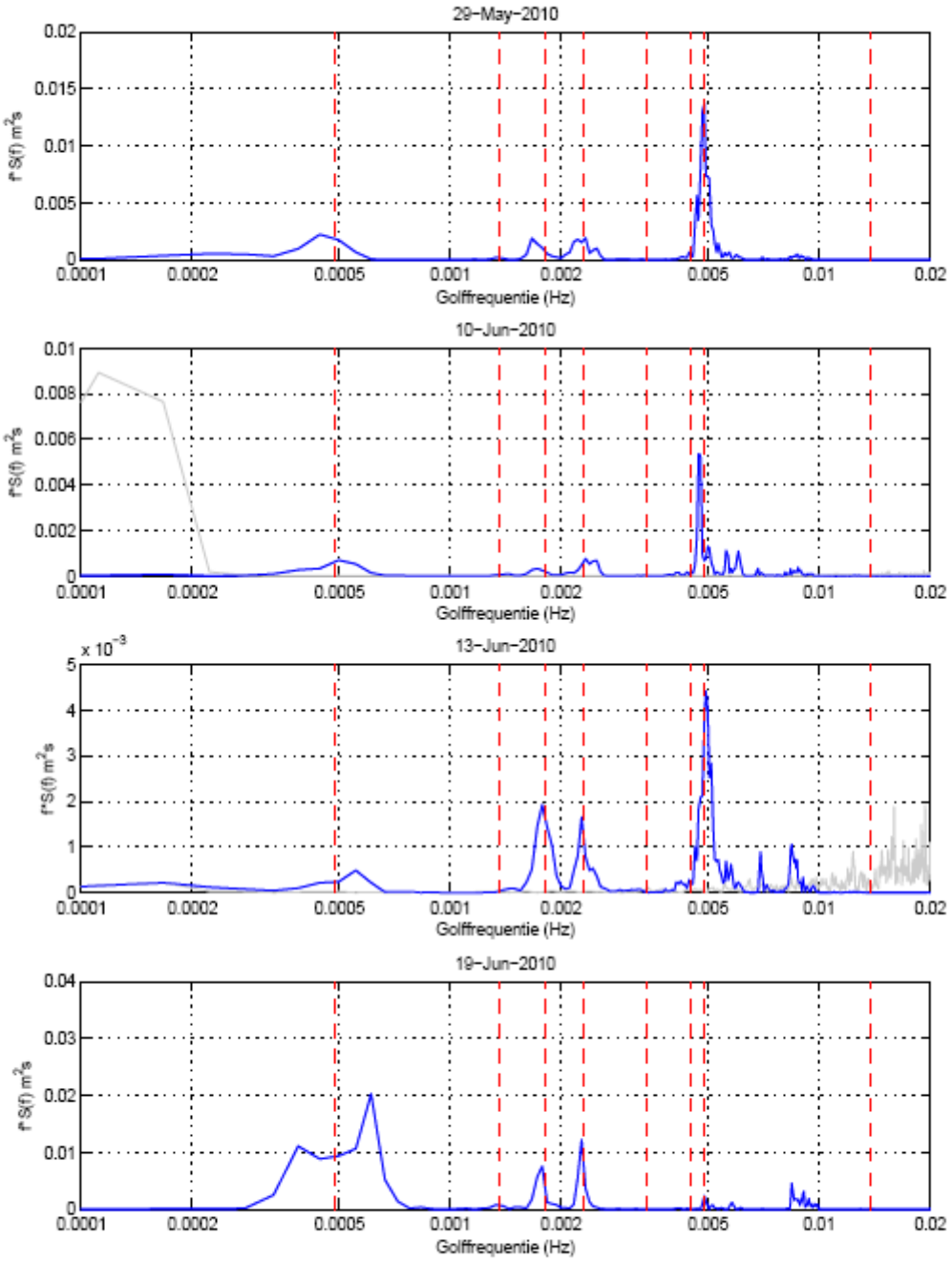

Figure A.8: One dimensional wave spectra derived at the Vissers harbor

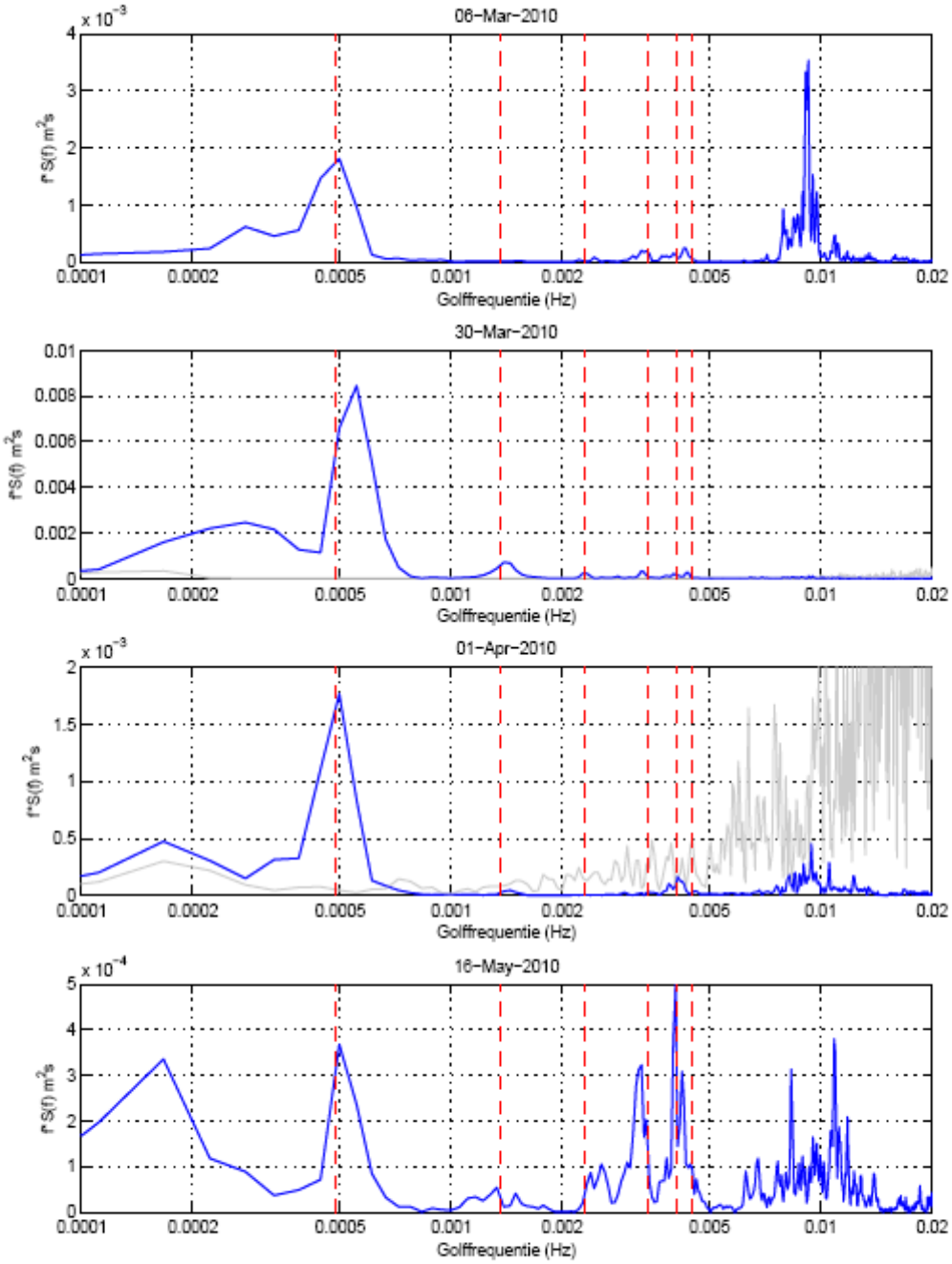

Figure A.9: One dimensional wave spectra derived at the Midden ship lock

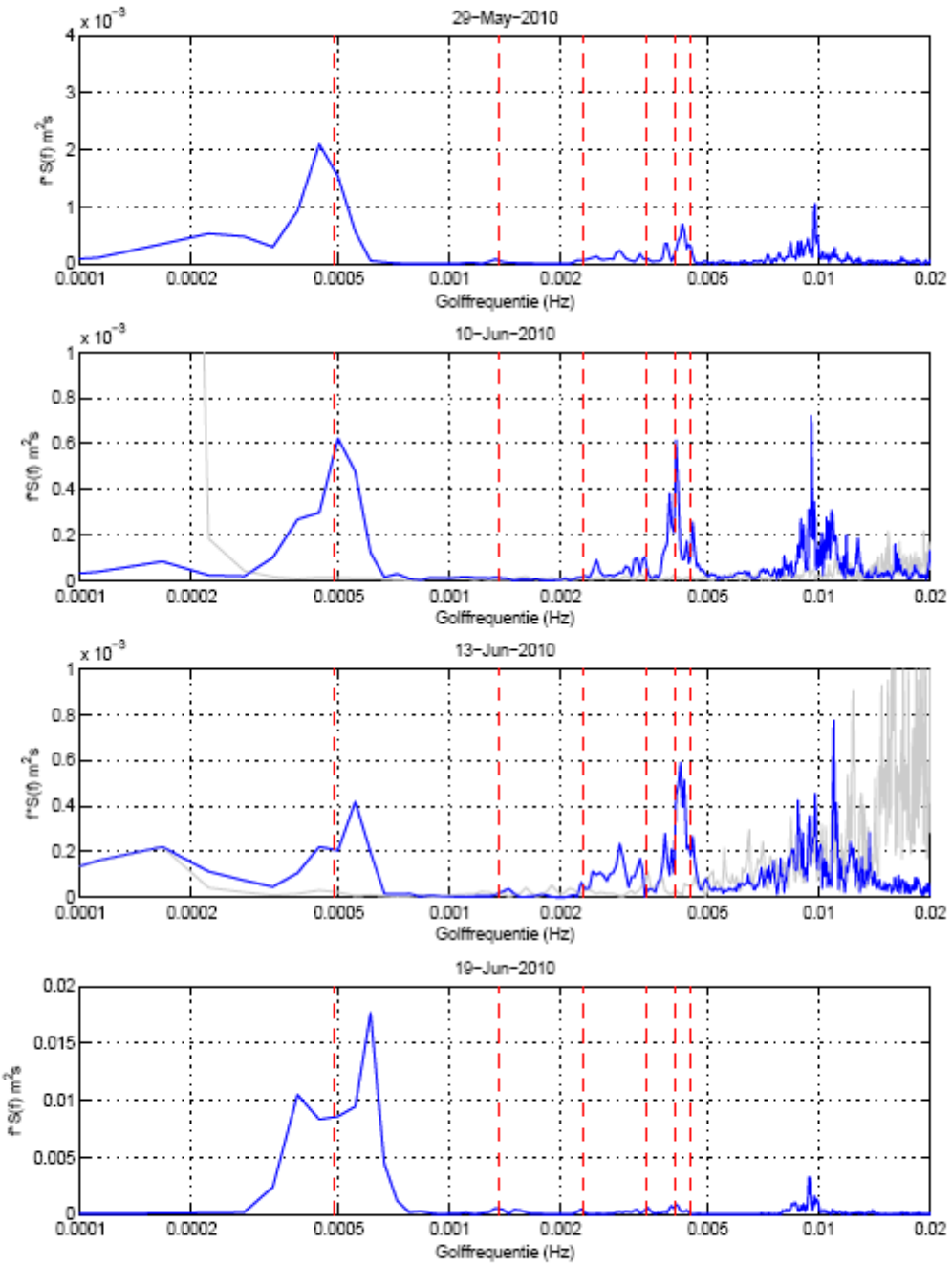

Figure A.10: One dimensional wave spectra derived at the Midden ship lock

Appendix B

Bulk carrier analyses

B.1 Relation between resonance frequencies of ships with different dimensions

In this appendix, graphs are implemented to analyze whether there is a relation between ship dimensions and the resonance frequencies that cause severe ship movement. The data dots in the graphs represent several ships which have been analyzed in earlier publications on ship resonance. In every graph a red line is added in the bottom of the figure. This line represents the period band in which commonly stated ships should experience resonance in its degree of free movement. The y axis does not represent any value, it only provides space between the data points. In case a vertical line/band can been drawn through the dots it signifies that a relation exists between the resonance periods of the ships. However, this analysis clearly shows that a relation for different ship dimensions for all degrees of free movement is hard to find.

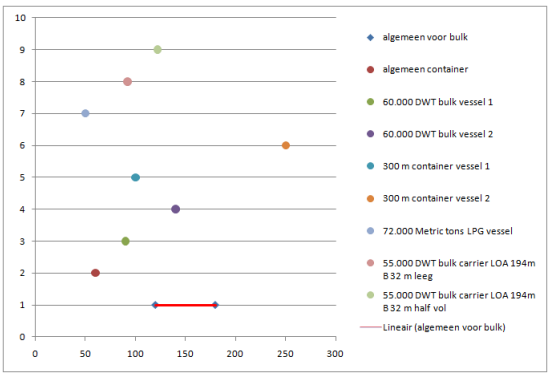

Figure B.1: Relations for surge periods for different ship dimensions. The x axis concerns the wave period that causes ship resonance, the y axis represents the ship type

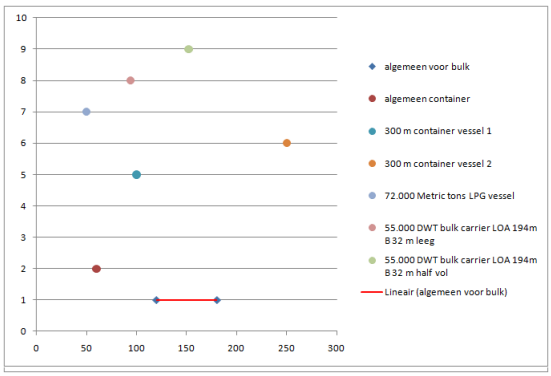

Figure B.2: Relations for sway periods for different ship dimensions. The x axis concerns the wave period that causes ship resonance, the y axis represents the ship type

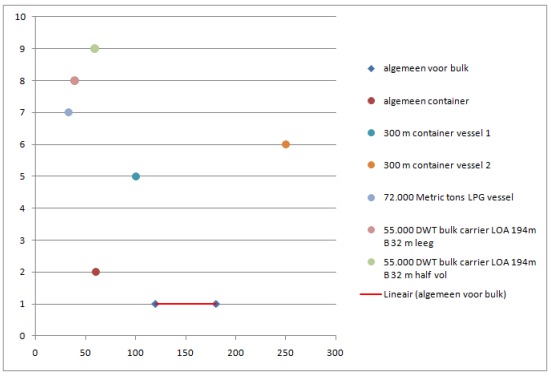

Figure B.3: Relations for yaw periods for different ship dimensions. The x axis concerns the wave period that causes ship resonance, the y axis represents the ship type

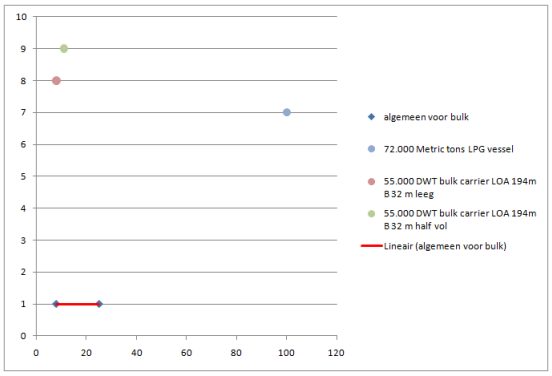

Figure B.4: Relations for heave periods for different ship dimensions. The x axis concerns the wave period that causes ship resonance, the y axis represents the ship type

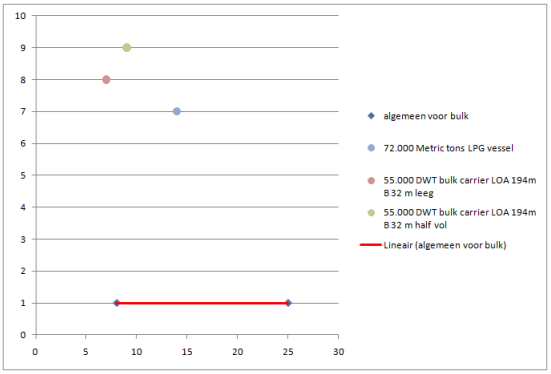

Figure B.5: Relations for roll periods for different ship dimensions. The x axis concerns the wave period that causes ship resonance, the y axis represents the ship type

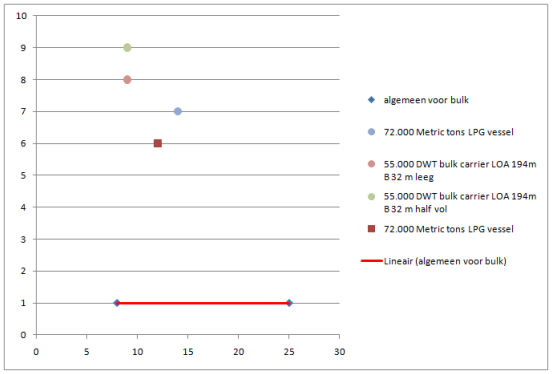

Figure B.6: Relations for pitch periods for different ship dimensions. The x axis concerns the wave period that causes ship resonance, the y axis represents the ship type

B.2 Response Amplitude Operator of a 200.000 DWT ship in open water

After consult with em. prof. dr. ir. Pinkster, the former head of Marine Technology at the TU Delft, results of a 3 Dimensional diffraction model called DELFRAC have been provided concerning a 300 meter LOA bulk carrier in 20 meter deep water. This program is commonly used in marine engineering to calculate resonance frequencies of a ship's movement in it degrees of freedom.
In the modeled situation the bulk carrier is assumed to be free in all degrees of its movement (as if the vessel lay still at open sea). This assumption is different from the real situation, were the bulk carrier is moored to a berthing location in the new basin. However, as this ROA analysis is the best information at hand for the study the results will be used for this thesis.
Especially the orizontal motions of the bulk vessel will be different in the real situation as the berthing location counteracts theses motions strongly due to the reaction of the breasting dolphins and mooring lines. Results in the real situation will be more damped due to the mooring situation.

The analysis is carried out for wave periods between 6 and 250 seconds.

B.3 Overview of the modeled bulk carrier in Delfrac

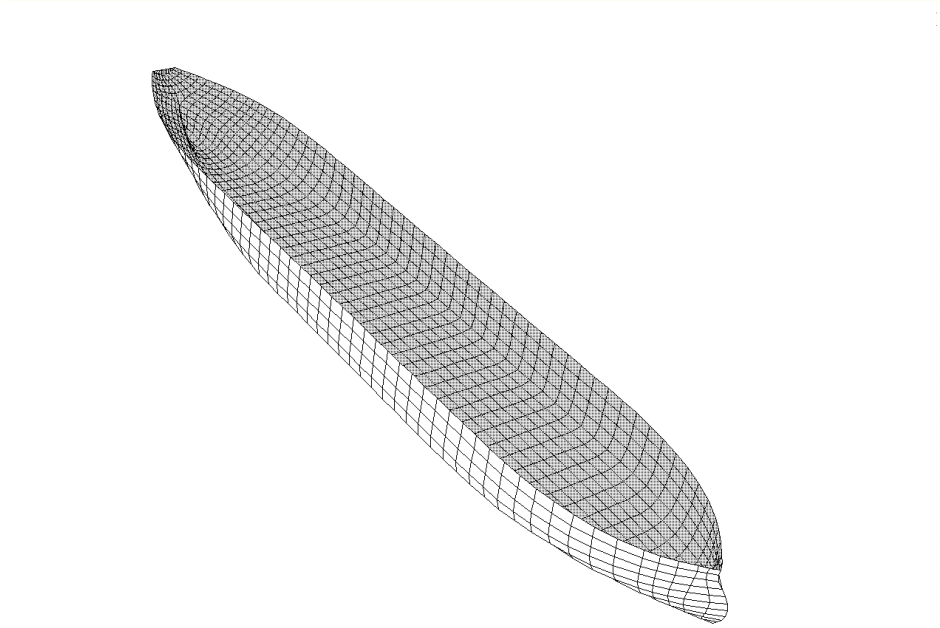

Figure B.7: The bulk carrier modeled in DELFRAC

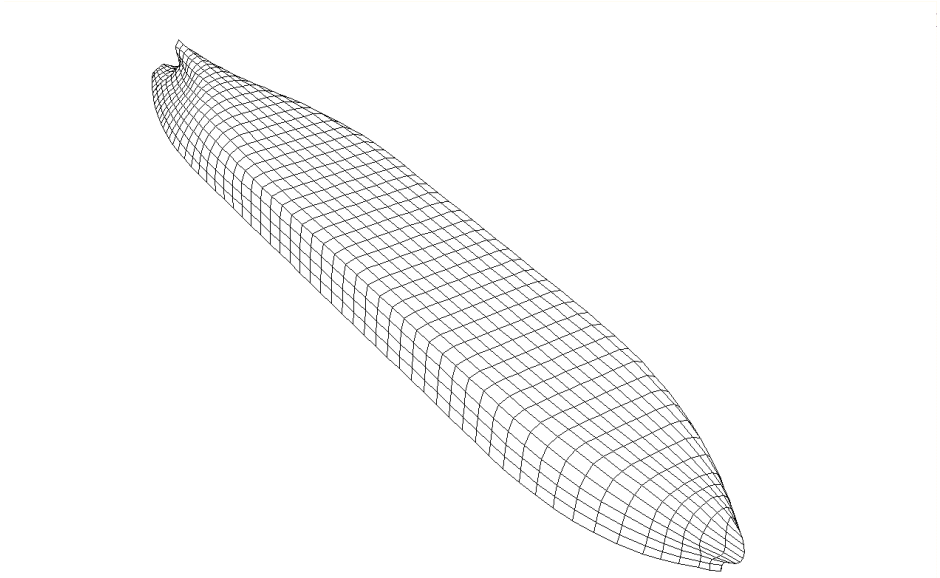

Figure B.8: The bulk carrier, bottom view

B.3.1 Results of the RAO's in all degrees of free ship movement

It can be seen that severe ship motion concerning surge occurs for the low frequencies belonging to wave periods up to 200 seconds (see figure B.9. This is the case for all incoming wave directions except for waves arriving straight at the stern. This is obvious as those waves arrive perpendicular to the surge motion of the bulk vessel and therefore cannot influence this motion.
Conclusions can be drawn that the ship's surge motion is strongly reacting to low wave frequencies around 0.005 Hz.

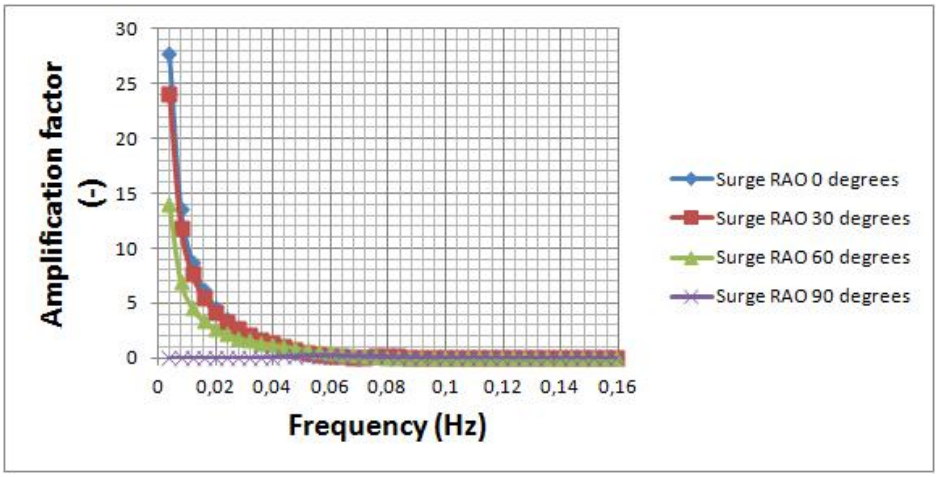

Figure B.9: RAO results for surge movement of the bulk carrier

When looking at the DELFRAC results for the bulk carrier's sway motion (figure B.10 it can be concluded that results are identical. Only in the opposite incoming wave direction. This is what would be expected as sway is perpendicular to surge therefore waves arriving perpendicular to the ship (in an angle of 90 degrees) have most effect on the sway motion and as waves arrive in a more parallel direction the effect on the sway motion becomes less. As is the case for surge motion the low wave frequencies cause the highest ship movement.

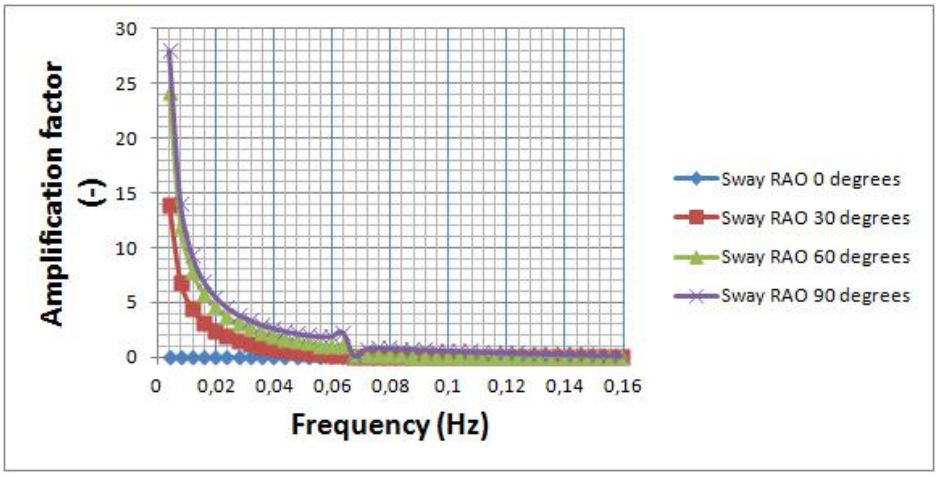

Figure B.10: RAO for sway movement of the bulk carrier

Yaw is the horizontal angular movement of the bulk carrier around its middle point. When waves arrive the ship from an angle of zero or 90 degrees, this will have little effect on this angular movement. However waves approaching in angle will effect the yaw motion of the ship. It can be concluded that waves arriving from a 60 degrees angle have the highest effect on yaw. Both for the 30 and 60 degree incoming waves the low wave frequencies provide the highest yaw movement.
As stated before this analysis assumes that the bulk carrier is positioned in open water. In the real situation berthing dolphins will counteract yaw movement of the vessel. Taking this into it can be assumed that the effect of the yaw motion of the moored bulk carrier will be a lot less in the real situation than as analyzed in figure B.11

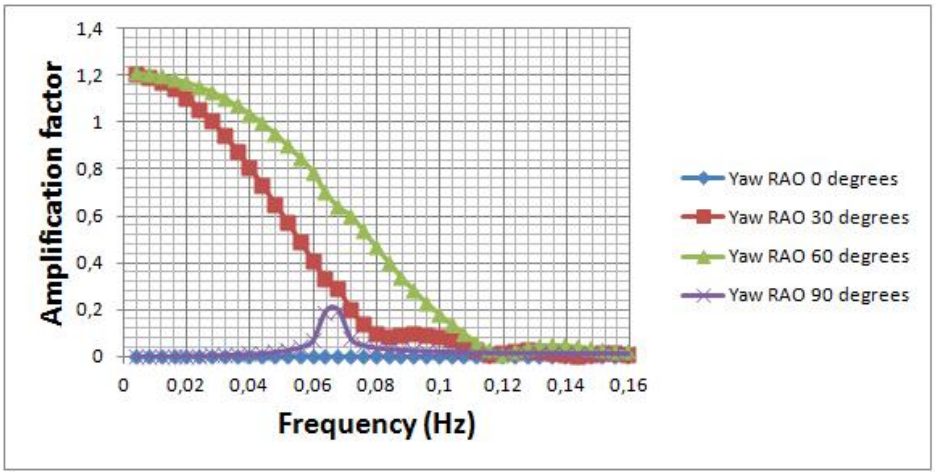

Figure B.11: RAO for yaw movement of the bulk carrier

When looking at figure B.12 it can be seen that for the heave motion of the bulk vessel two high ship agitation situations occur. The first situation concerns waves arriving under an angle of zero and 30 degrees of the stern. The ship reacts the most to low frequency waves coming from this direction. When waves arrive more perpendicular towards the stern of the vessel it can be seen that that the heave agitation peaks are situated around the higher wave frequencies coinciding with wave periods around 20 seconds. The agitation effects of these waves are higher than for the longer waves ariving more parallel to the ship's stern.

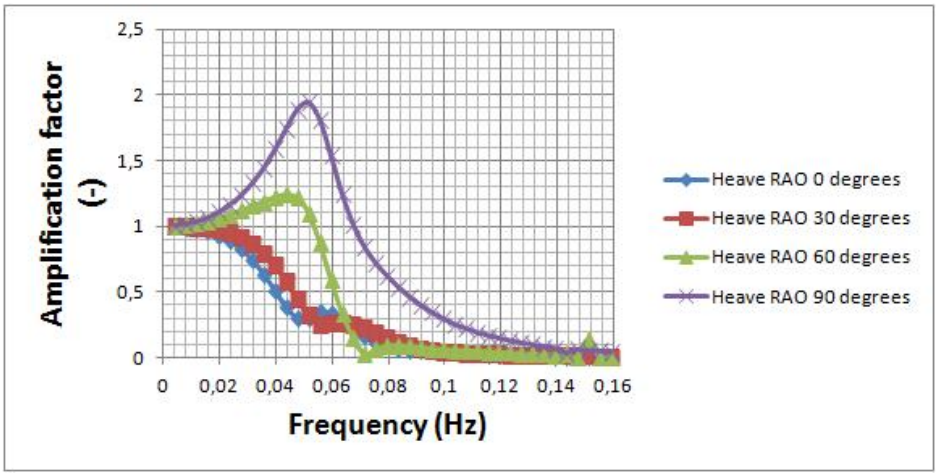

Figure B.12: RAO for heave movement of the bulk carrier

The agitation peaks for roll motion are clearly occurring around the wave frequency of 0.06 Hz coinciding with a wave period of 17 seconds. Figure B.13 clearly shows that for all incoming directions the agitation peak arises at this same frequency. Again as roll concerns angular movement in direction of the width of the ship incoming waves under an angle of zero degrees from the stern have no influence on this movement as a logical result waves arriving from an perpendicular angle towards the ships bow have most influence on roll motion.

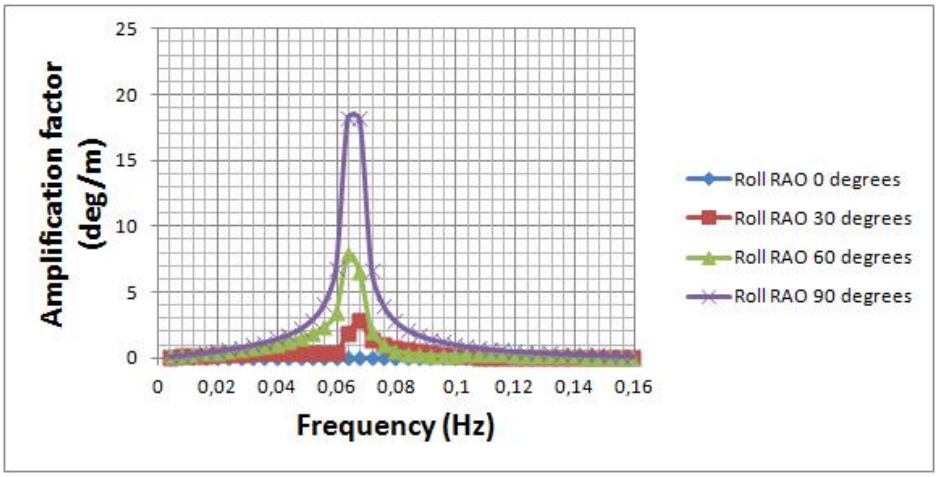

Figure B.13: RAO for roll movement of the bulk carrier

When looking at figure B.14, as pitch is exactly the opposite movement for roll (same relation

as surge and sway) waves arriving from an angle of zero degrees have most influence and waves arriving from a 90 degrees angle have the least influence on this motion. However in contradiction to what has been stated at the roll motion, all incoming wave angles influence the ship's agitation in case of pitch. Highest agitation occurs for incoming waves under an angle of 60 degrees from the ship's stern at a frequency of 0.06 Hz (wave period of around 17 seconds).

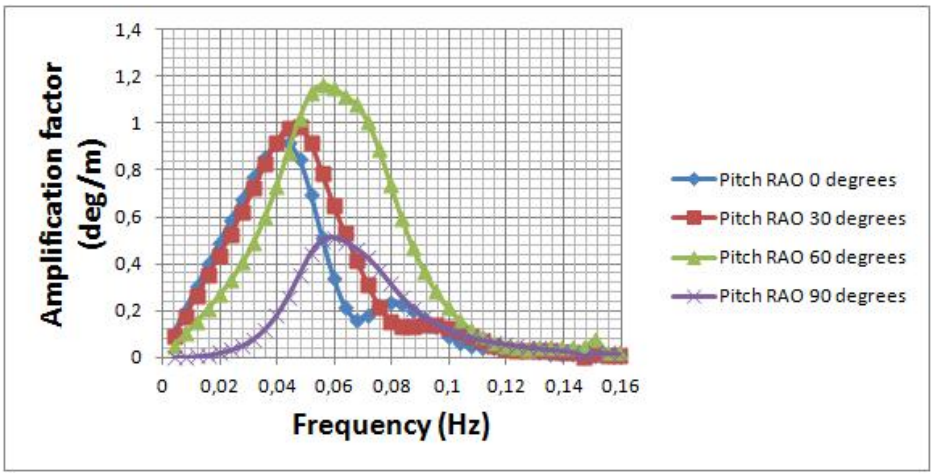

Figure B.14: RAO for pitch movement of the bulk carrier

Appendix C

Basin resonance

C.1 Derivation of a half closed basin resonance wave periods

C.1.1 Calculating resonance frequencies for harbor basins

The resonance and amplification factors of incoming waves depend on the geometrics and bathymetry of the basin. For a long and small half closed harbor basin the simplest oscillation shape is an oscillation shape of the basin with a length of ¼ of the length of the incoming wave in the direction of the length of the basin [7]. This oscillation shape is visualized by a node just outside the basin opening and an anti node at the end of the harbor (see figure C.1). When waves reflect from quay to quay in direction of the width of the basin, the natural frequencies of the basin will be characterized by anti nodes at both quays and a node in the basin. The length of the incoming resonating wave therefore consists of a length of ½ the width of the basin(see figure C.2).

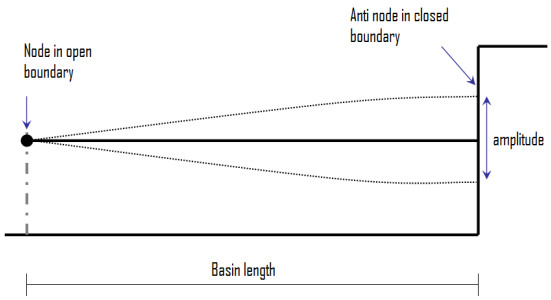

Figure C.1: First harmonic oscillation of a half closed basin

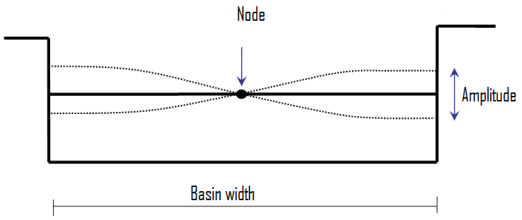

Figure C.2: First harmonic oscillation of a closed basin

In anti nodes the amplitude of the wave grows to its maximum value while the velocity of the wave reduces to zero. At the nodes maximum velocities are measured in combination with minimal wave amplitudes. This form of resonance is called a first mode type of oscillation. There can also be resonance at higher modes. At these higher mode standing waves there will be more nodes and anti nodes in the harbor basin. For further details about the theory the open channel flow lecture book can be referred to [7].
It has to be taken into account that shapes of a harbor basin scarcely have the form of a perfect rectangle, estimations derived through the method described above assume perfect rectangular forms.

The wave periods belonging to basin resonance can be calculated using the following formula [5]:

$$T_{basin} = \frac{L}{\sqrt{g * d}} \tag{C.1}$$

In which:

T_{basin} = natural period of the basin
L = Wave length of incoming wave (depending on the calculated mode standing wave)
g = gravitational acceleration
d = depth of the basin

This formula can be rewritten including the wave number k:

$$T_{basin} = \frac{2\pi}{k * \sqrt{g * d}} \tag{C.2}$$

T_{basin} = natural period of the basin
k = wave number of the incoming wave
g = gravitational acceleration
d = depth of the basin

Because:

$$L = \frac{2\pi}{k} \tag{C.3}$$

L = wave length of the incoming wave
k = wave number of the incoming wave

The wave length (L) in formula C.1 depends on the mode standing wave that is calculated. Figure C.1 shows that for a first mode standing wave the incoming wave length should be four times the basin length:

$$L_{halfopen} = 4 * l_{basin} \tag{C.4}$$

However, for higher mode standing waves the incoming wave length decreases. Therefore the general notation of this formula can be rewritten as:

$$L_{halfopen} = \frac{4 * l_{basin}}{2n + 1} \tag{C.5}$$

in which n determines the mode of the standing wave.

For a closed basin (see figure C.2) the incoming wave length is determined by:

$$L_{closed} = \frac{2 * l_{basin}}{m} \tag{C.6}$$

in which m determines the mode of the standing wave.

It should be taken into account that the natural period of the new basin is determined by a combination of wave oscillation in x (length) and y (width) direction of the basin. When determining the wave resonance periods the wave number k is a combination of wave numbers in two directions and can be computed as:

$$k = \sqrt{{k_x}^2 + {k_y}^2} \tag{C.7}$$

To derive k_x and k_y a number of steps have to be followed. The new basin is assumed to be a rectangular basin with an open boundary at $x = 0$, a closed boundary at $x = l$ and closed boundaries at $y = 0$ and $y = b$.
Resonance in the x direction occurs when incoming waves have a length of:

$$L_x = \frac{4l_{\text{basin}}}{2n+1} \tag{C.8}$$

L_x = wave length of incoming wave
l_{basin} = length of the basin
n = number of harmonics

The wave number k_x is given by:

$$k_x = \frac{2\pi}{L_x} \tag{C.9}$$

Substituting equation C.8 in equation C.9 gives:

$$k_x = \frac{\pi(2n+1)}{2l_{basin}} \tag{C.10}$$

If the basin would experience resonance in the y direction, the width of the basin should be interpreted as a closed basin. For a standing wave to occur in this direction, the length of waves in the y directions should be:

$$L_y = \frac{2B_{basin}}{(m)} \tag{C.11}$$

L_y = wave length of incoming wave
B_{basin} = width of the basin
m = number of harmonics

The wave number k_y is given by:

$$k_y = \frac{2\pi}{L_y} \tag{C.12}$$

Substituting equation C.11 in equation C.12 gives:

$$k_y = \frac{2\pi(m)}{2B_{basin}} \tag{C.13}$$

The wave number k can now be calculated using formula C.7.
When implementing the wave number k obtained in formula C.7 into formula C.2 the natural period belonging to the chosen mode standing wave is calculated.

To examine the natural periods belonging to the different mode standing waves inside the new basin, all combinations between wave numbers in x and y direction should be computed.

C.2 Resonance frequencies of the outer harbor basins

C.2.1 Resonance frequencies of the new basin

For calculating the resonance frequencies, dimensions used for the length and width of the new basin will be implemented conform the criteria mentioned in chapter 3.2.2. Table C.1 provides the dimensions used. The resulting resonance frequencies of the new basin are shown in table C.2.

Table C.1: Dimensions of the new basin

Basin length (m)	360
Basin width (m)	220
Basin depth (m)	20

Table C.2: Table of resonance frequencies (Hz) of the new basin

		basin length		
		1^{st} harmonic	2^{nd} harmonic	3^{rd} harmonic
basin width	0^{th} harmonic	0.0097	0.0289	0.0472
	1^{st} harmonic	0.0393	0.0472	0.0593
	2^{nd} harmonic	0.0728	0.0765	0.0832
	3^{rd} harmonic	0.1011	0.1031	0.1070

The important resonant frequencies appear to have values between 0.0097 and 0.1700 Hz. This complies with wave periods between 9 and 100 seconds. This first analysis implies that only looking at the influence of the new basin on incoming waves, the bulk carrier will not suffer severe horizontal movements due to basin resonance. Vertical movement could be enforced as wave periods between 10 and 25 seconds do cause resonance in the new basin

C.2.2 Resonance frequencies of the IJmond harbor

Table C.3 shows the dimensions of the IJmond harbor, table C.4 shows the wave frequencies for which resonance of the basin will occur.

Table C.3: Dimensions of the IJmond harbor

Basin length (m)	394
Basin width (m)	192
Basin depth (m)	11

Table C.4: Table of resonance frequencies (Hz) of the IJmond harbor

		basin length		
		1^{st} harmonic	2^{nd} harmonic	3^{rd} harmonic
basin width	0^{th} harmonic	0.0067	0.0197	0.0327
	1^{st} harmonic	0.0277	0.0332	0.0421
	2^{nd} harmonic	0.0534	0.0563	0.0616
	3^{rd} harmonic	0.0778	0.0796	0.0831

C.2.3 Resonance frequencies of the Vissers harbor

Table C.5 shows the dimensions of the Vissers harbor, table C.6 shows the wave frequencies for which resonance of the basin will occur.

Table C.5: Dimensions of the Vissers harbor

Basin length (m)	1075
Basin width (m)	130
Basin depth (m)	8

Table C.6: Table of resonance frequencies (Hz) of the Vissers harbor

		basin length			
		1^{st} harmonic	2^{nd} harmonic	3^{rd} harmonic	4^{rd} harmonic
basin width	0^{th} harmonic	0.0021	0.0062	0.0103	0.0144
	1^{st} harmonic	0.0332	0.0337	0.0346	0.0360
	2^{nd} harmonic	0.0651	0.0654	0.0658	0.0665
	3^{rd} harmonic	0.0951	0.0952	0.0955	0.0959

C.2.4 Resonance frequencies of the Haring harbor

The Haring harbor does not have a rectangular shape as it bends to the right at 3/4 of the length. For the estimation of the resonance frequencies this bend is neglected and the basin is assumed as a rectangular basin. Table C.7 shows the dimensions of the Haring harbor, table C.8 shows the wave frequencies for which resonance of the basin will occur.

Table C.7: Dimensions of the Haring harbor

Basin length (m)	668
Basin width (m)	120
Basin depth (m)	9

Table C.8: Table of resonance frequencies (Hz) of the Haring harbor harbor

		basin length		
		1^{st} harmonic	2^{nd} harmonic	3^{rd} harmonic
basin width	0^{th} harmonic	0.0035	0.0105	0.0176
	1^{st} harmonic	0.0389	0.0402	0.0425
	2^{nd} harmonic	0.0757	0.0762	0.0773
	3^{rd} harmonic	0.1090	0.1094	0.1100

Appendix D

One dimensional energy density spectra measured in the outer harbor

In chapter 4.4 it is explained that the spectra shown in figures 4.5, 4.6, 4.7 and 4.8 are representative for all spectra measured during the November 2010 period. This appendix shows the entire collection of spectra measured during November 2010. Figures D.1 and D.4 show the the whole collection of spectra measured at the Northern breakwater and the Averij depot. Figures D.2, D.3, D.5 and D.6 show the division between the spectra measured during calm weather conditions and the 12 November storm.

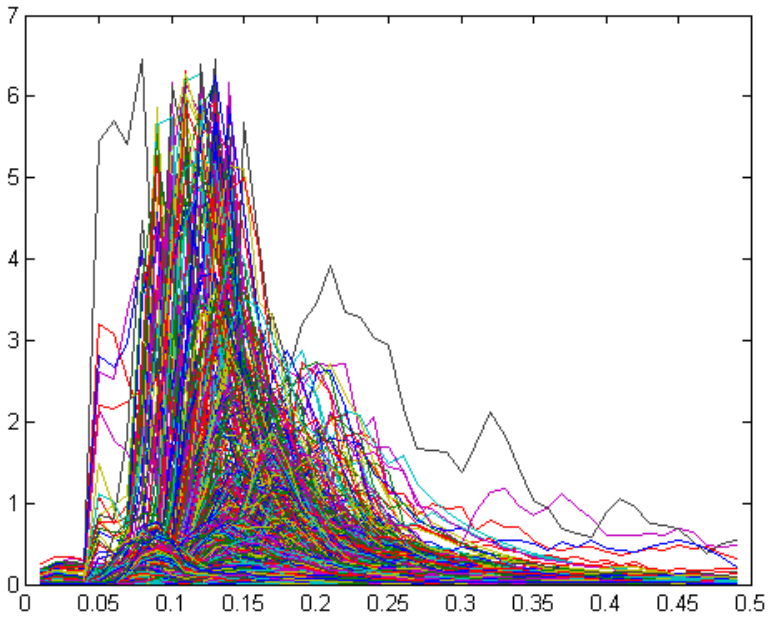

Figure D.1: All one dimensional energy density spectra measured at the northern breakwater

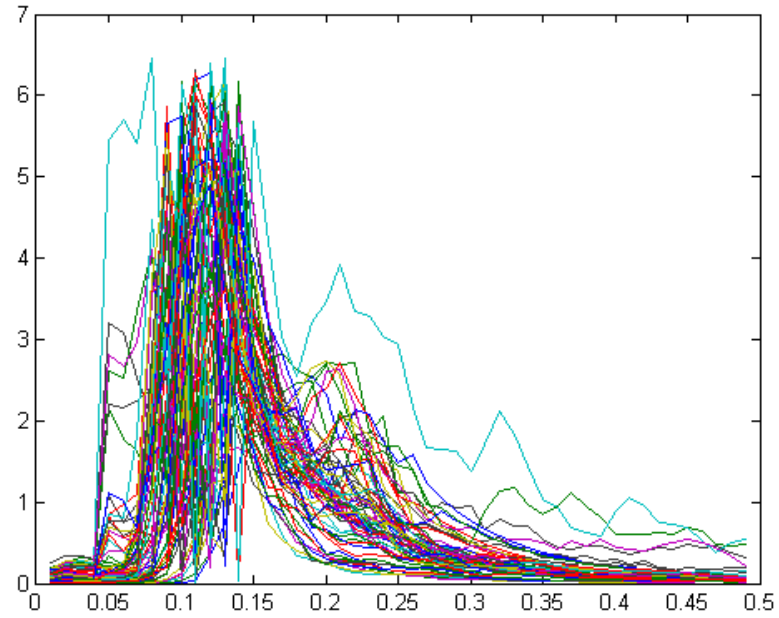

Figure D.2: One dimensional energy density spectra measured at the northern breakwater during the 12 November storm

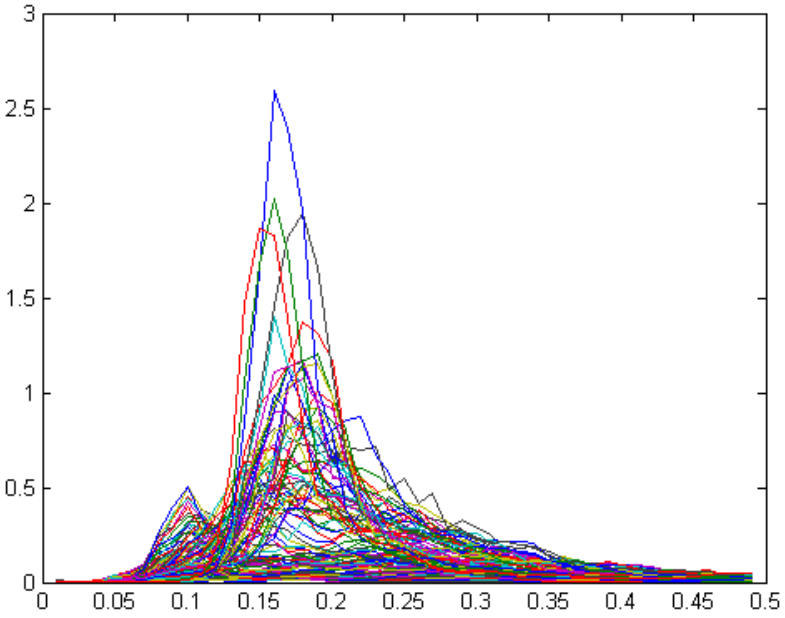

Figure D.3: One dimensional energy density spectra measured at the northern breakwater during November, not including the 12 November storm

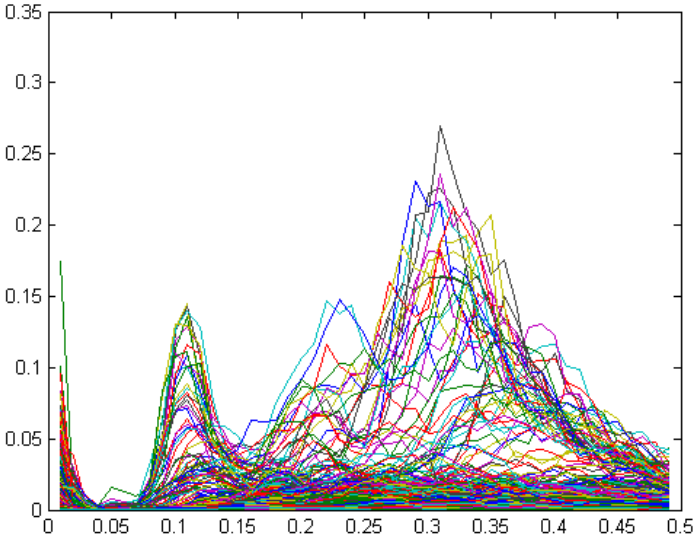

Figure D.4: All one dimensional energy density spectra measured during November 2001 at the Averij depot

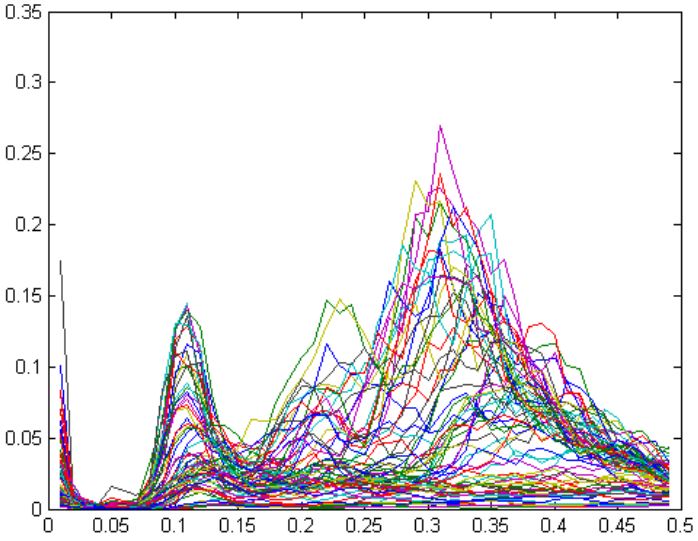

Figure D.5: One dimensional energy density spectra measured at the Averij depot during the 12 November storm

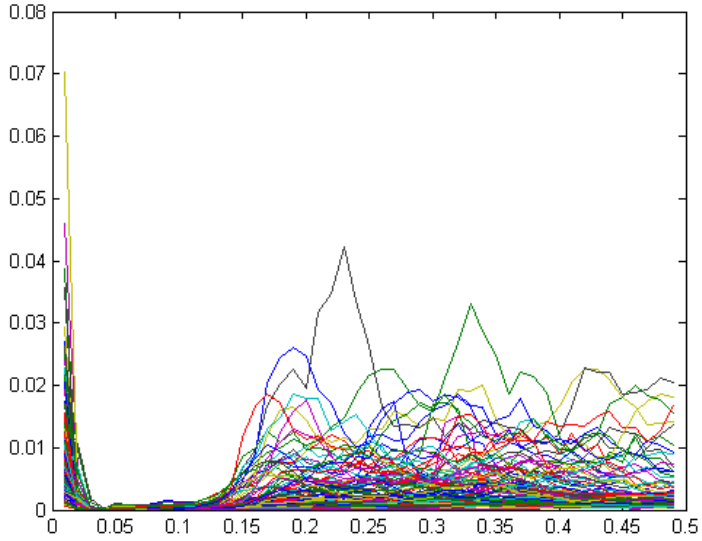

Figure D.6: One dimensional energy density spectra measured at the Averij depot during November, not including the 12 November storm

Appendix E

PHAROS model preparations

E.1 Model grid adjustments for the PHAROS models

In chapter 5.3.2 it is explained that the new basin grid has been added to the existing basin grid. Figures E.1 and E.2 show the current harbor grid and the harbor grid including the addition of the new basin.
Figures E.3 and E.4 show a close up of the grid size of the new basin concerning both the long and short wave model.

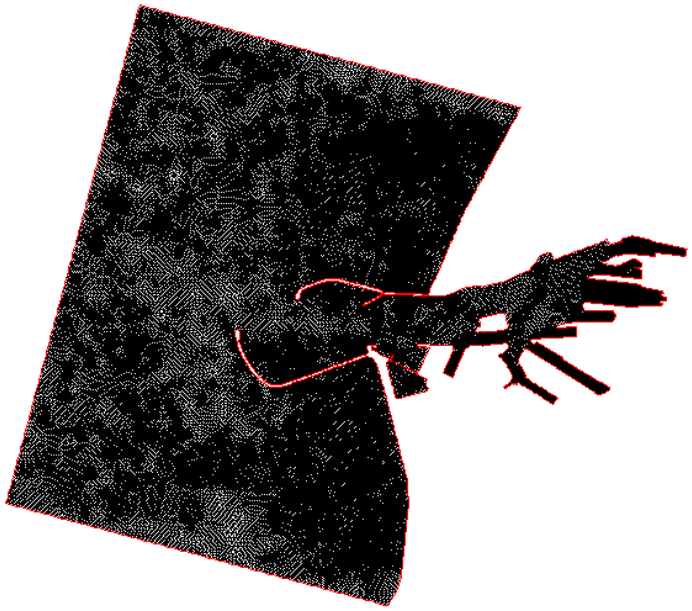

Figure E.1: Long wave model grid for the current situation

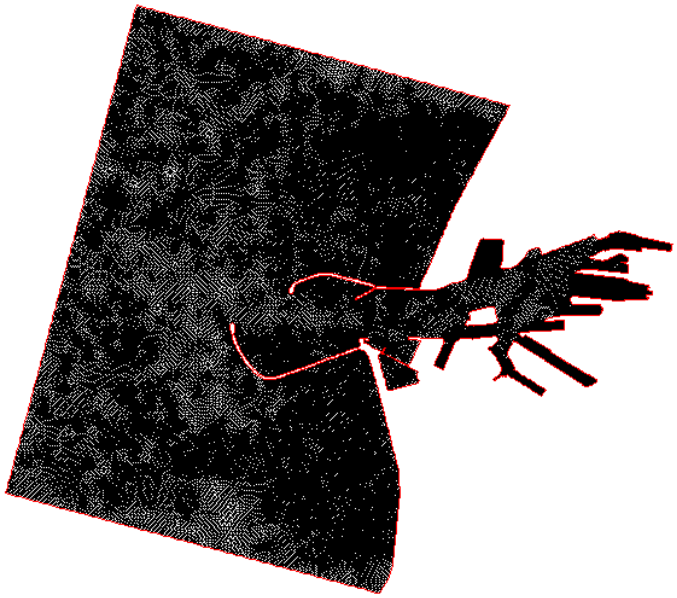

Figure E.2: Long wave model grid for the situation concerning the new harbor basin

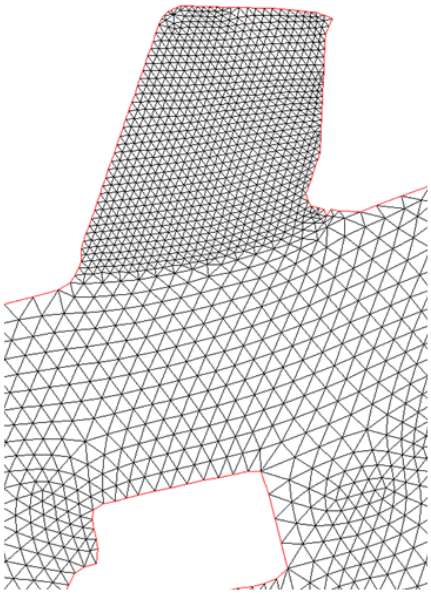

Figure E.3: Long wave model grid close up at the location of the new harbor basin

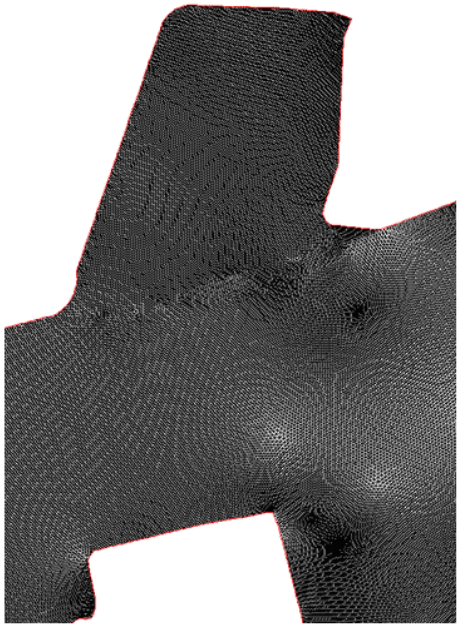

Figure E.4: Short wave model grid close up at the location of the new harbor basin

E.2 Explanation PHAROS parameters

A short description of the most important PHAROS parameters is given in this appendix. For a detailed description of the use of all model parameters reference is moade to the PHAROS manual [16].

E.2.1 General parameters

In the Pharos model a number of parameters can be adjusted. The significant wave height of the incoming waves at the model boundary has to be chosen. The main wave direction of the incoming waves has to be determined and the water level (which is uniform for the whole grid) has to be chosen. When the seiches option is selected, the user can use a band of frequencies as input for the model instead of just one wave period.

E.2.2 Reflection parameters

In the model all the embankment structures and elements considering the harbor shorelines can be addressed with different reflection coefficients and the angle of the incoming waves can be given for every element. It is also possible to adjust the transmission coefficients of the elements if it is desired to simulate wave overtopping of structures as breakwaters and harbor quays.

E.2.3 Physical parameters

Bottom friction can be added to the model by means of Jonsson using the Nikuradse roughness parameter and the viscosity coefficient. Entrance losses, due to sudden narrowing of inlets at harbor basins, can be added to the model grid and when necessary wave breaking can be implemented using breaking coefficients as the breaking index γ_{br} and the maximum wave steepness coefficient γ_{st}.

E.3 Reflection coefficients used in the short wave model

Table E.1 provides the values of the reflection coefficient used for the short waves PHAROS model [6].

Table E.1: Reflection coefficients used in the Short wave model, Source Deltares [6]

Type of shoreline	reflection coefficient (R)
Beaches	0.10
Slopes directly encountering incoming waves	0.3 - 0.5
Slopes not directly encountering incoming waves	0.3 -0.8
Quay walls	0.8 - 0.9

It is assumed that slopes that are directly encountered with wave impacts experience wave impact of relatively steep waves. Waves that encounter the slopes indirectly have already been reflected and are relatively flat and will therefore reflect for larger parts.

To determine whether these values are realistic, reference is made to two earlier studies. The first is a 'Technical Standards and Commentaries for Port & Harbour Facilities in Japan' and the second is a 'Random Seas and Design of Maritime Structures' study by Goda. Reflection coefficients of both studies are summarized in a technical summary provided by WSP on a study of the Ashdod harbor in Israel [43]. Tables E.2 and E.3 show the results for the reflection coefficients concerning these studies.

Table E.2: Reflection coefficients defined for Technical Standards and Commentaries for Port & Harbour Facilities in Japan [43]

Type of shoreline	reflection coefficient (R)
Quay wall	0.7 - 1.0
Rubble mound	0.3 - 0.6
natural beach	0.05 -0.6

Table E.3: Reflection coefficients defined by Goda, [43]

Type of shoreline	reflection coefficient (R)
Vertical wall	0.7 - 1.0
Slopes of rubble stones	0.3 - 0.6
Slopes of energy dissipating concrete	0.3 -0.5
Natural beaches	0.05 - 0.2

As can be seen the chosen values for the short waves model coincide with the results of the earlier investigations.

E.4 Determining the incoming wave angle α

The reflection behavior of the boundary condition is different for other directions. This means that in case the user specifies a wave angle different from the one that is actually present at the considered boundary, the reflection coefficient will be different from the value specified by the user. This behavior is the result of the inherent mathematical characteristics of the reflection boundary condition formulation.
Figure E.5 shows the behavior of the reflection boundary condition for different combinations of prescribed reflection coefficient and wave angle. For wave directions more normal to the boundary than the wave angle specified by the user, the actual reflection coefficient is larger than the specified one; it is smaller otherwise. Note that the deviation from the specified reflection coefficient due to a certain mismatch between the user estimated direction α and the actual direction(s) θ calculated inside the domain becomes larger for wave angles further away from the normal direction. Particular attention should therefore be given to situations in which waves propagate more parallel to a boundary.

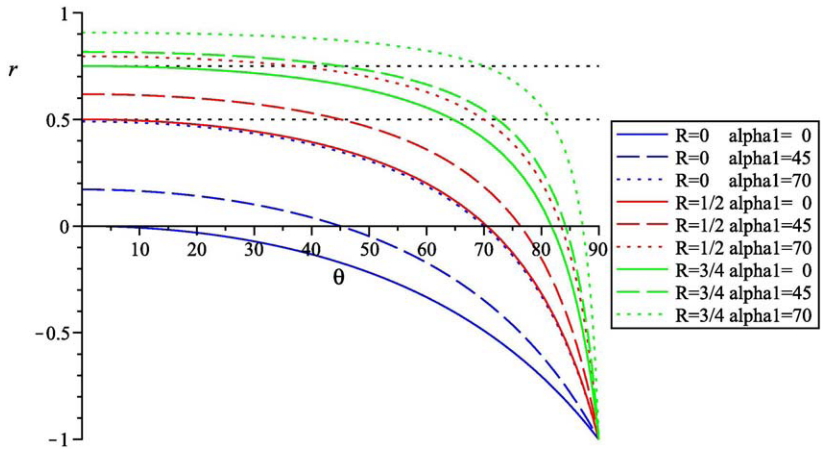

Figure E.5: Actual reflection coefficient r of boundary condition as a function of angle θ with which the waves approach the considered boundary, for several combinations of user-specified reflection coefficient R and estimated wave angle α

The above description indicates that when applying this boundary condition, its characteristics (and limitations) need to be taken into account. However, the method is very stable and versatile when it comes to practical applications and numerical aspects. When the above characteristics are taken into account, then accurate results are obtained.
Note that the actual reflection coefficient r can have a negative value. The absolute value of r is in this case the reflection coefficient, however the minus sign results in a reflected wave in anti-phase at the boundary (node at the boundary instead of an anti-node). Especially in cases where the wave direction is almost parallel to the boundary, the user should pay attention to this.

Appendix F

PHAROS output results

F.1 Results of output locations for wave agitation in the new basin

As discussed in chapter 5.5.1 15 output locations have been created in the PHAROS models to analyze wave amplification inside the new basin. The resulting amplification factor for every location is demonstrated in this appendix for the frequency range between 0.004 and 0.034 Hz (coinciding with wave periods between 30 to 250 seconds). All amplification factors are based on a incoming wave height of 0.05 meter as explained in chapter 5.4.1.

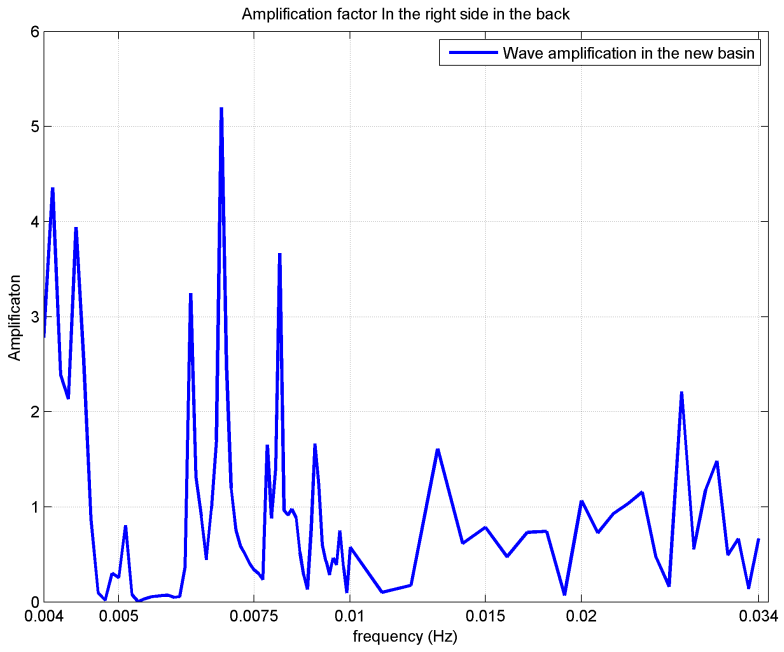

Figure F.1: Wave agitation in the right side in the back

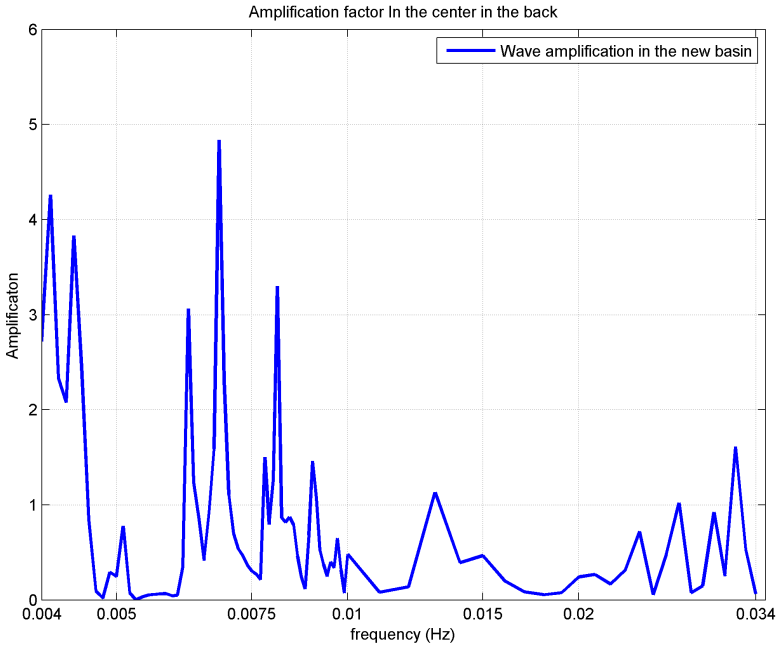

Figure F.2: Wave agitation in the center in the back

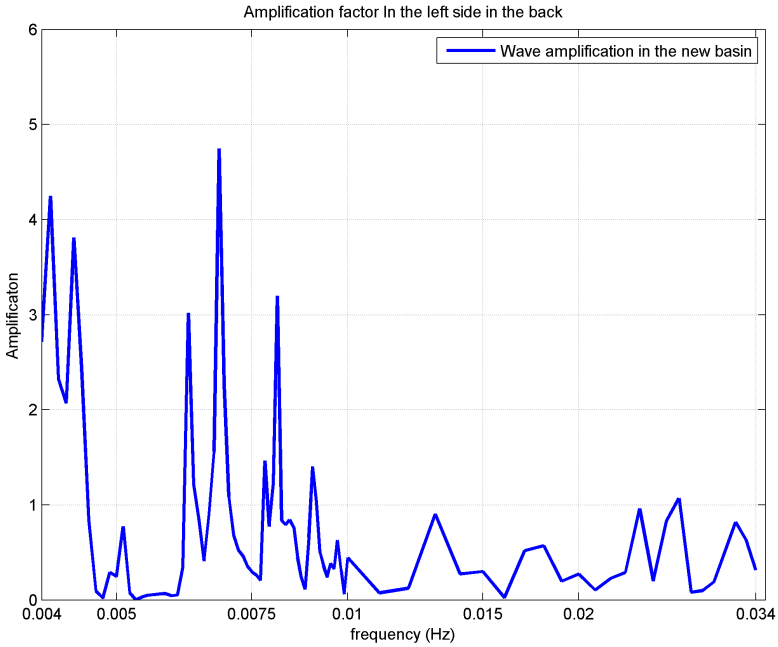

Figure F.3: Wave agitation in the left side in the back

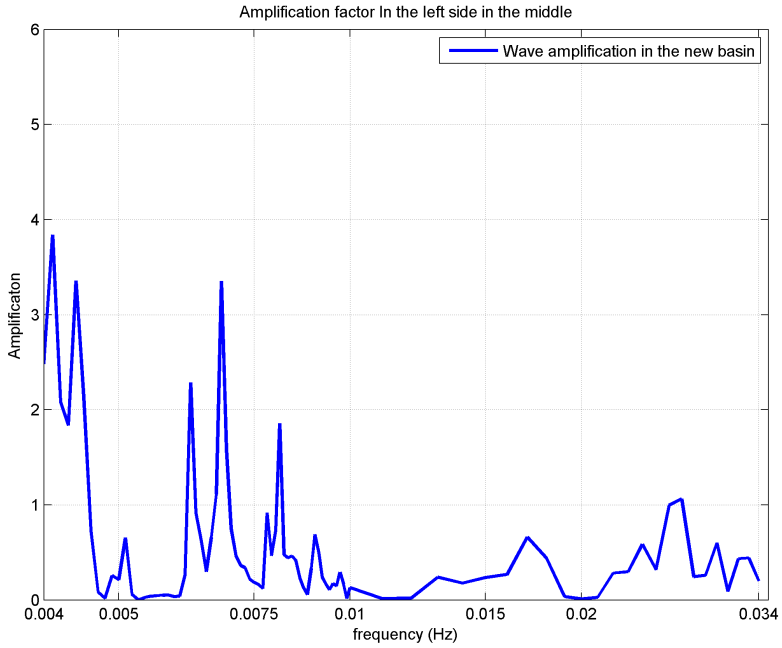

Figure F.4: Wave agitation in the left side in the middle

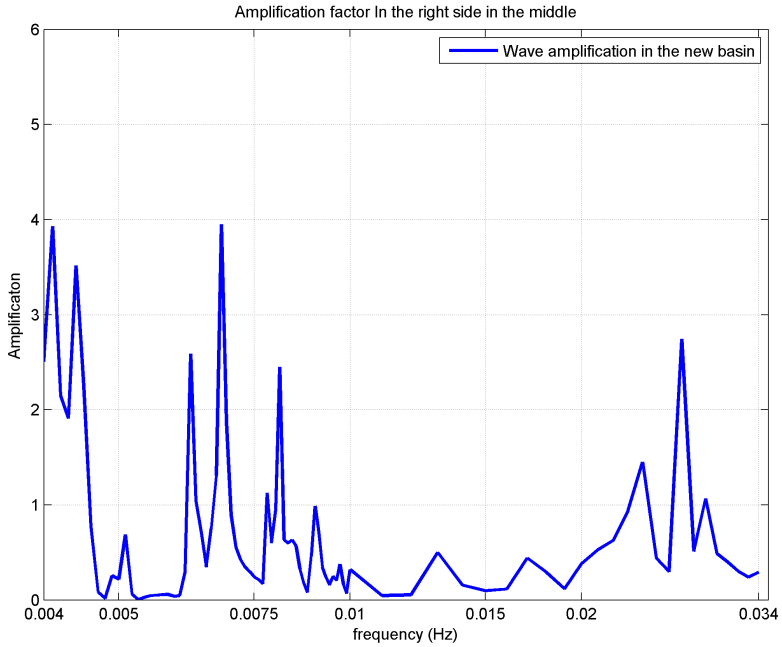

Figure F.5: Wave agitation in the right side in the middle

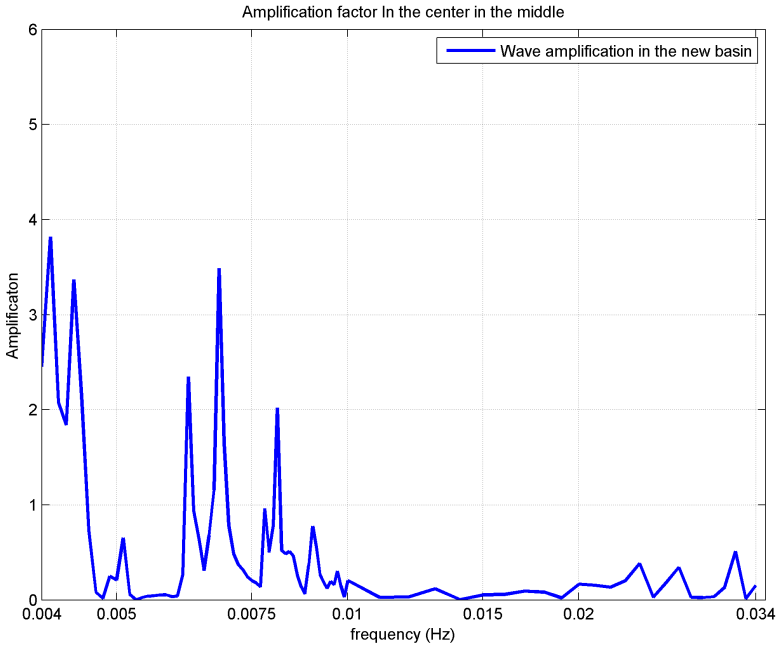

Figure F.6: Wave agitation in the center in the middle

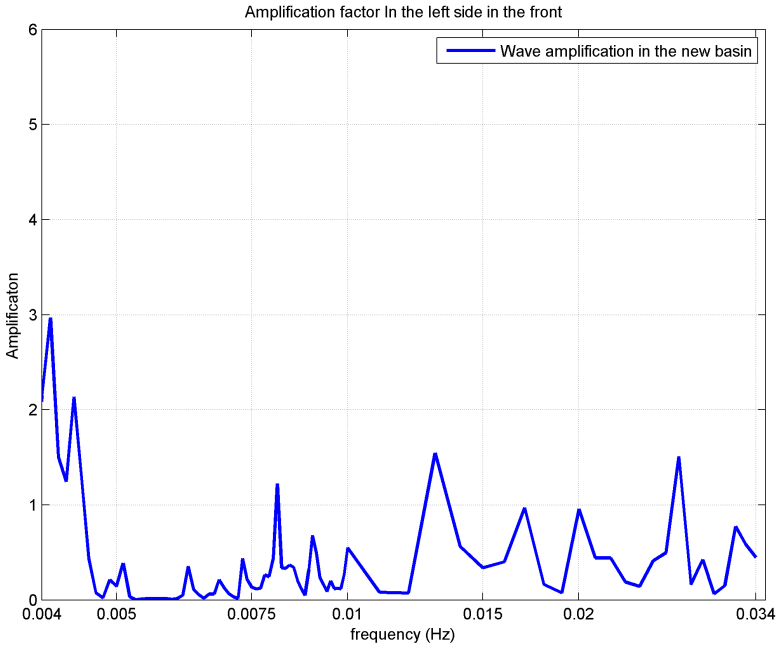

Figure F.7: Wave agitation in the left side in the front

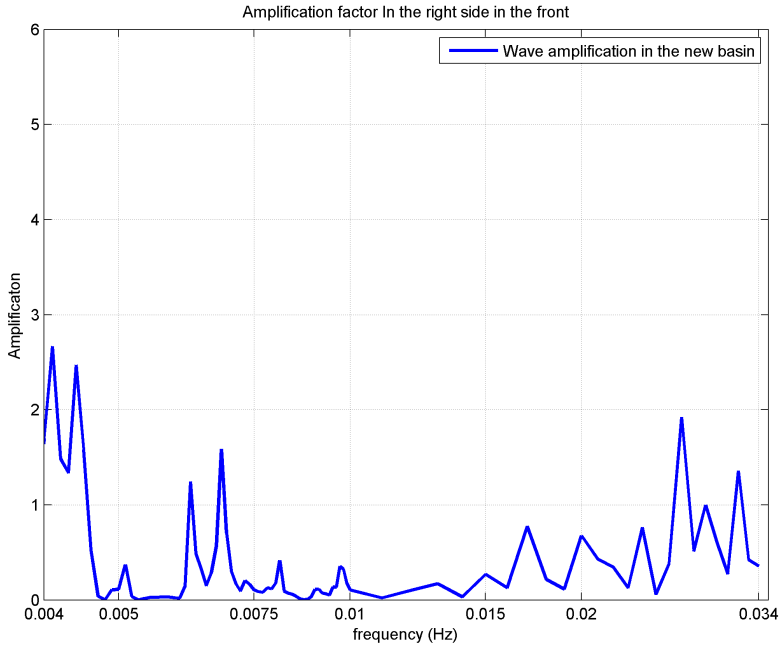

Figure F.8: Wave agitation in the right side in the front

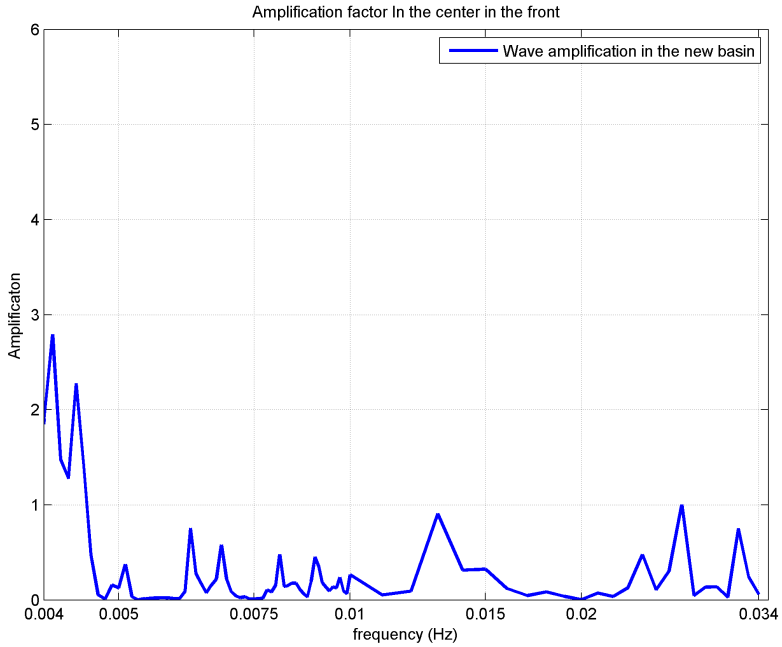

Figure F.9: Wave agitation in the center in the front

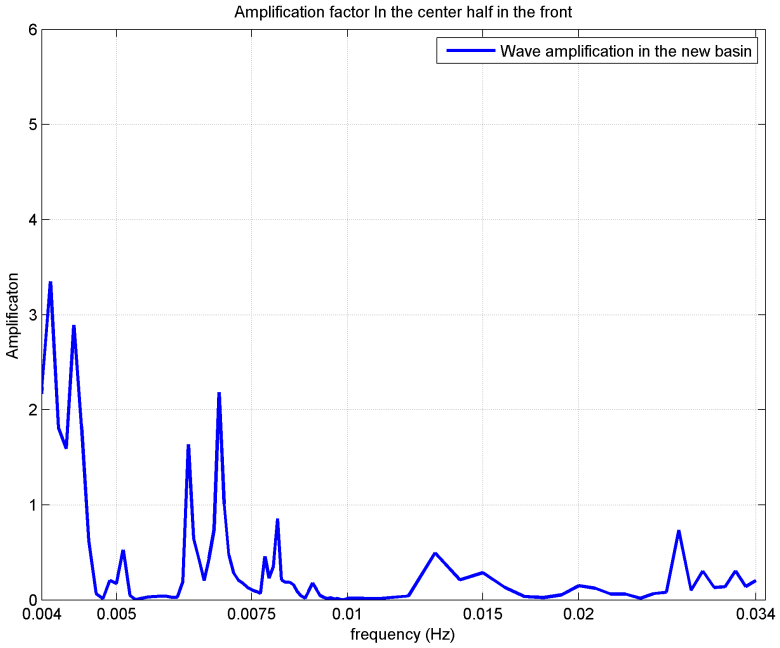

Figure F.10: Wave agitation in the center half in the front

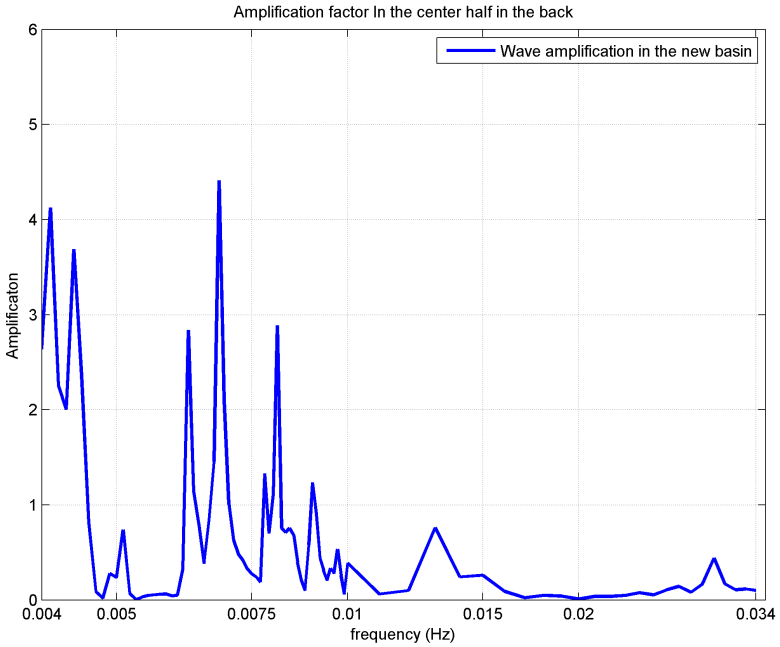

Figure F.11: Wave agitation in the center half in the back

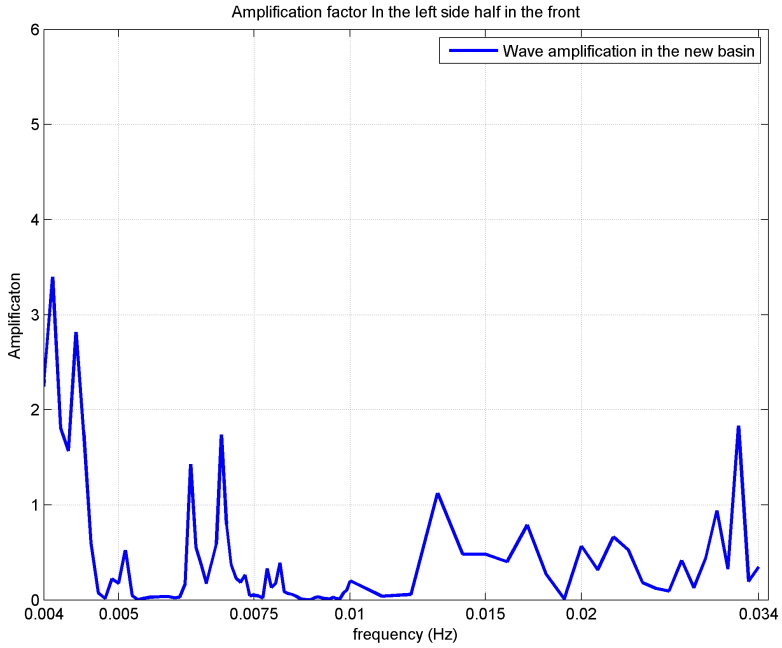

Figure F.12: Wave agitation in the left side half in the front

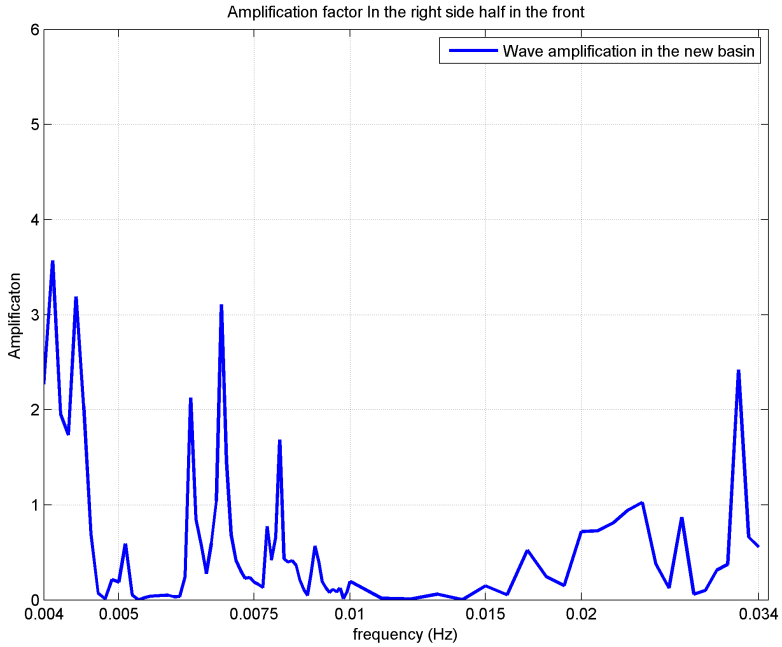

Figure F.13: Wave agitation in the right side half in the front

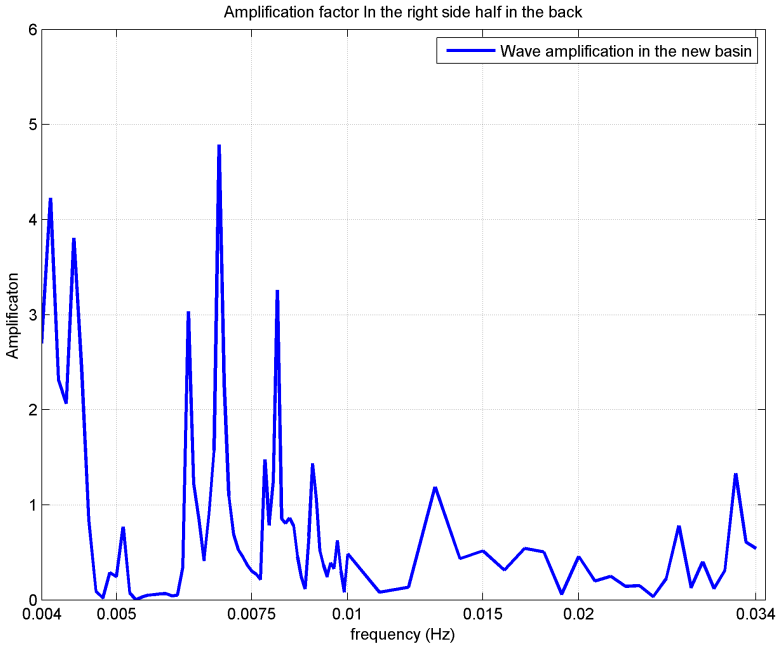

Figure F.14: Wave agitation in the right side half in the back

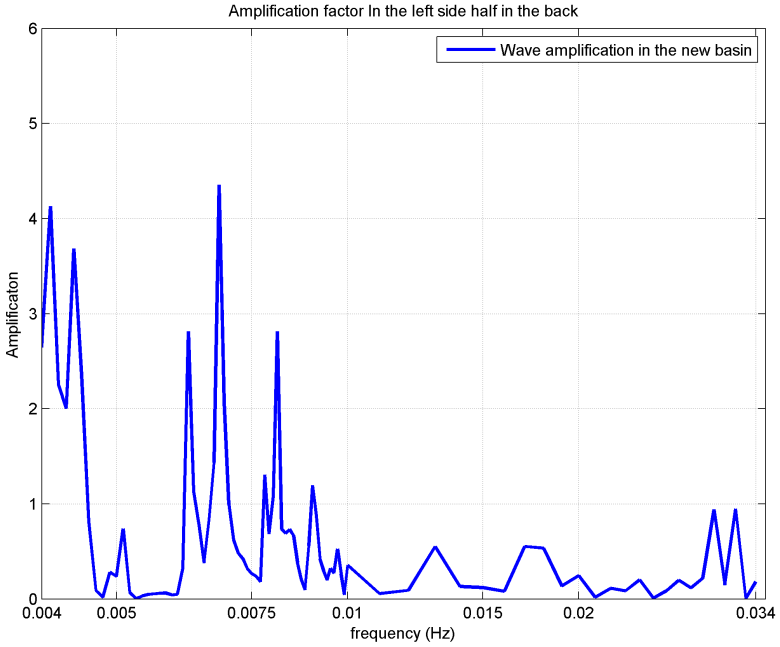

Figure F.15: Wave agitation in the left side half in the back

F.2 Results of wave height plots concerning the new basin

The following figures belong to the peak wave agitation frequencies discussed in table 5.4 in chapter 5.5.1. The figures, obtained from the PHAROS long wave model, provide better insight in wave patters that occur during the measured agitation peaks for certain wave periods. This way it can be determined whether a standing wave pattern occurs and what kind of mode that is present.

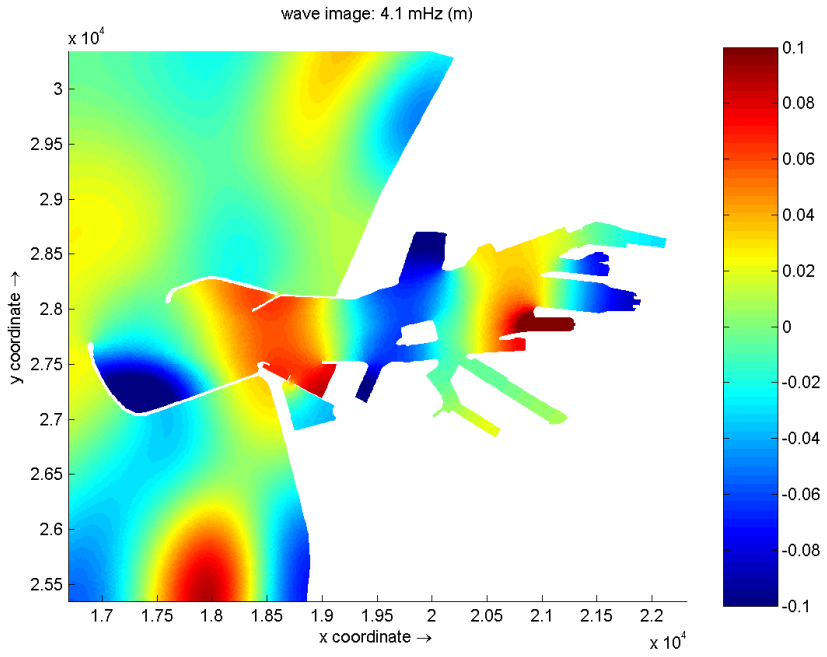

Figure F.16: 4^{th} mode standing wave covering the entire outer harbor for a frequency of 4.1 mHz

The period of a 4^{th} mode standing wave covering the entire outer harbor is calculated using the theory explained in appendix C.1. Using a harbor length of 5.2 kilometer and an average harbor depth of 15 meter. It follows from equation C.1 that the belonging wave period should be 244 seconds. This period complies with a wave frequency of 0.0041 Hz which is the same period as modeled by the PHAROS model.

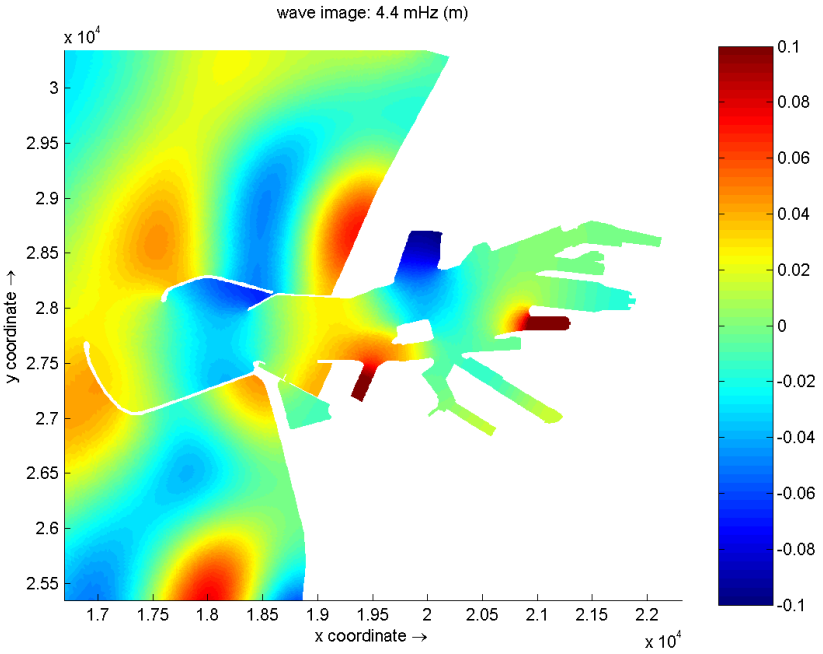

Figure F.17: 1^{st} mode standing waves between the new basin and the IJmond harbor for a frequency of 4.4 mHz

Theoretically the wave period for a 1^{st} mode standing waves between the new basin and the IJmond harbor should be 237 seconds. This complies with a wave frequency of 0.042 Hz. This result is very close to the modeled result provided by the PHAROS model. Dimensions used are a distance of 1660 meter between the two basin ends and an average depth of 20 meter.

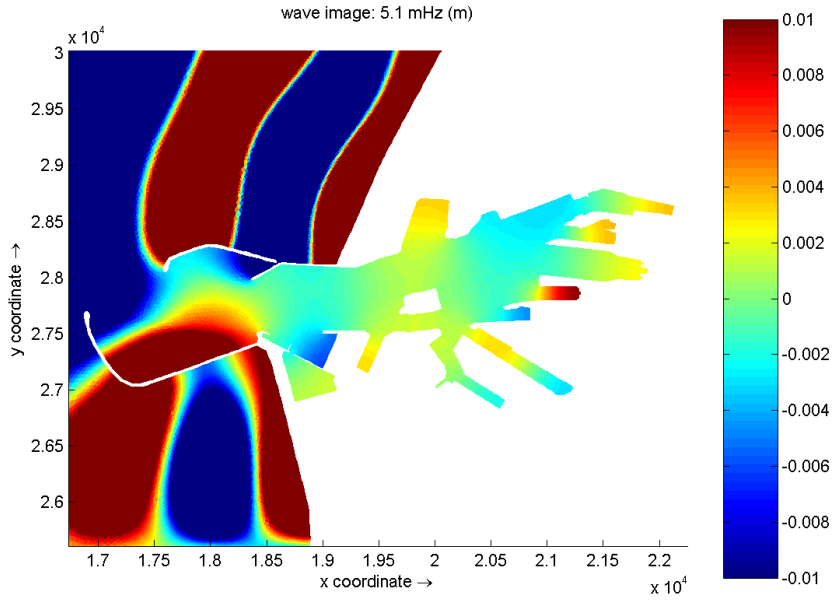

Figure F.18: Higher mode standing wave covering the entire outer harbor for a frequency of 5.1 mHz

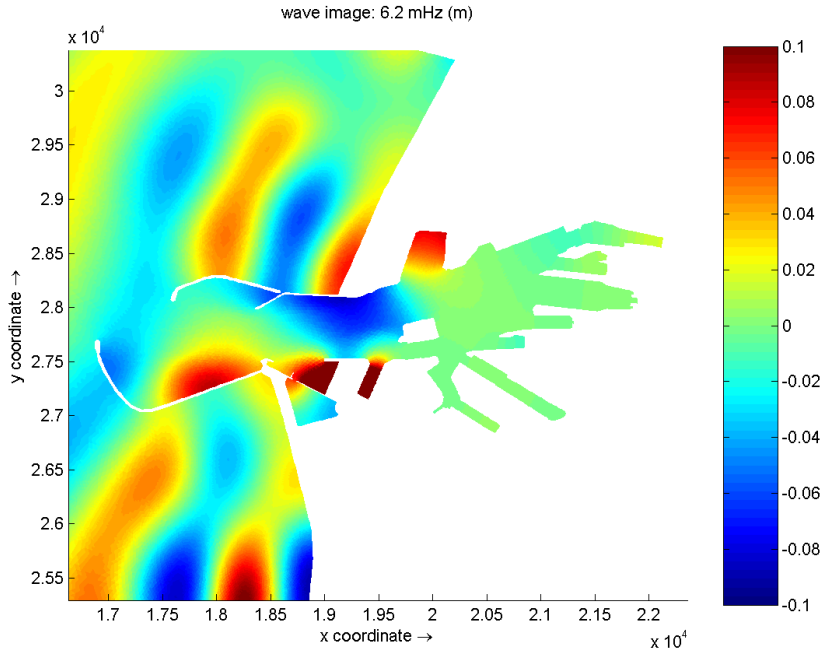

Figure F.19: Higher harmonic standing waves involving the new basin and harbor entrance for a frequency of 6.2 mHz

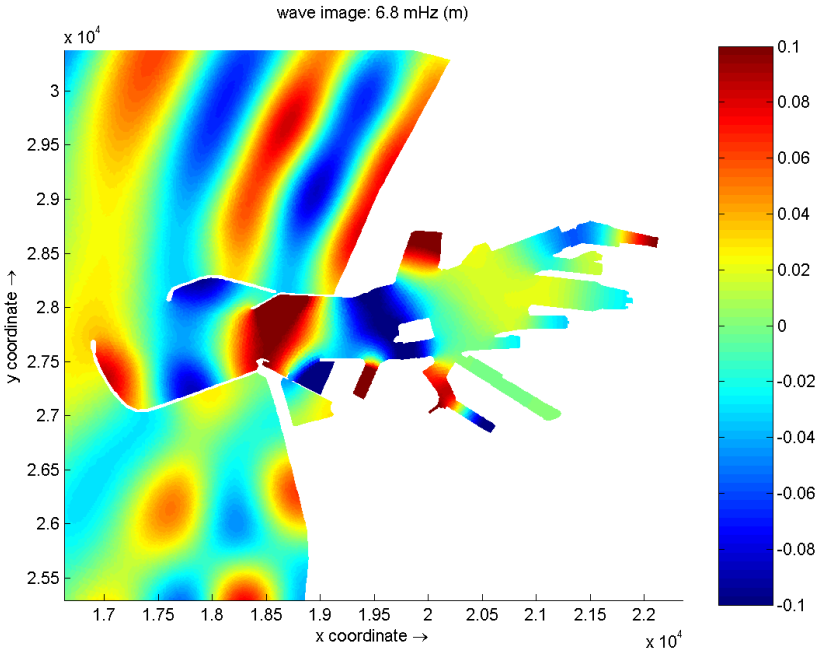

Figure F.20: Higher harmonic standing waves involving the new basin and harbor entrance for a frequency of 6.8 mHz

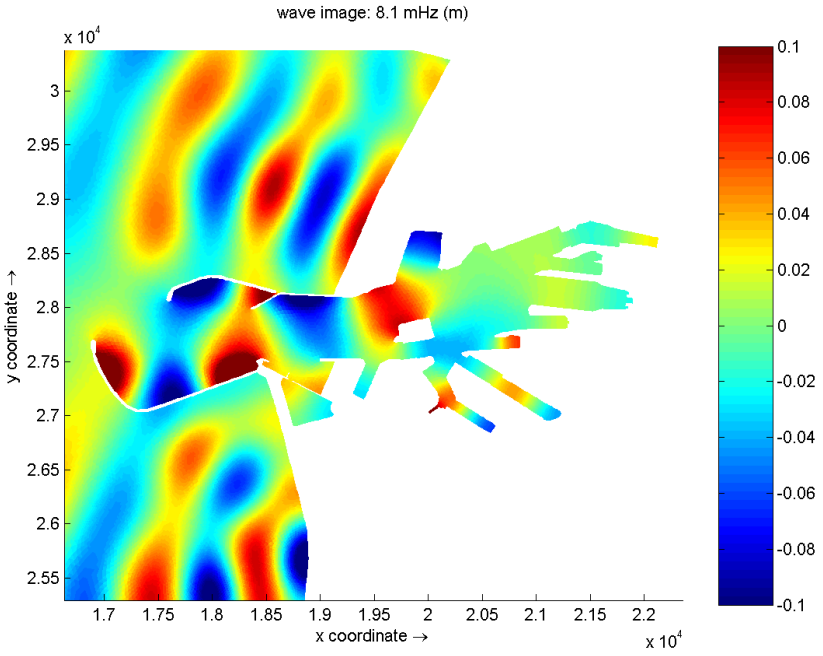

Figure F.21: Higher harmonic standing waves involving the new basin and harbor entrance for a frequency of 8.1 mHz

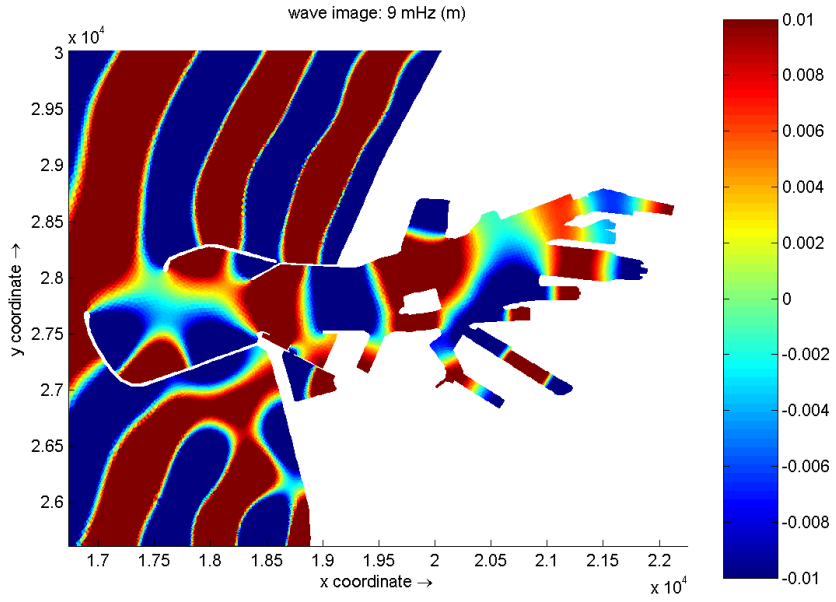

Figure F.22: Higher harmonic standing waves involving the new basin and harbor entrance for a frequency of 9.0 mHz

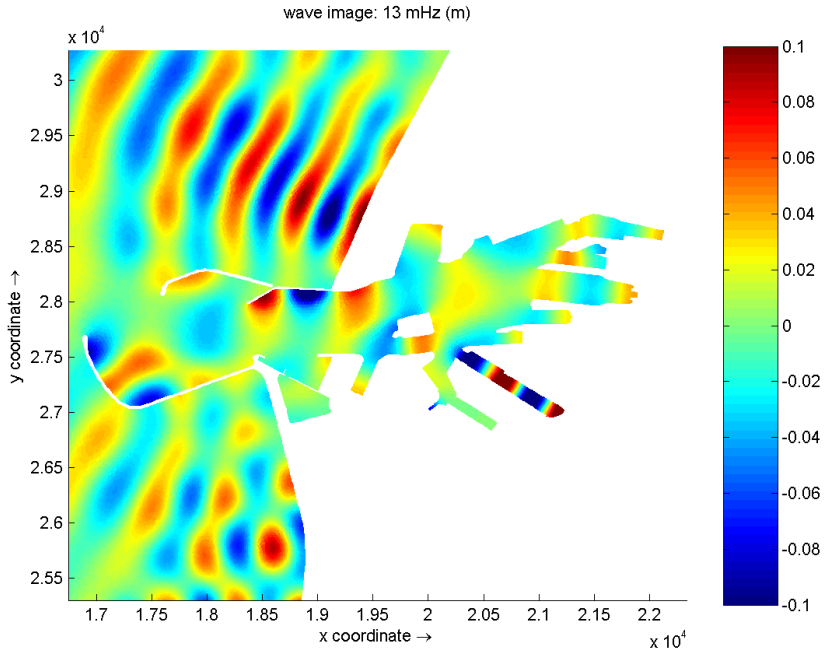

Figure F.23: Higher harmonic standing waves involving the new basin and harbor entrance for a frequency of 13.0 mHz

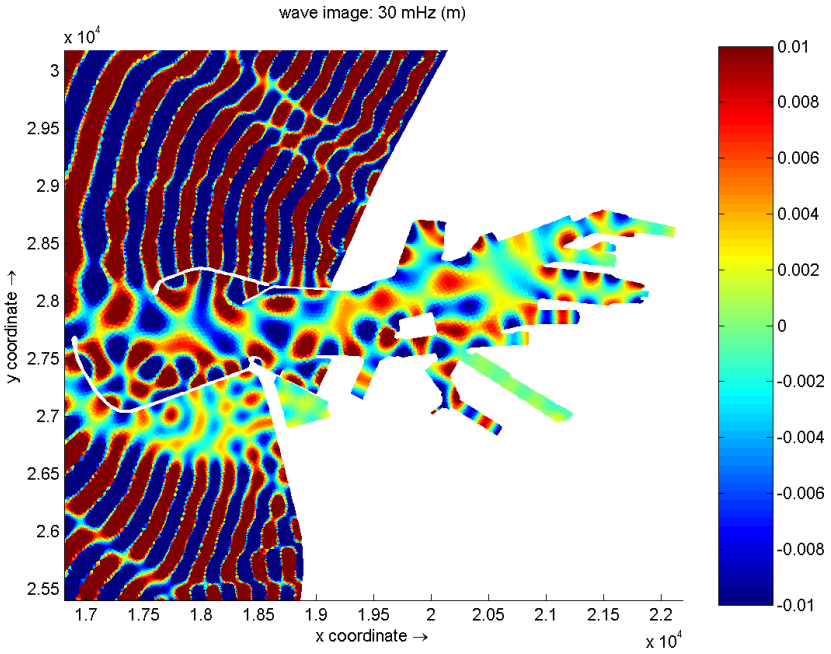

Figure F.24: Local random wave agitation in the new basin for a frequency of 30 mHz

F.3 Comparing wave agitation for different output locations inside the basins

To analyze wave agitation in the harbor basin it is chosen to situate the output locations in the far ends of the harbor basins. To determine whether this is a correct approach another set of output locations have been implemented a little more inside the basins to see what the results of wave agitation is at those locations. The figuresin this appendix show the different output locations for every harbor basin and the difference in wave agitation for both locations. The results concerning the output locations at the far end of the basins are colored blue while the results concerning the location more inside the basins are colored red. The figures clearly show that in all situations the wave agitation is highest at the far end of the basins. This result is complying the explanation given in chapter 4 about maximum agitation in anti nodes of a standing wave.
All figures are provided on the following pages of this appendix.

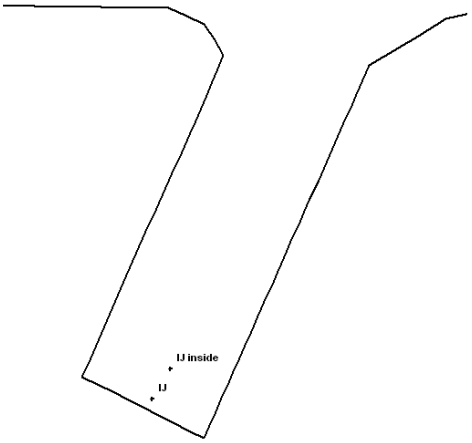

Figure F.25: Overview of the two different output locations inside the IJmond harbor

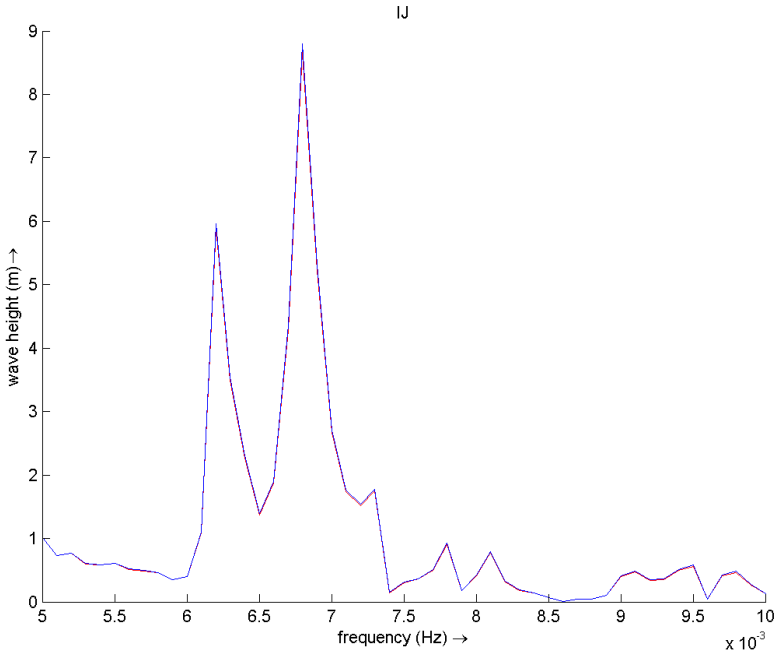

Figure F.26: Wave agitation graphs of the IJmond harbor output locations. The blue graph concerns the location at the end and red graph concerns the location further inside the basin

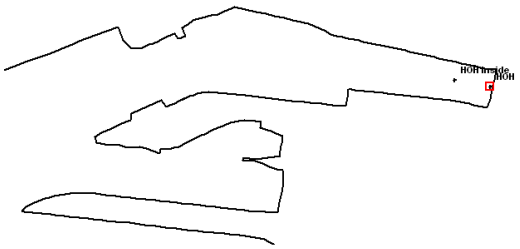

Figure F.27: Overview of the two different output locations inside the Haring harbor

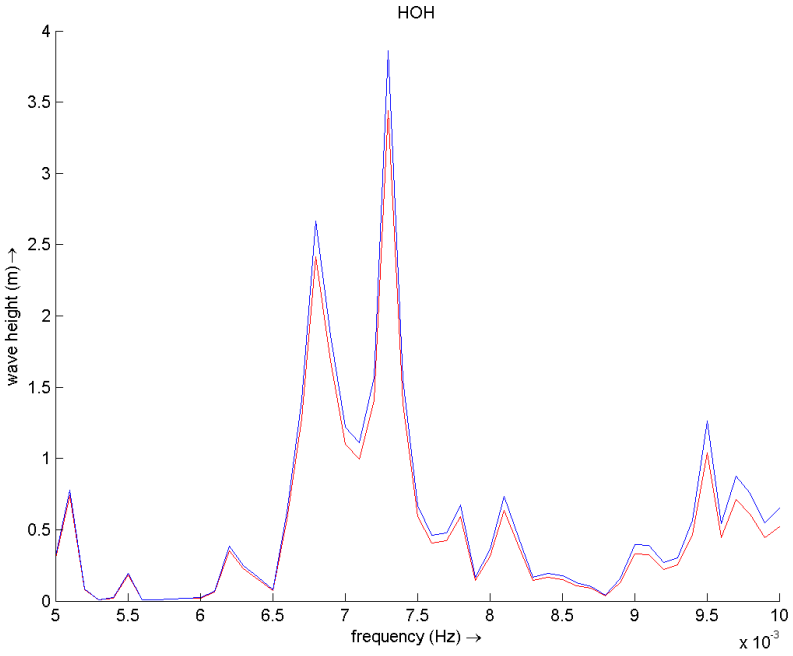

Figure F.28: Wave agitation graphs of the Hoogoven harbor output locations. The blue graph concerns the location at the end and red graph concerns the location further inside the basin

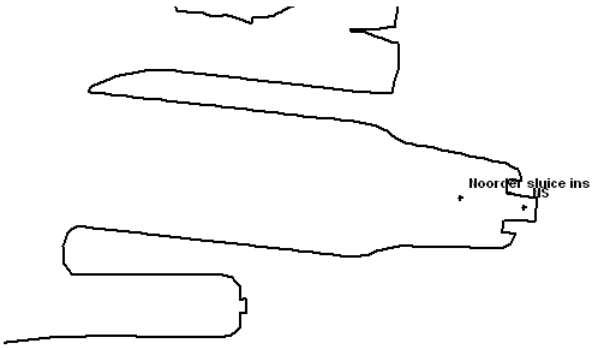

Figure F.29: Overview of the two different output locations inside the Noordersluice

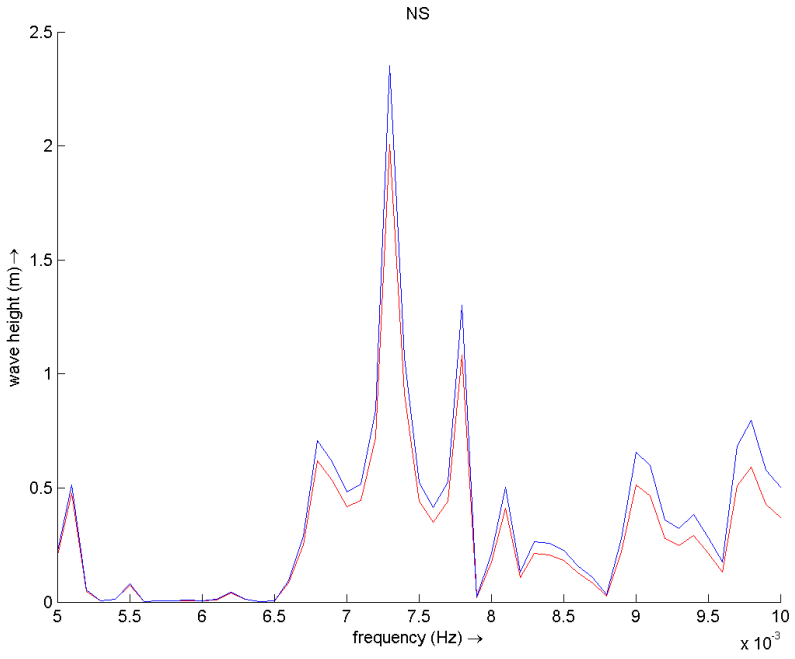

Figure F.30: Wave agitation graphs of the Noorder sluice output locations. The blue graph concerns the location at the end and red graph concerns the location further inside the basin

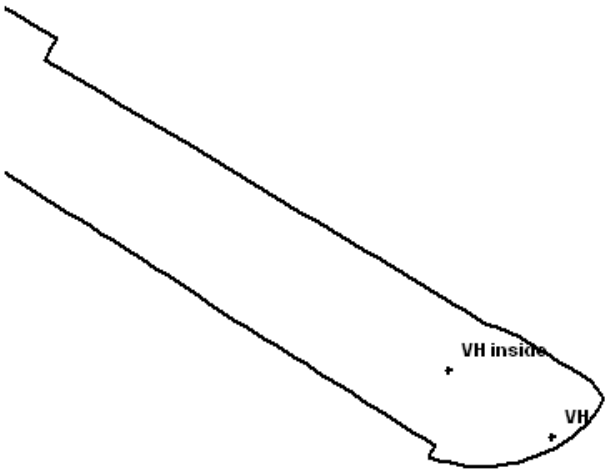

Figure F.31: Overview of the two different output locations inside the Vissers harbor

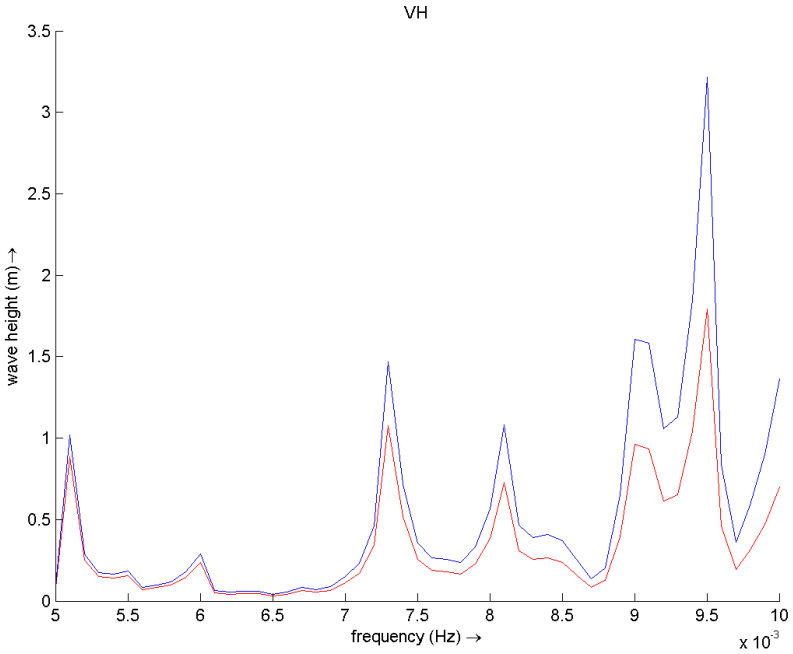

Figure F.32: Wave agitation graphs of the Vissers harbor output locations. The blue graph concerns the location at the end and red graph concerns the location further inside the basin

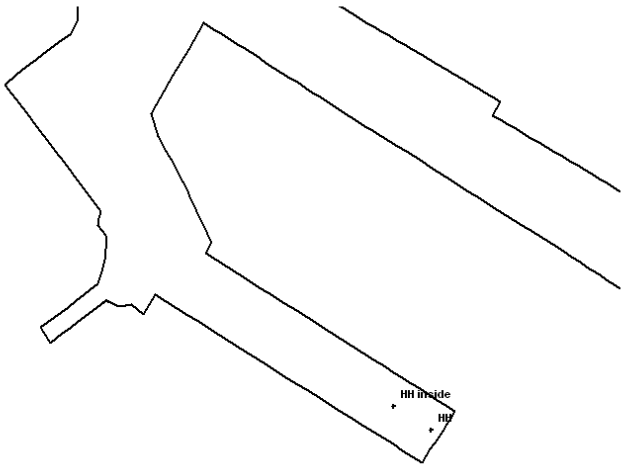

Figure F.33: Overview of the two different output locations inside the Haring harbor

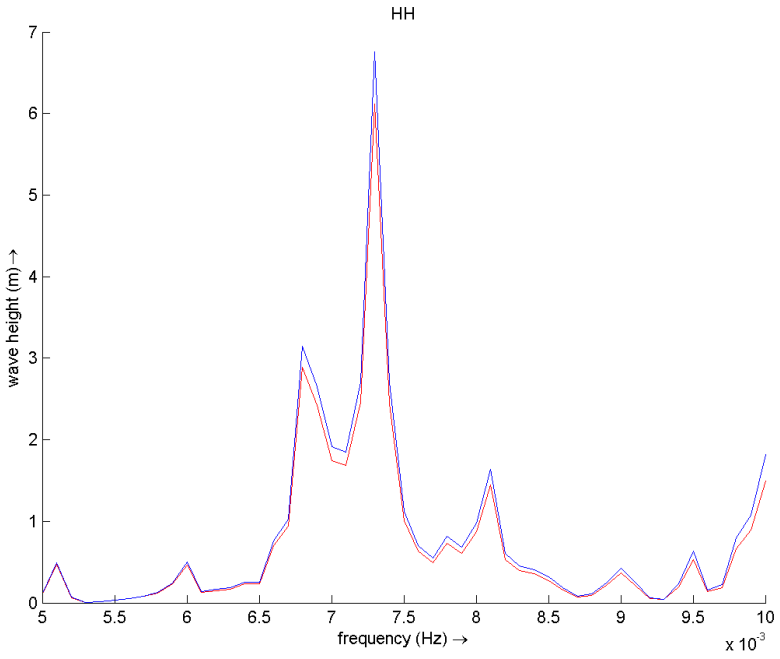

Figure F.34: Wave agitation graphs of the Haring harbor output locations. The blue graph concerns the location at the end and red graph concerns the location further inside the basin

F.4 Wave amplification for swell waves in the outer harbor

Chapter 5.6.1 concludes that swell does not penetrate the outer harbor. This appendix demonstrates the wave penetration results of all wave periods between 10 and 30 seconds.

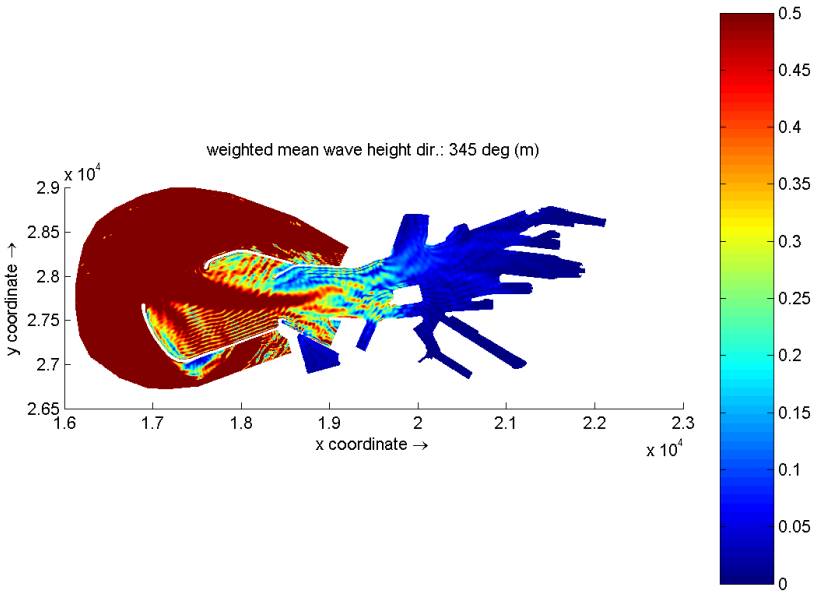

Figure F.35: Wave amplification in the outer harbor for an incoming wave period of 10 seconds

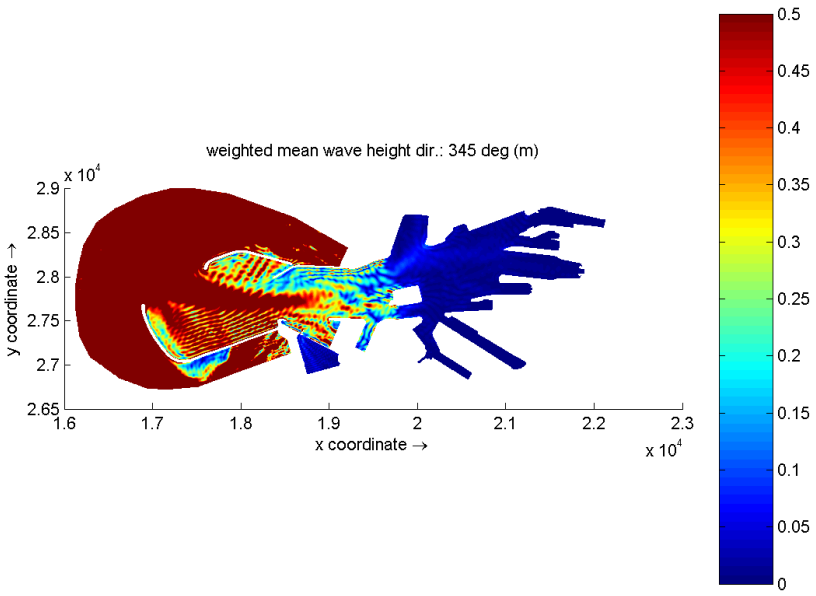

Figure F.36: Wave amplification in the outer harbor for an incoming wave period of 11 seconds

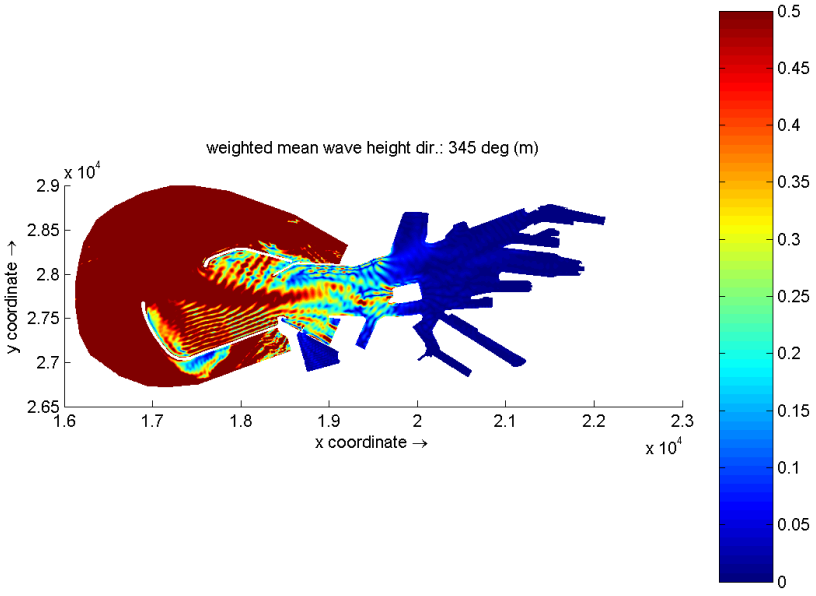

Figure F.37: Wave amplification in the outer harbor for an incoming wave period of 12 seconds

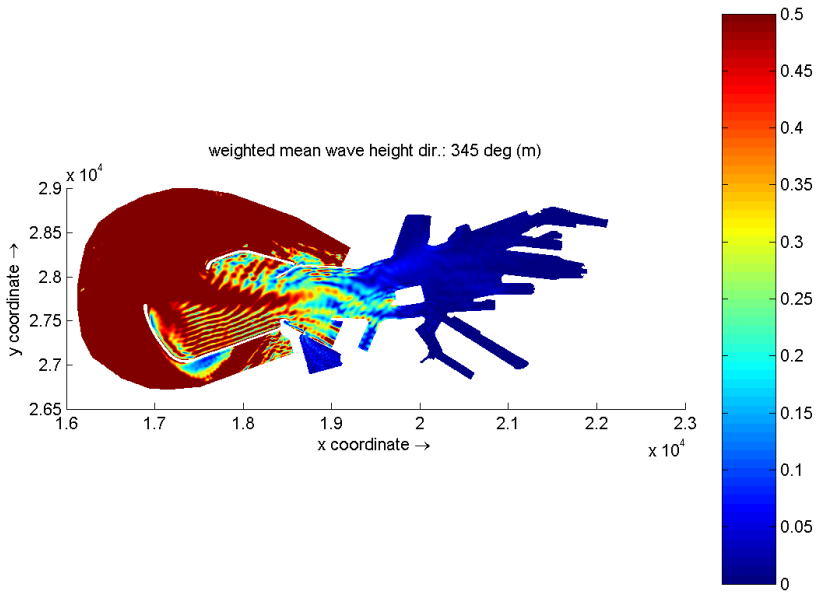

Figure F.38: Wave amplification in the outer harbor for an incoming wave period of 13 seconds

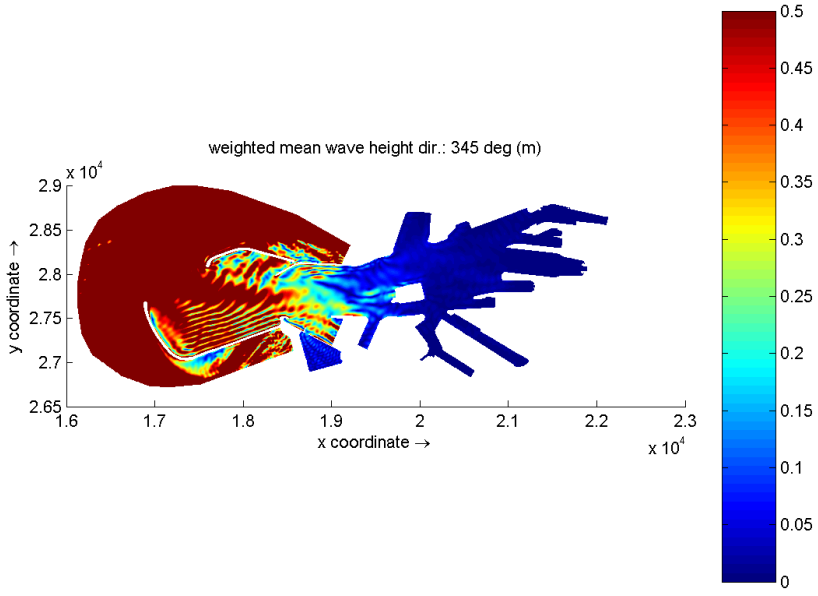

Figure F.39: Wave amplification in the outer harbor for an incoming wave period of 14 seconds

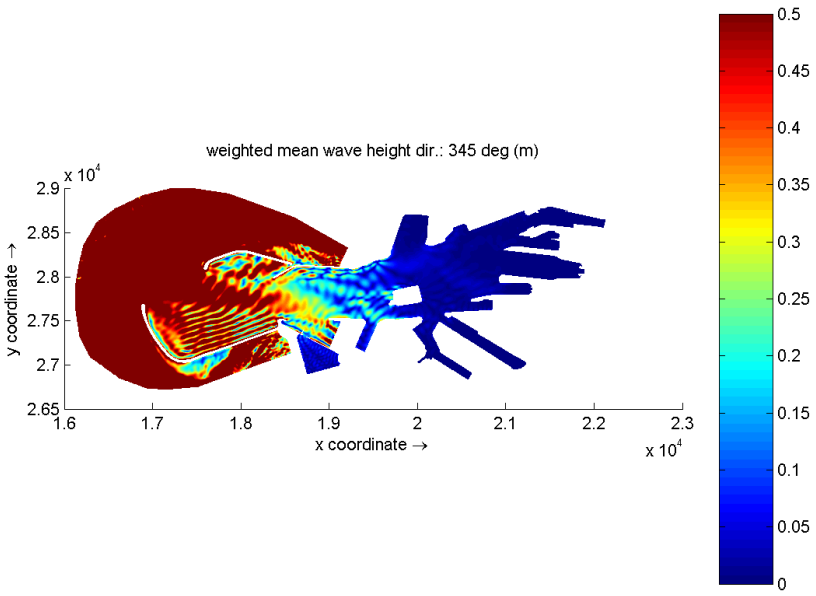

Figure F.40: Wave amplification in the outer harbor for an incoming wave period of 15 seconds

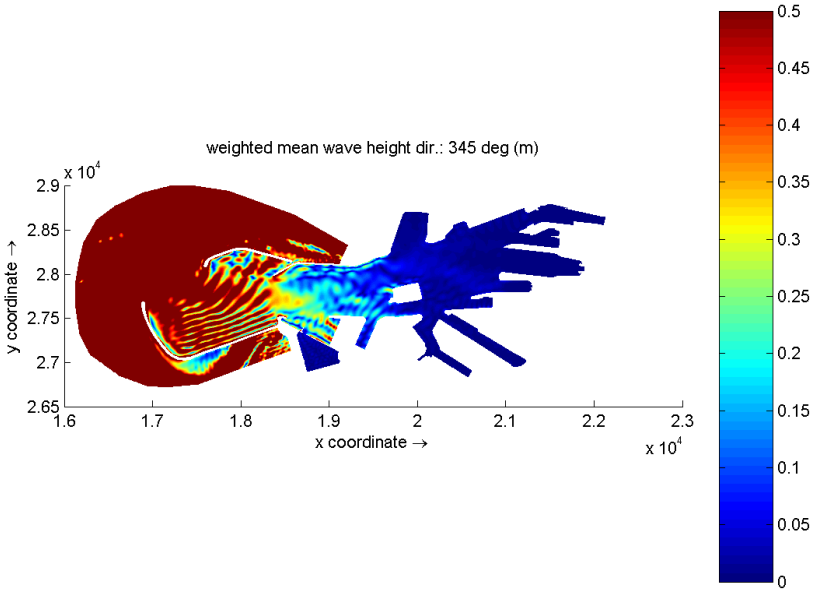

Figure F.41: Wave amplification in the outer harbor for an incoming wave period of 16 seconds

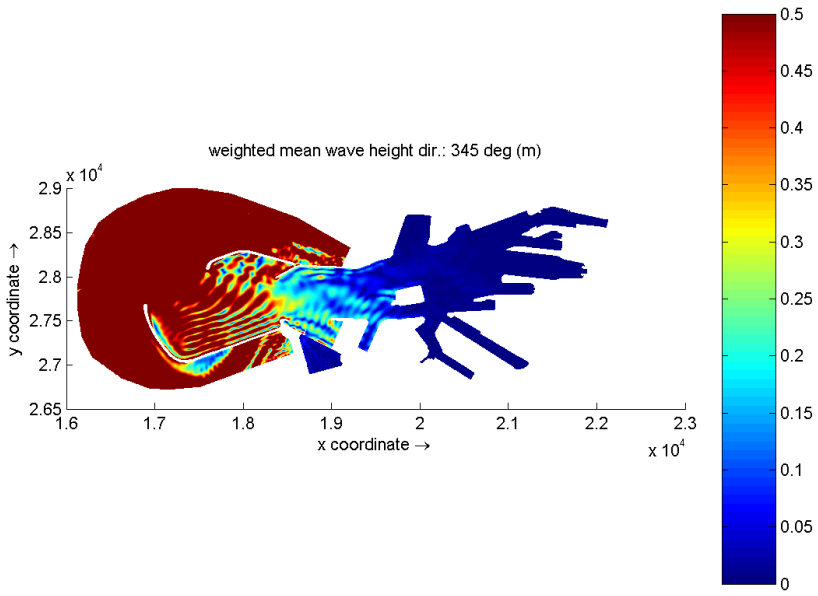

Figure F.42: Wave amplification in the outer harbor for an incoming wave period of 17 seconds

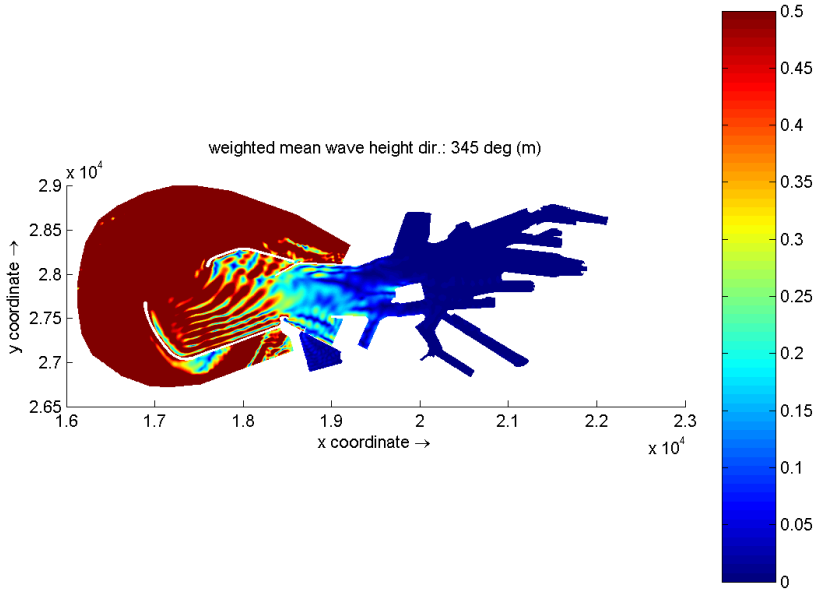

Figure F.43: Wave amplification in the outer harbor for an incoming wave period of 18 seconds

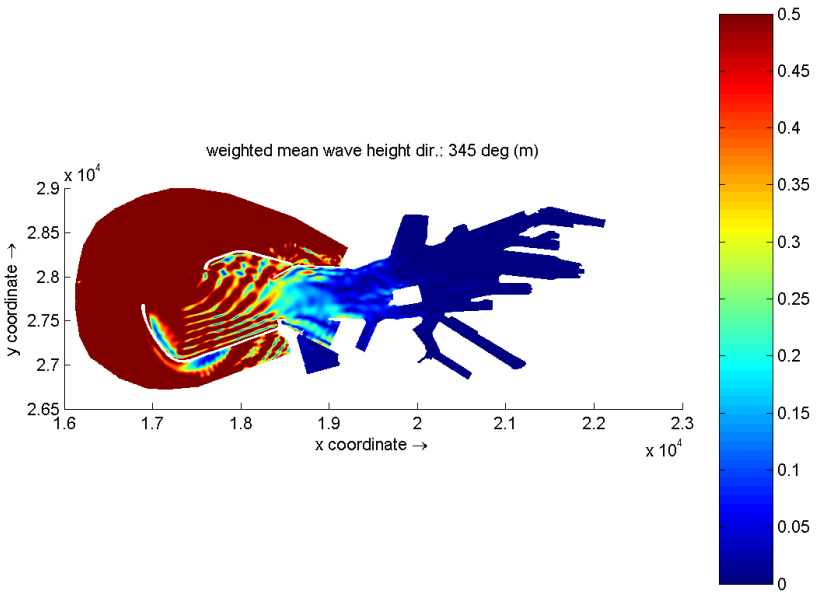

Figure F.44: Wave amplification in the outer harbor for an incoming wave period of 19 seconds

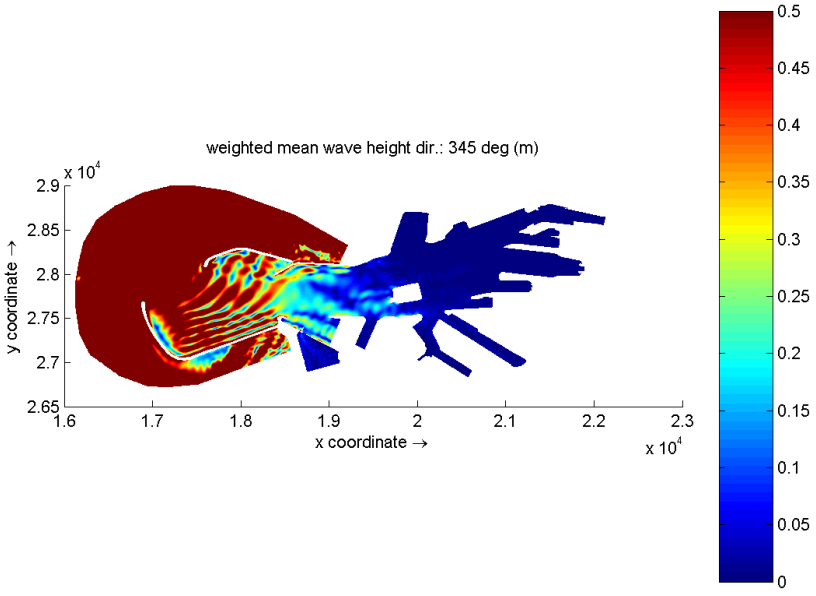

Figure F.45: Wave amplification in the outer harbor for an incoming wave period of 20 seconds

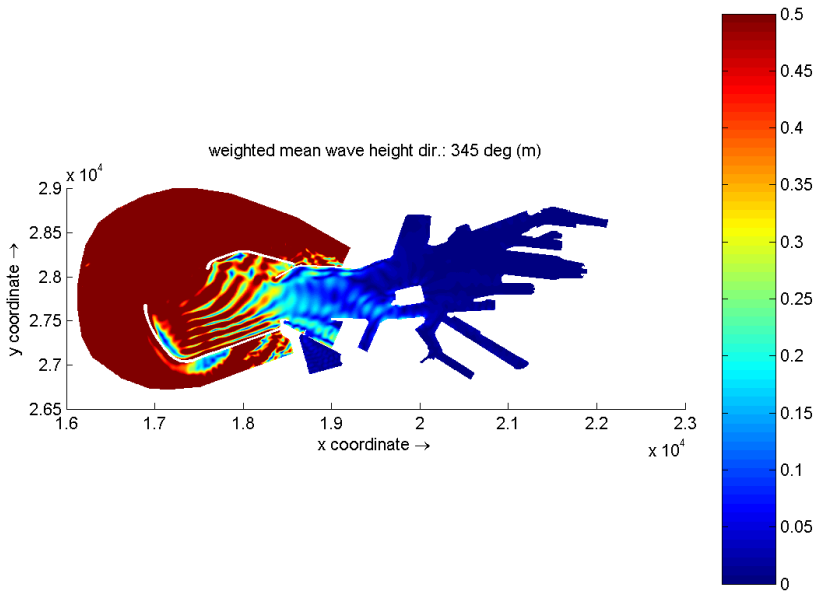

Figure F.46: Wave amplification in the outer harbor for an incoming wave period of 21 seconds

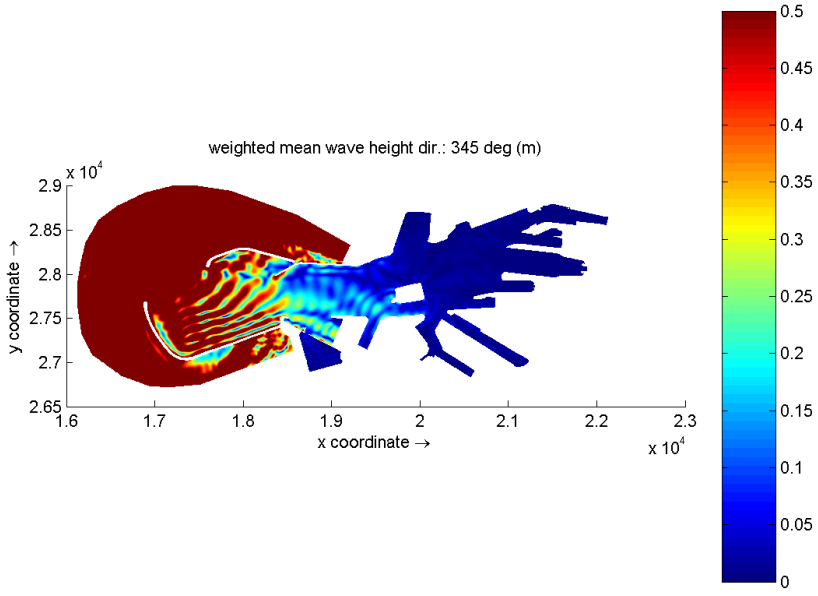

Figure F.47: Wave amplification in the outer harbor for an incoming wave period of 22 seconds

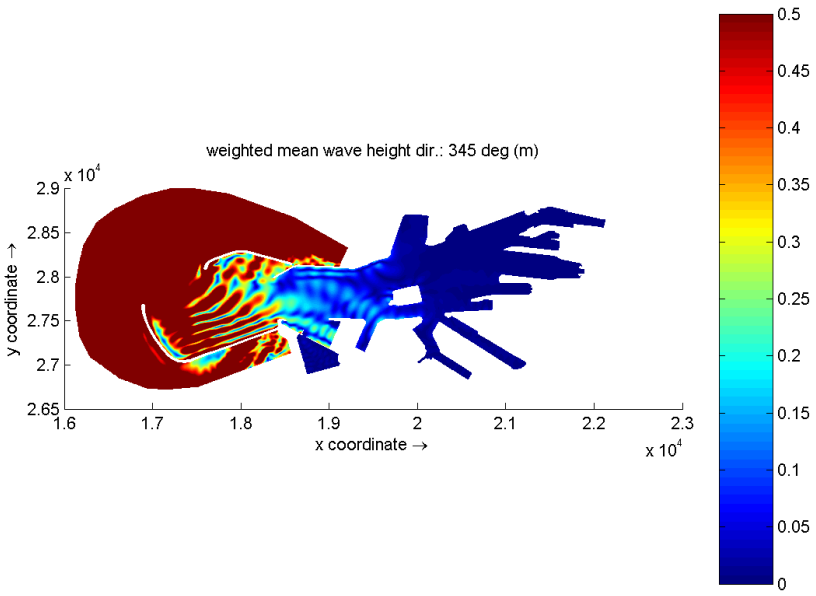

Figure F.48: Wave amplification in the outer harbor for an incoming wave period of 23 seconds

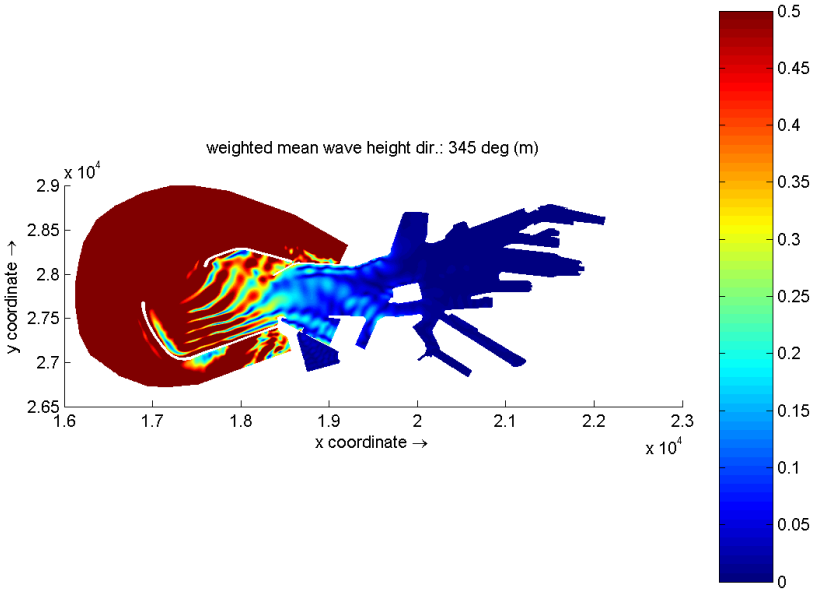

Figure F.49: Wave amplification in the outer harbor for an incoming wave period of 24 seconds

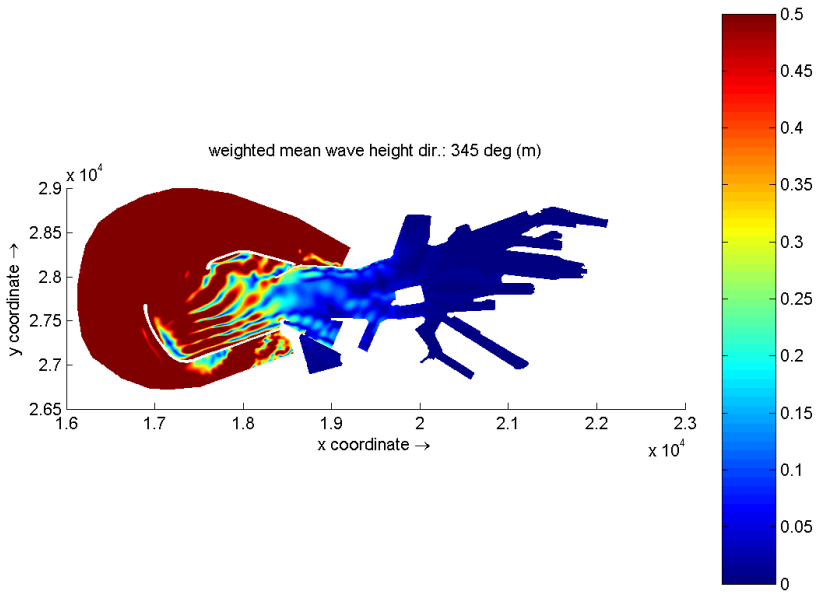

Figure F.50: Wave amplification in the outer harbor for an incoming wave period of 25 seconds

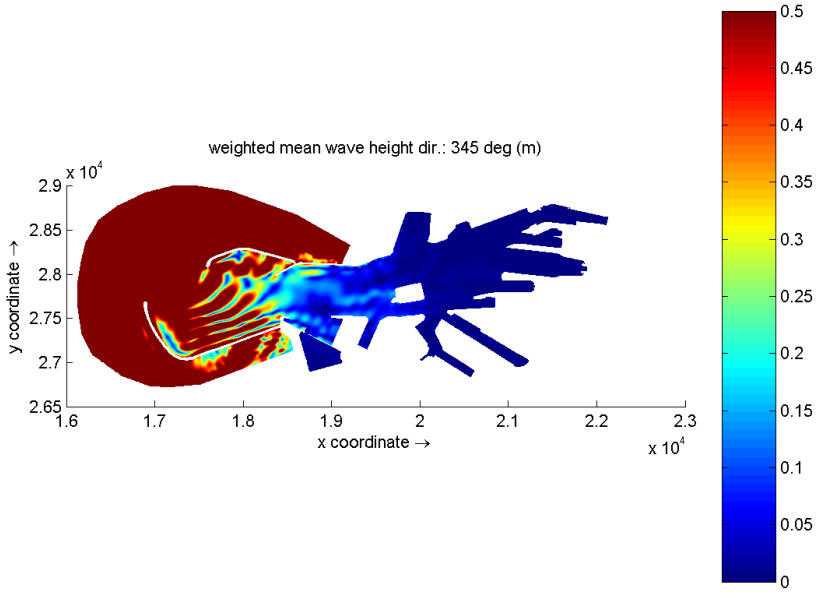

Figure F.51: Wave amplification in the outer harbor for an incoming wave period of 26 seconds

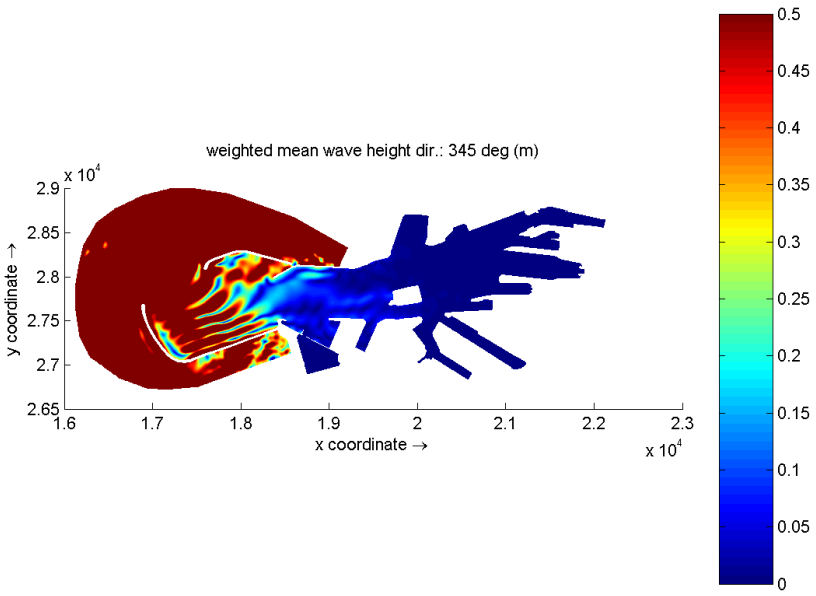

Figure F.52: Wave amplification in the outer harbor for an incoming wave period of 27 seconds

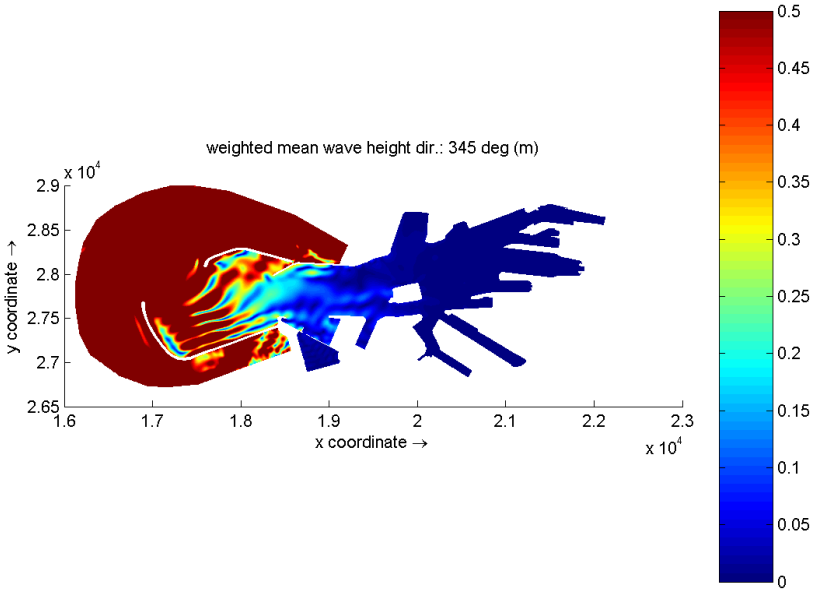

Figure F.53: Wave amplification in the outer harbor for an incoming wave period of 28 seconds

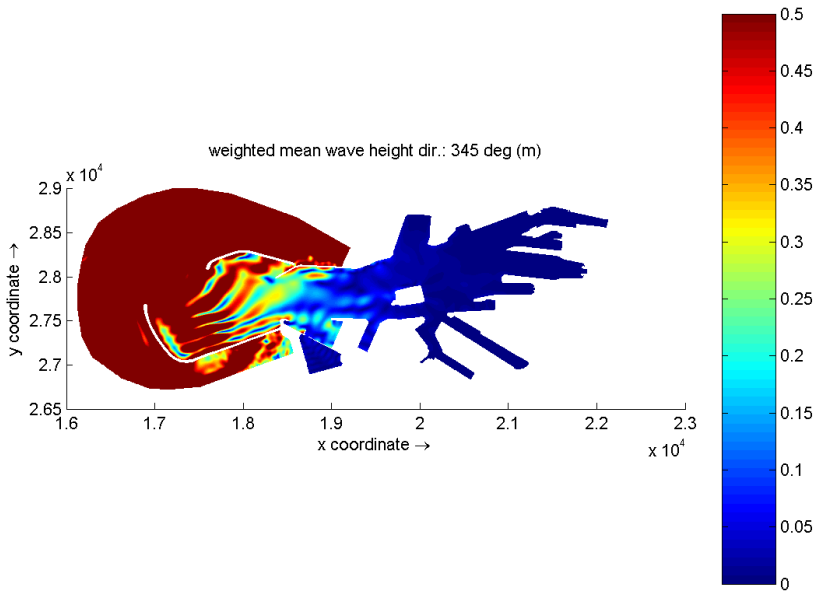

Figure F.54: Wave amplification in the outer harbor for an incoming wave period of 29 seconds

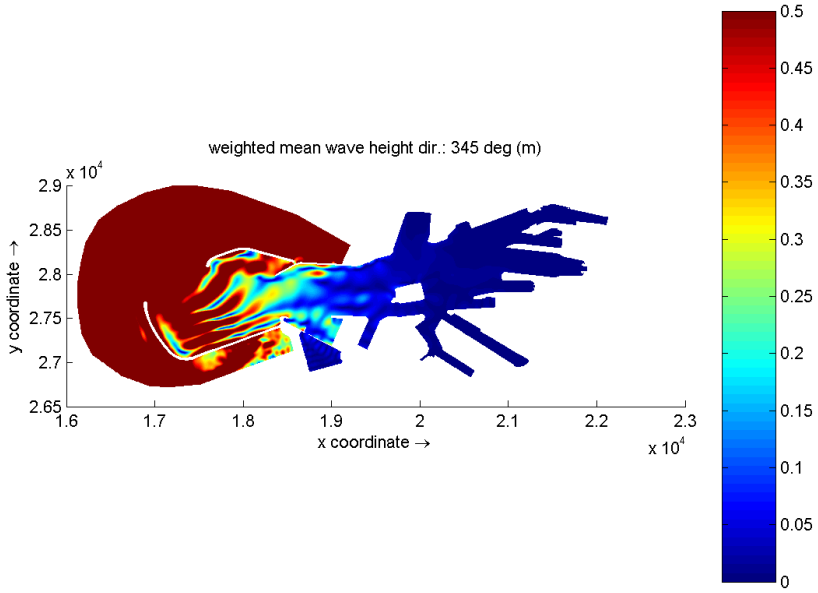

Figure F.55: Wave amplification in the outer harbor for an incoming wave period of 30 seconds

F.5 Comparing wave amplification in the outer harbor considering the current harbor layout and the layout with the new basin

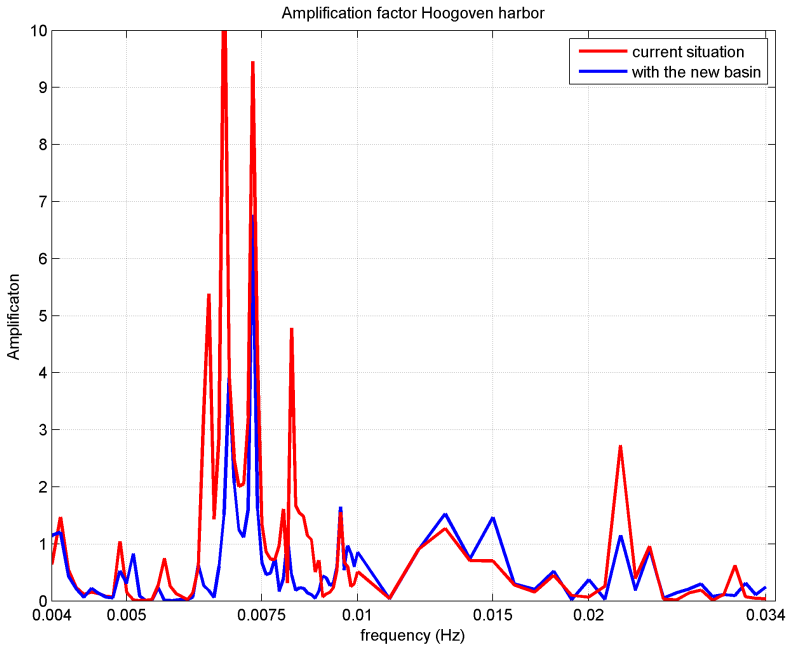

Figure F.56: Comparing wave amplification in the Hoogoven harbor considering the current harbor layout and the layout with the new basin

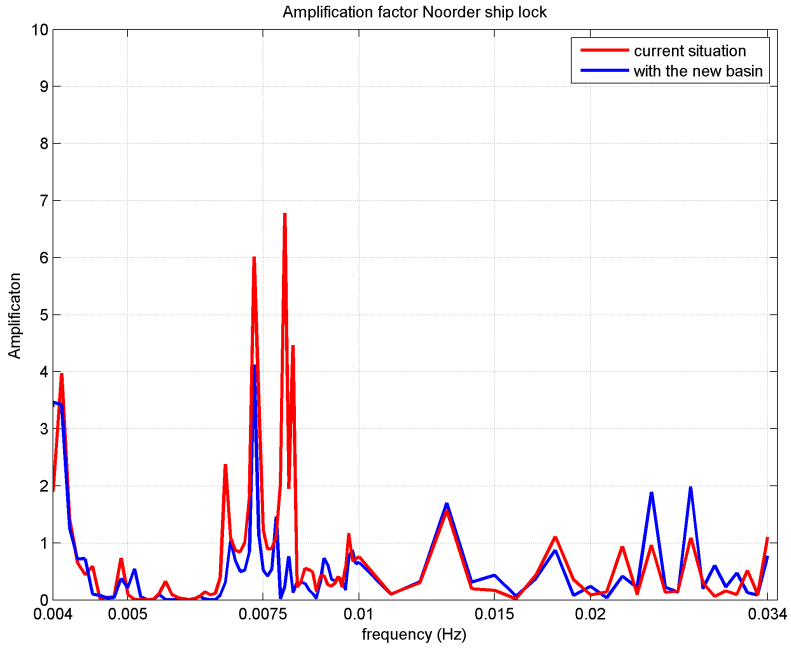

Figure F.57: Comparing wave amplification in the Noorder ship lock considering the current harbor layout and the layout with the new basin

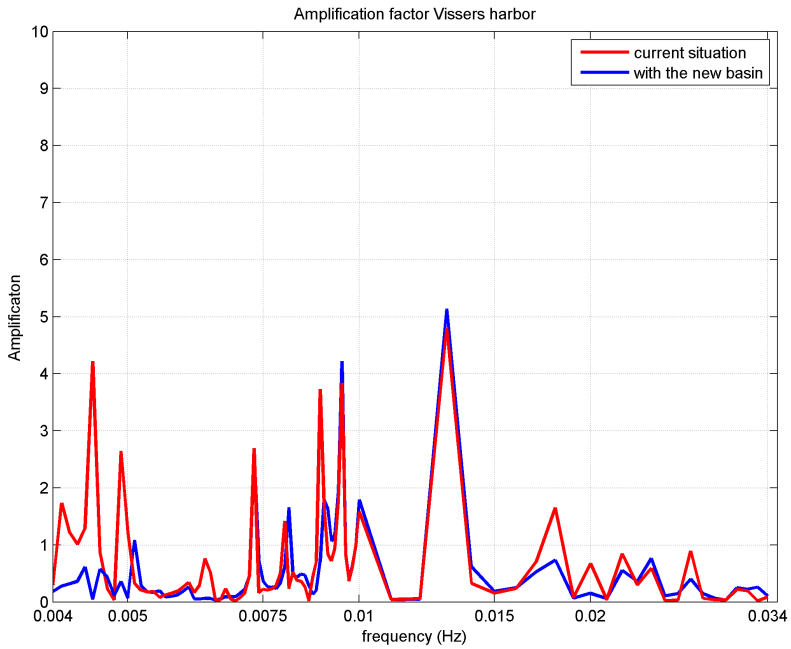

Figure F.58: Comparing wave amplification in the Vissers harbor considering the current harbor layout and the layout with the new basin

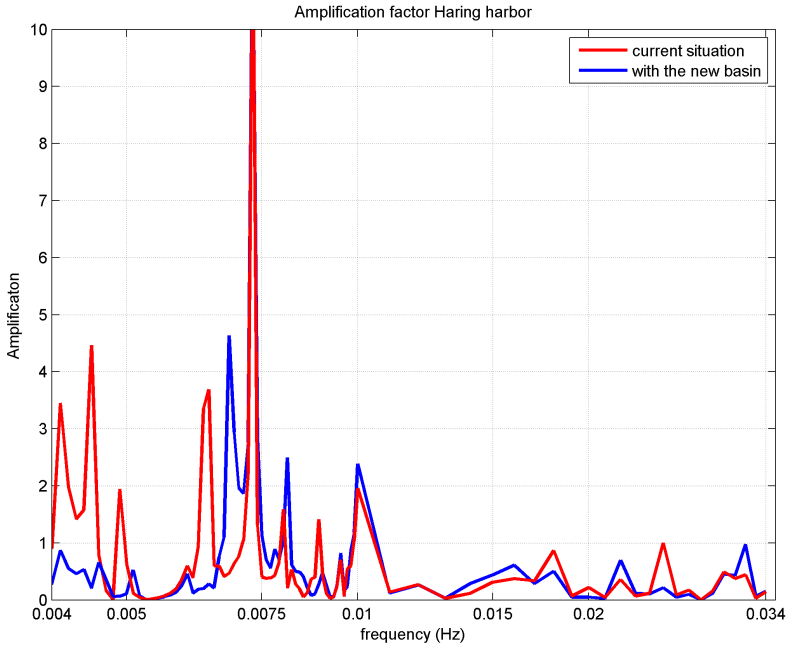

Figure F.59: Comparing wave amplification in the Haring harbor considering the current harbor layout and the layout with the new basin

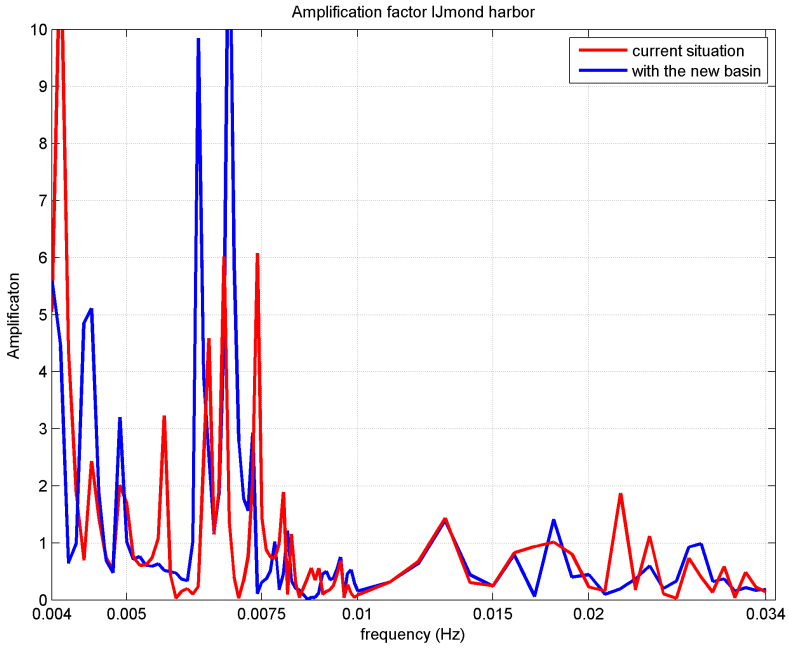

Figure F.60: Comparing wave amplification in the IJmond harbor considering the current harbor layout and the layout with the new basin

F.6 Comparing wave amplification in the outer harbor considering the new basin and adjusted new basin

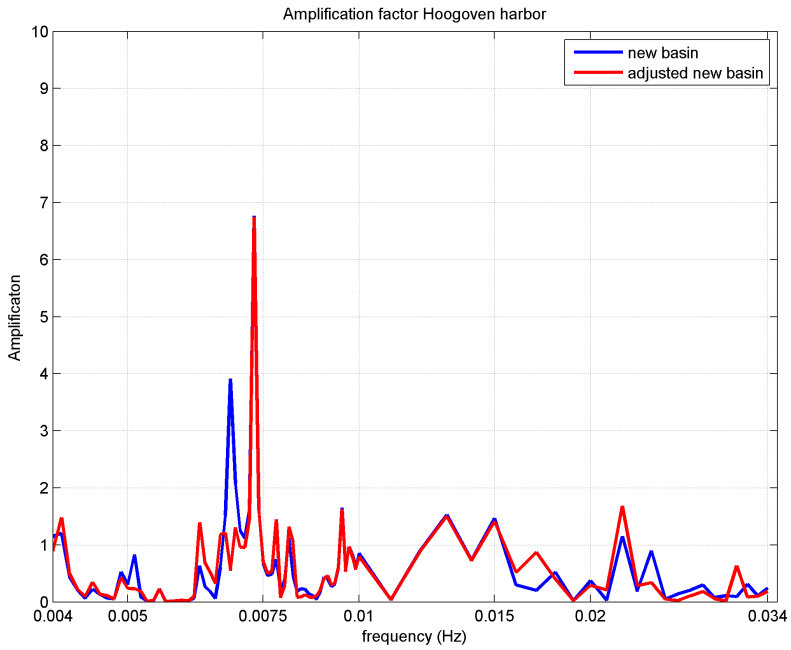

Figure F.61: Comparing wave amplification in the Hoogoven harbor considering the new basin and adjusted new basin

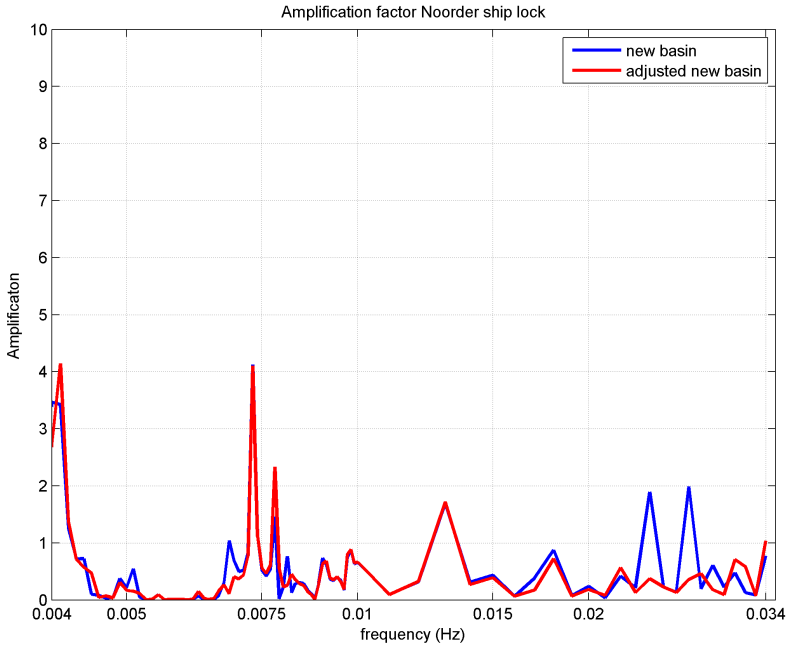

Figure F.62: Comparing wave amplification at the Noorder ship lock considering the new basin and adjusted new basin

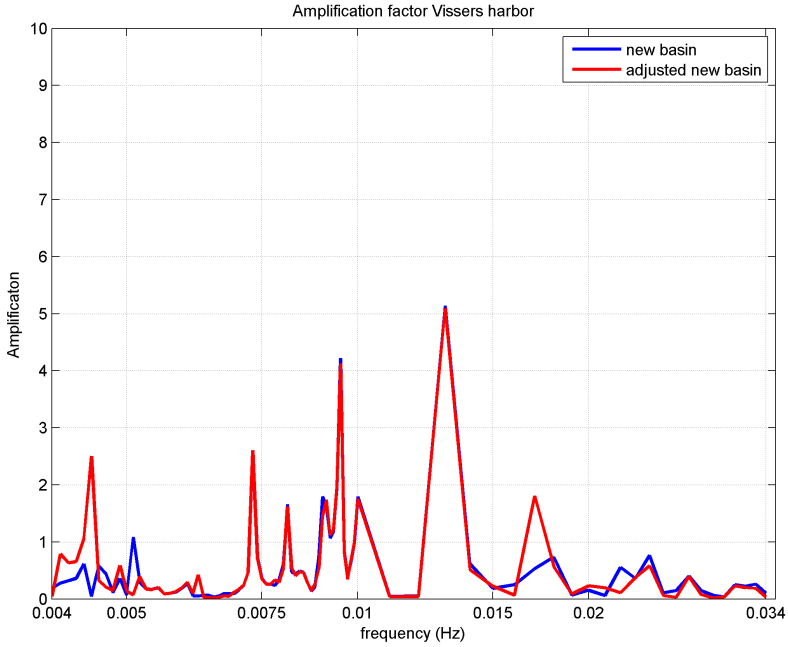

Figure F.63: Comparing wave amplification in the Vissers harbor considering the new basin and adjusted new basin

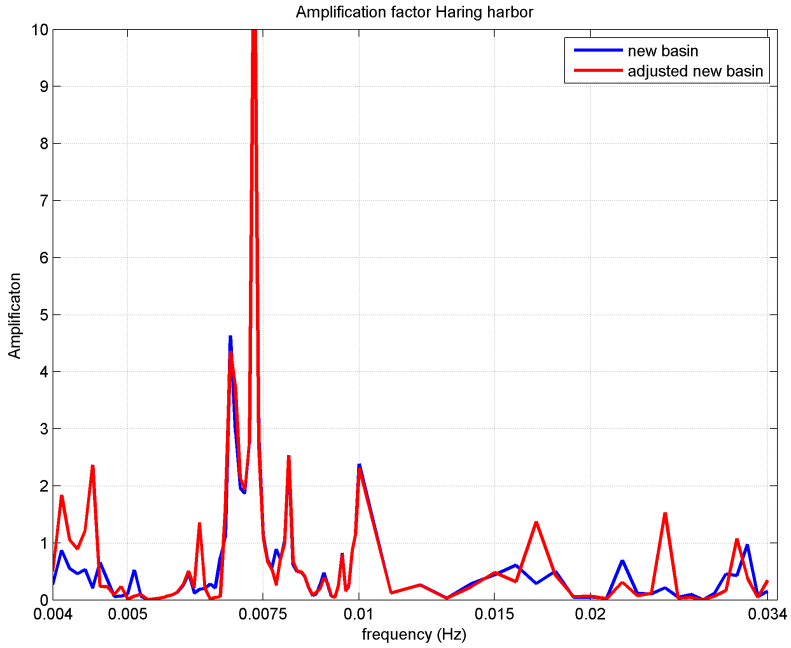

Figure F.64: Comparing wave amplification in the Haring harbor considering the new basin and adjusted new basin

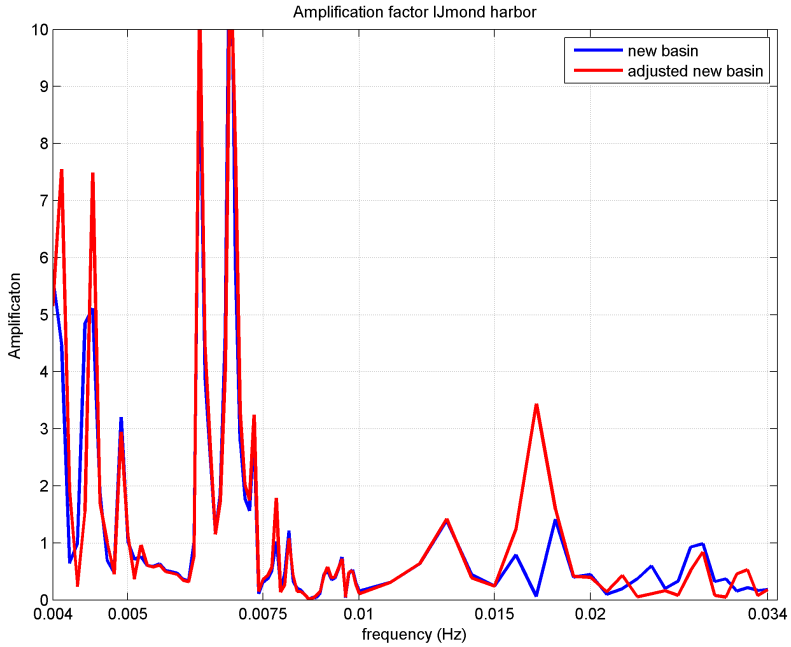

Figure F.65: Comparing wave amplification in the IJmond harbor considering the new basin and adjusted new basin